AN ABSTRACT OF THE THESIS OF

W. Scott Pegau for the degree of Doctor of Philosophy in Oceanography presented on February 23, 1996. Title: The Effects of Physical Parameters on the Absorption Coefficient of Natural Waters.

Abstract approved:

Redacted for privacy

J. Ronald V. Zaneveld

The absorption coefficient is one of the fundamental parameters used for studies in hydrologic optics. The significance of this parameter makes it important to understand how to properly measure it and how the absorption of components, such as water, depend on physical parameters such as temperature and salinity. A discussion is provided of a majority of the techniques available for measuring the absorption coefficient. Results from a comparison of the techniques indicates that natural variability in the optical properties is an important factor to consider when comparing or reporting measured values of the absorption coefficient. The agreement between methods was found to be best at longer wavelengths where the absorption by water is a significant portion of the total absorption coefficient. In order to test the accuracy of measurements of the absorption coefficient a practical IOP closure equation is

developed. Application of the equation to field measurements is limited by our ability to measure the volume scattering function.

The dependence of the absorption coefficient of water on temperature and salinity is investigated. It was found that the absorption coefficient in the near infrared portion of the spectrum is strongly dependent on temperature and salinity. In the visible region the only portion with a temperature dependence > 0.001 $m^{-1}/°C$ is in the neighborhood of 610 nm. A model of the absorption coefficient of water is used to develop a spectrally continuous temperature dependence curve. The only measured visible wavelength with a significant dependence was at 412 nm. It was found that in some spectral regions the temperature and salinity had opposite effects on the absorption coefficient.

The temperature dependence of the absorption coefficient in the near infrared region creates a difference in the absorption coefficients of water and ice. Two optical techniques are developed and tested to measure frazil concentrations. One of the methods uses the difference in absorption properties of water and ice to measure frazil concentrations. This technique should allow frazil measurements to be made even when other types of particles are present in the water column.

The Effects of Physical Parameters on the Absorption Coefficient of Natural Waters

by

W. Scott Pegau

A THESIS

submitted to

Oregon State University

in partial fulfillment of
the requirements for the
degree of

Doctor of Philosophy

Completed February 23, 1996
Commencement June 1996

Doctor of Philosophy thesis of W. Scott Pegau presented on February 23, 1996

APPROVED:

Redacted for privacy

Major Professor, representing Oceanography

Redacted for privacy

Dean of College of Oceanic and Atmospheric Sciences

Redacted for privacy

Dean of Graduate School

I understand that my thesis will become part of the permanent collection of Oregon State University libraries. My signature below authorizes release of my thesis to any reader upon request.

Redacted for privacy

W. Scott Pegau, Author

ACKNOWLEDGMENTS

I thank my major advisor, Dr. J. Ronald V. Zaneveld, for his guidance in research, teaching, and other aspects of life as a researcher. Because of the well rounded education and unselfish approach to research he has provided, I feel that the transition from being a student to being on my own will go as smoothly as possible. I also value the kindness he and his family have shown to my wife and me. In all aspects it has been a rewarding experience working with him.

I am grateful to Dr. Clayton Paulson for including me in his Arctic research and his work in developing the frazil measurement techniques. He has provided invaluable help in expanding my research directions as well as providing insights to classroom material when I had difficulties. I thank the other members of my committee, Dr. Timothy Cowles, Dr. Barry Sherr, and Dr. Robert Olson, their time and effort as committee members is greatly appreciated. I look forward to interacting with my committee members in my future research endeavors.

I thank all of the co-authors on the various chapters of this thesis for sharing their data with me and their helpful comments on the text. The efforts of Dr. James Mueller are especially appreciated. His many comments on content and style greatly improved the comparison of absorption measurement paper. I thank Steve Daly and Jim Lever for their cooperation in providing use of the facilities of the Cold Regions Research and Engineering Laboratory to test the optical frazil measurement techniques.

I thank the Office of Naval Research Environmental Optics program managers, Dr. Curt Mobley, Dr. Gary Gilbert, and Dr. Steven Ackleson, for providing funding for a majority of this research. Parts of the research have also been funded by the High Latitude section of ONR, NASA, and NSF.

Most importantly I must thank my wife, Cathy Pegau, for being so understanding when I had to work late on a project or for a class. I know of no other person who would be as understanding when I had long stretches of time traveling to meetings or cruises. She was even willing to drive me to and from the airports in Portland and Eugene at ungodly hours with a minimum of fuss. To her I give my deepest love.

CONTRIBUTION OF AUTHORS

Dr. Ronald Zaneveld was involved in the analysis and writing of all of the enclosed chapters. The data, method description, and error analysis of the spectrophotometer data used in Chapter two was provided by Dr. Joan Cleveland. Dr. Willard Wells, William Doss, and Robert Stone provided similar analysis of the Compound Radiometer. Dr. James Mueller provided the sections concerning the Tethered Optical Profiler and Gershun's equation. Dr. Alan Weidemann and Dan Kennedy were responsible for the sections involving the Integrating Cavity Absorption Meter. Robert Maffione provided the sections involving the Isotropic Point Source. Dr. Charles Trees provided information on pigment composition during the experiment. All of the above co-authors helped in developing the analysis and discussion of the collected data. Dr. Mueller provided much assistance in developing the final version of this manuscript.

Dr. Kenneth Voss provided the General Angle Scattering Meter data used in Chapter 3 along with comments on the analysis provided in the manuscript. Deric Gray was responsible for making the laboratory measurements used in Chapter 5. Dr. Clayton Paulson provided the field data used in Chapter 6. He also helped in collection and analysis of the laboratory data. He has provided strong guidance in the writing of the manuscript.

TABLE OF CONTENTS

TABLE OF CONTENTS (Continued)

TABLE OF CONTENTS (Continued)

TABLE OF CONTENTS (Continued)

Page

LIST OF FIGURES

LIST OF FIGURES (Continued)

LIST OF FIGURES (Continued)

LIST OF TABLES

DEDICATION

This thesis is dedicated to the memory of Shelly Dawn Clay, an inspiration and friend forever.

THE EFFECTS OF PHYSICAL PARAMETERS ON THE ABSORPTION COEFFICIENT OF NATURAL WATERS

CHAPTER 1

GENERAL INTRODUCTION

Absorption and scattering are the two fundamental processes by which light interacts with aqueous systems. This thesis focuses on the spectral absorption coefficient [$a(\lambda)$]. Special attention will be paid to the absorption coefficient of the only component included in all aqueous systems, water.

The absorption coefficient is defined to be the proportion of radiant flux lost due to absorption from a beam normal to an infinitesimally thin layer of the medium, divided by the thickness of the layer [e.g., Jerlov, 1976]. Because it is not dependent on the natural radiance field the absorption coefficient is an inherent optical property (IOP) [Preisendorfer, 1976]. The absorption coefficient is one of the two IOP that must be known to solve the equation of radiative transfer in a plane parallel medium with no internal sources or inelastic scattering. For this case the equation of radiative transfer can be written as:

$$\cos\theta \frac{dL(\Omega)}{dz} = -(a+b)L(\Omega) + \int_0^{4\pi} \beta(\Omega,\Omega')\, L(\Omega')d\Omega', \qquad (1.1)$$

where $L(\Omega)$ is the radiance at a given solid angle Ω, a is the absorption coefficient, $\beta(\Omega,\Omega')$ is the volume scattering function, and b is the scattering coefficient. The

scattering coefficient is obtained by integrating the volume scattering function over all solid angles. Using this equation we can calculate the apparent optical properties (AOP) such as the irradiance levels (E, and E_0), the diffuse attenuation coefficient (K), the remote sensing reflectance, as well as the radiance distribution at any depth. The absorption coefficient thus has an integral role in studies that require the AOP. These studies include, but are not limited to, the short-wave radiation contribution to the heat budget, visibility predictions, and productivity investigations [Kirk, 1994].

In the inverse problem, the total absorption coefficient (a_t) is used to determine the concentrations of dissolved and suspended matter. This is possible because the total absorption coefficient can be divided into the individual component contributions. In hydrologic optics the division is often into water (a_w) , dissolved materials (a_d), and particulate contribution (a_p).

$$a_t = a_w + a_d + a_p \tag{1.2}$$

The particulate component can be further divided into phytoplankton pigments, detritus, and tripton [Kirk, 1994; Roesler et al., 1989]. This division is not clean, for example, the absorption properties of protists and heterotrophic bacteria are presently lumped into the detritus category. There is no reason not to change the divisions to suit the interests of the investigator. As an example, another manner in which to divide the particulate absorption is to break it into particle size categories.

It is difficult to isolate one component of the total absorption. The absorption by water must be accounted for when measuring the absorption coefficient of dissolved materials. The opposite is also true; dissolved materials have historically been difficult

to remove from the water, which creates problems in making high quality measurements of pure water absorption. Similarly, absorption of the particulate component is commonly measured on wet filter pads and may contain some dissolved materials as well as water in the measurement. Thus, it is important to consider absorption by all components when determining the absorption coefficient of individual components.

In some instances the instruments used to measure the absorption coefficient require a knowledge of the optical properties of a reference material, such as water, to interpret the measurements. The two commercially available systems for measuring the absorption coefficient, spectrophotometers and the WETLabs ac-9 [Moore, 1994], use pure water as a reference for some or all of the measurements. These instruments also require that a correction be made for scattered light that is not measured. Some of the scattering correction schemes use the measured absorption coefficient at a near infrared wavelength to estimate the scattering error [Zaneveld et al., 1994; Green and Blough, 1994]. It therefore is important to know the optical properties of the reference medium in the near infrared as well as the visible regions of the spectrum to prevent the scattering correction from propagating measurement errors to shorter wavelengths.

Despite the importance of the absorption coefficient in studies of radiative transfer, even the most recent texts about optical oceanography [Kirk, 1994; Mobley, 1994] provide little detail about the theory of absorption or measurement techniques used to determine the absorption coefficient. The lack of detail in the theory of absorption is understandable because of the complexity of any liquid system [Franks,

1972]. The water molecule is a polar molecule which allows the individual molecules in water to form hydrogen bonds with each other, creating a complex liquid. There are several possible structures for the water dimer which is the simplest form of a water macromolecule [Rao, 1972]. The water molecules can also form trimers and larger molecular clusters. It is changes in the structure of liquid water that leads to the temperature and salinity dependence of the absorption coefficient. To estimate the absorption coefficient from theory using the Schrödinger equation requires a knowledge of the probability of existence of each molecular arrangement and an understanding of the energy potentials of the atoms in all of the possible arrangements [Richards, 1979]. The ab initio calculation of the molecular arrangements and potentials is limited by the ability of computers to handle many-body problems and by the assumptions used in creating the models [Rao, 1972; Richards, 1979; Wood, 1979]. A full development of the theory of absorption is not included in this work and readers are referred to the seven volume set edited by F. Franks (1972), titled, "Water: a comprehensive treatise" as a starting point in studying the structure and theoretical approaches used towards understanding the properties of water.

Because of the difficulty in formulating a complete theoretical description of absorption in natural waters, it is important to develop an understanding of absorption by empirical means. Measurement of the absorption coefficient in the visible region of the spectrum is extremely difficult. The difficulties arise because of the high transparency of water in this region and in devising a method to account for errors in the measurement caused by scattered light. Scattering errors are caused by not

collecting all of the scattered light and/or by an increased pathlength due to scattering. The complexity of making absorption measurements has led to the development of several laboratory and in-situ devices for measuring the absorption coefficient. The focus of the second chapter, titled "A comparison of methods for the measurement of the absorption coefficient in natural waters," is a review of the majority of the techniques presently used for measuring the absorption coefficient in natural waters. A simple description of the methodology used by each technique is included along with an error analysis. The absorption coefficients measured during a 1992 experiment at Lake Pend Oreille are compared.

A comparison of absorption measurement methods indicates the variability among the methods but cannot determine which measurement is most accurate. In the third chapter titled, "Toward closure of the inherent optical properties in natural waters," closure of the inherent optical properties is discussed as a means to check the accuracy of measurements of the absorption coefficient. The IOP closure equation is reformulated into an equation applicable to realistic measurements. An attempt to perform closure using the practical IOP closure equation is carried out using measurements of c, a, and $\beta(\theta)$ from 10 to 170° collected during the same experiment described in chapter 2.

The accurate measurement of the absorption coefficient in natural waters is difficult to perform. Part of the difficulty is caused by a poor understanding of which environmental parameters the absorption coefficient of water is dependent on. Chapters four and five are devoted to the determination of the effect of temperature

and salinity on the absorption coefficient in the visible and near-infrared portions of the spectrum. In chapter 4, titled "Temperature-dependent absorption of water in the red and near-infrared portions of the spectrum," a spectrophotometer was used to determine how the shape of the absorption spectrum changes as a function of temperature in the red and near infrared portions of the spectrum. In chapter 5, titled "Absorption of visible and near-infrared light in water: the dependence on temperature and salinity," measurements are made using WETLabs ac-9s and a WETLabs a-3 to determine the absolute magnitude of the dependence of the absorption coefficient on temperature and salinity. The laboratory measurements are validated using field measurements. The field measurements are used to argue that a constant temperature dependence in the blue-green portion of the spectrum that has previously been reported [Højerslev and Trabjerg, 1990; Buiteveld, et al., 1994] cannot exist.

The factors that cause the absorption coefficient of water to depend on temperature and salinity create differences in the spectral absorption coefficients of ice and liquid water. Based on the difference in the absorption properties of water and ice, an instrument was developed to measure the concentration of frazil crystals within the water column. A description of the method and results from tests in a laboratory flume are presented in chapter 6, titled "Optical measurements of frazil concentration."

This thesis describes the different ways in which the absorption coefficient is measured in natural waters. A practical IOP closure equation is developed for testing the consistency of absorption coefficient measurements. The roles of the environmental parameters of temperature and salinity are then investigated using

laboratory and field measurements of the absorption coefficient. Finally, the temperature dependence of the absorption coefficient is used to develop a method for measuring frazil concentration within the water column.

CHAPTER 2

A COMPARISON OF METHODS FOR THE MEASUREMENT OF THE ABSORPTION COEFFICIENT IN NATURAL WATERS

W. Scott Pegau, Joan S. Cleveland, W. Doss, C. Dan Kennedy, Robert A. Maffione, James L. Mueller, R. Stone, Charles C. Trees, Alan D. Weidemann, Willard H. Wells, and J. Ronald V. Zaneveld

Published in *Journal of Geophysical Research*
July 15, 1995, 20 pages

2.1 ABSTRACT

In the spring of 1992 an optical closure experiment was conducted at Lake Pend Oreille, Idaho. A primary objective of the experiment was to compare techniques for the measurement of the spectral absorption coefficient and other inherent optical properties of natural waters. Daily averages of absorption coefficients measured using six methods are compared at wavelengths of 456, 488 and 532 nm. Overall agreement was within 40% at 456 nm and improved with increasing wavelength to 25% at 532 nm. These absorption measurements were distributed over the final 9 days of the experiment, when bio-optical conditions in Lake Pend Oreille (as indexed by the $c_p(660)$ and chlorophyll a fluorescence profiles) were representative of those observed throughout the experiment. However, profiles of stimulated chlorophyll a fluorescence and beam transmission showed that bio-optical properties in the lake varied strongly on all time and space scales. Therefore, environmental variability contributed significantly to deviations between daily mean absorption coefficients measured using the different techniques.

2.2 INTRODUCTION

In the spring of 1992 an optical closure experiment was performed at Lake Pend Oreille, Idaho. The experiment was designed to test mathematical relationships between measured sets of several optical properties, and to compare results from

different techniques used to measure individual optical properties, including the spectral volume absorption coefficient.

Absorption is one of the fundamental processes that determine the shape and magnitude of the light field in a medium. The absorption coefficient is the proportion of the flux lost due to absorption from a beam normal to an infinitesimally thin layer of the medium, divided by the thickness of the layer [e.g., *Jerlov*, 1976]. The absorption coefficient, the volume scattering function, and the input radiance distribution are necessary to solve the radiative transfer equation for the radiance distribution as a function of depth. Thus, the absorption coefficient has a key role in determining any optical property that is dependent on the radiance distribution including the remotely sensed reflectance, the diffuse attenuation coefficient, and irradiance.

In addition to its importance for modeling radiative energy transfer in water, the absorption coefficient is important for studies of phytoplankton productivity and taxonomy. The total absorption coefficient can be partitioned into a sum of the absorption coefficients due to dissolved organic matter, phytoplankton, detrital particles, and water. Spectral characteristics of absorption by phytoplankton result from, and can therefore be used to identify, photosynthetic and auxiliary pigments characteristic of particular phytoplankton taxonomic groups [*Sathyendranath et al.*, 1987]. Investigations and models of primary production must include spectral absorption coefficients of photosynthetic pigments, which determine the ability of phytoplankton to collect light for use in photosynthesis.

The importance of the absorption coefficient and the difficulty of measuring it accurately in low signal, scattering suspensions has led to the development of a variety of techniques to measure it. In situ measurement techniques include the reflecting tube absorption meter [*Zaneveld et al.*, 1990; *Moore et al.* 1992], methods that use an isotropic point source [*Sorenson and Honey,* 1968; *Maffione et al.*, 1993], and a number of methods that use a natural light field and Gershun's equation relating the absorption coefficient to the apparent optical properties [*Tyler,* 1960; *Højerslev,* 1975; *Spitzer and Wernand,* 1981; *Doss and Wells,* 1992; *Voss and Chapin,* 1992]. Laboratory measurement techniques include the integrating cavity absorption meter [*Fry et al.,* 1992], optoacoustic measurements [*Trees and Voss,* 1990], photothermal measurements [*Bennett et al.,* 1986], and measurements of the component portions using a spectrophotometer [*Yentsch*, 1962; *Kiefer and SooHoo*, 1982; *Roesler et al.*, 1989].

During the April/May 1992 optical closure experiment in Lake Pend Oreille, spectral absorption coefficients were measured using six different techniques, including laboratory measurements that use water samples and in situ measurements. Most of these methods had never been compared. In this paper we compare these techniques for the measurement of the spectral absorption coefficients of natural water and investigate the relative uncertainties between methods. We also examine the data for evidence of systematic deviations in absorption estimates which may result from the different measurement volumes, calibration techniques, and wavelength bandpass characteristics of the methods.

The Lake Pend Oreille site was selected primarily because *Tyler*'s [1960] optical measurements there indicated that, in late winter and early spring, we could expect to find a well-mixed water column having a relatively homogeneous distribution of bio-optical properties. Unfortunately, the spring of 1992 was an unusually warm season and the lake had begun to stratify both thermally and bio-optically. These conditions resulted in significant spatial and temporal variability which detracted from our comparisons, but which made the lake a more typical optical environment.

A second important consideration in our choice of this site was the availability of a Navy barge moored in 200 m of water, which provided an ideal platform from which to deploy several optical systems simultaneously. It is rarely possible to deploy more than one measurement system at a time from a research vessel at sea. The barge and other essential logistical support facilities are maintained by the Acoustic Research Detachment of the U.S. Navy's David Taylor Research Center (DTRC) in and near Bayview, Idaho.

2.3 METHODS

The six individual absorption measurement techniques used in the optical closure experiment, and ancillary measurements made to characterize bio-optical variability associated with particles, are briefly described in this section. The absorption measurement systems, in the order described below, are the Reflecting Tube

Absorption Meter (RTAM), the Tethered Optical Profiling System (TOPS), the Isotropic Point Source (IPS), the Compound Radiometer (CR), the Integrating Cavity Absorption Meter (ICAM) and a spectrophotometer. The three wavelengths at which most of the instruments were operated were 456, 488, and 532 nm. Dates, measurement wavelengths, and sampling depths for each absorption measurement system are listed in Table 2.1. The IPS, spectrophotometer and TOPS were the only techniques with which measurements were made at all three wavelengths for the period of April 30 to May 7. A 456 nm RTAM was operated from April 30 to May 5, and a 532 nm RTAM was operated on all days. At depths below 50 m, where the IPS method worked best, absorption coefficients determined with the IPS, spectrophotometer, ICAM and the two RTAMs are compared. Absorption measurements by the TOPS, RTAMs, ICAM, CR and spectrophotometer are compared in the upper 30 m of the water column. Measurements by the IPS and TOPS, which both integrate absorption over large water volumes, cannot be compared directly, because the TOPS measurements require strong ambient daylight, and the IPS requires near or total darkness to derive accurate absorption coefficients.

Table 2.1. The dates, wavelengths, and depths sampled by each of the absorption techniques.

Instrument	Dates used	Wavelengths	Depths Sampled
Reflecting tube absorption meter	April 30 May 1, 4, 5, 6, 7	456 and 532nm with 10 nm bandpass filters	approximately every 20 cm from 0 to 80 m, (small volume measurement)
Tethered optical profiler (Gershun's)	April 29, 30 May 1, 4, 5, 6, 7	440, 453, 486, 518, and 530 nm with 10 nm bandpass filters	0 to 45 m, maximum depth dependent on wavelength, (large volume measurement)
Isotropic point source	April 23, 24, 27, 28, 29, 30 May 1, 4, 5, 6, 7	456, 488, and 532 nm with 10 nm bandpass filters	discrete samples between 10 and 90 m, sample size 10 to 15m, (large volume measurement)
Compound radiometer	May 1	450 nm with 10 nm bandpass filters	5 to 25 m (large volume measurement)
Integrating cavity absorption meter	April 27, 28, 29, 30 May 1	440, 456, 488, 532, 565, 600, 630, 676, and 712 nm with 3 nm bandpass	discrete water samples taken from 5 to 100 m (small volume measurement)
Spectrophotometer	April 23, 24, 27, 28, 29, 30 May 1, 4, 5, 6, 7	400 to 700 nm every nm with 4 nm bandpass	discrete water samples taken from 5 to 100 m (small volume measurement)

2.3.1 Sampling Site

We conducted the optical closure experiment from a Navy barge operated by the David Taylor Research Center located in Bayview, Idaho. The barge, moored in Scenic Bay, Lake Pend Oreille, in approximately 200 m of water (Figure 2.1), is 145 feet long and 78 feet wide. A 22 feet wide by 125 feet long well runs through the center of the barge and is open at its eastern end (Figure 2.2). The enclosed portion at the western edge of the barge contained wet and dry laboratories. A second smaller barge, containing electrical power transformers, was moored to the western end of the large barge.

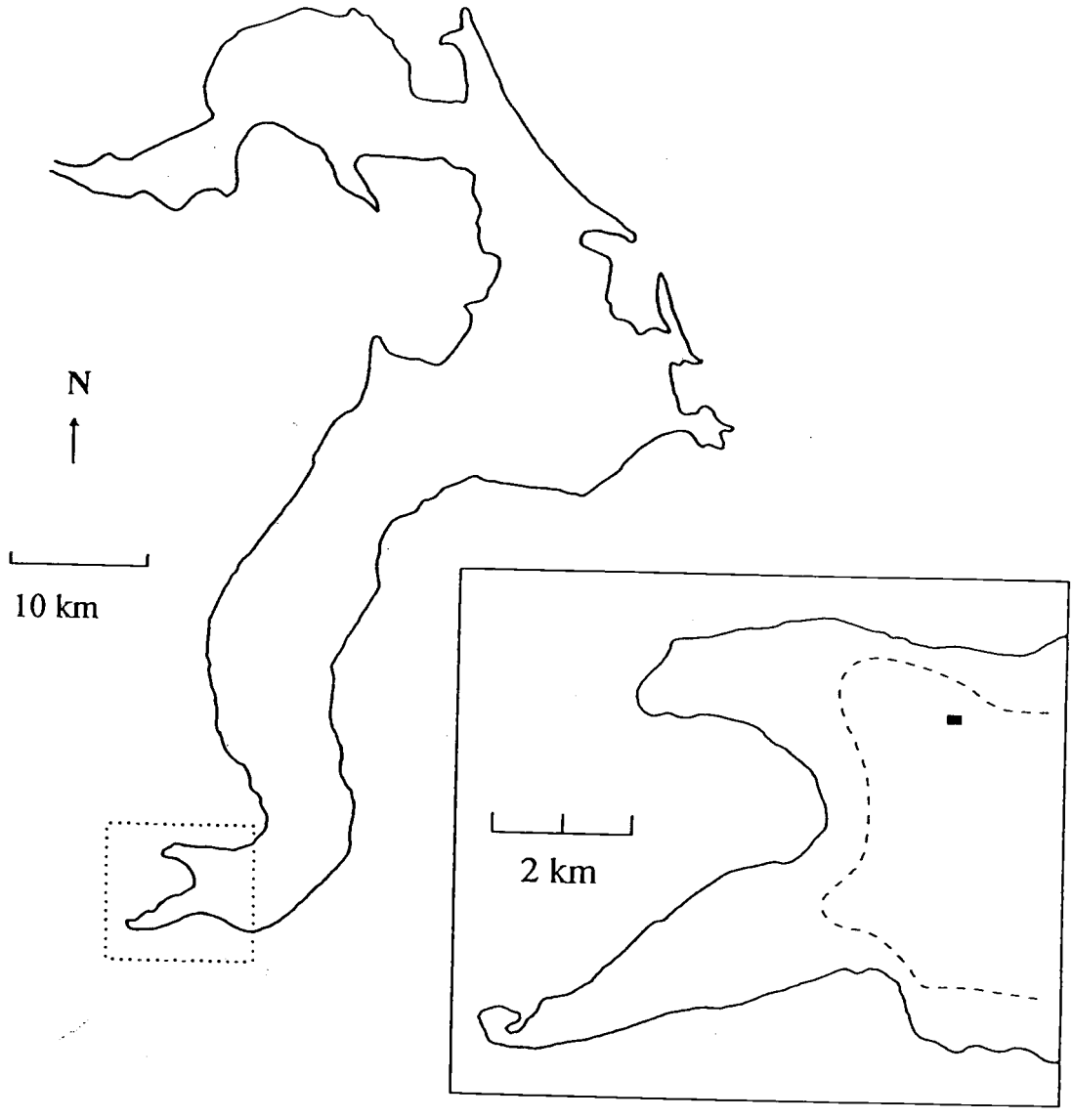

Figure 2.1. Map of Lake Pend Oreille, Idaho. The inset is of Scenic Bay, the dotted line represents the 100 m isobath, and the large dot is the location of the barge.

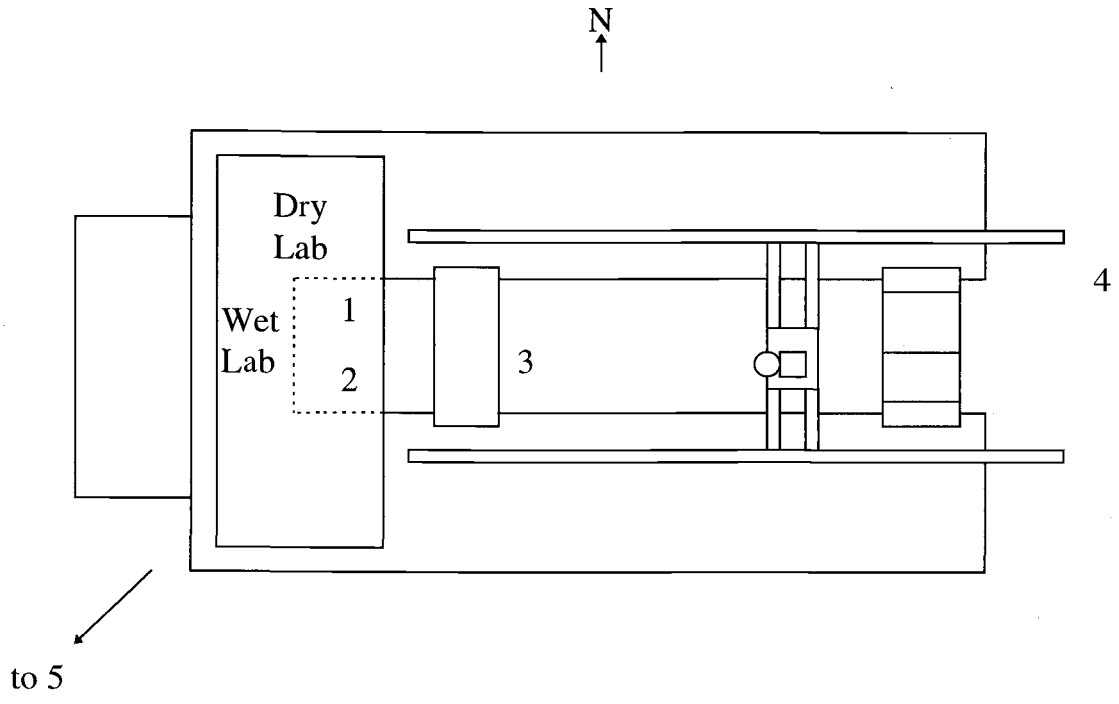

Figure 2.2. Layout of the barge including locations where the different instrumentation were used (1) is the reflecting tube absorption meters, (2) the CTD with water samples for the spectrophotometer and integrating cavity absorption meter, (3) the isotropic point source, (4) the compound radiometer, (5) the TOPS hauldown where vector and scalar irradiance measurements were made.

Water samples (taken with 8 l Niskin bottles attached to the CTD wire) and the reflecting tube absorption meter measurements were taken at the western end of the well (Figure 2.2). The IPS was deployed from a platform spanning the open well 10 m away from the CTD deployment location. The CR was operated at the eastern end of the barge. A hauldown mooring was used to deploy the TOPS irradiance sensors about 150 m SW of the barge, well away from possible light reflections and shadowing by the barge.

2.3.2 Ancillary Measurements

2.3.2.1 *Beam Attenuation at 660 nm and In Situ Chlorophyll a Fluorescence*

Beam attenuation at 660 nm (reported as the particulate portion of the beam attenuation coefficient [$c_p(660) = c(660) - c_{water}(660)$]) and chlorophyll-a fluorescence [reported as fluorometer voltage] were measured using Sea Tech, Inc. instruments located on the TOPS hauldown platform and on the CTD. A third fluorometer was attached to the instrument cage on which the reflecting tube absorption meters were mounted. These instrument packages were lowered and raised several times each day to obtain vertical profiles of optical properties, both within the well and outside of the influence of the barge. The time series of $c_p(660)$ and in situ chlorophyll a fluorescence provide estimates of the relative magnitudes of temporal variability in particulate concentrations and bio-optical properties within the water column at fixed horizontal positions in the lake.

2.3.2.2 *Chlorophyll a Concentrations*

Chlorophyll a concentrations were determined for water samples taken from Niskin bottle casts, typically twice daily at several discrete depths. The water samples were filtered through Whatman GF/F glass-fiber filters and pigments were extracted in 90% acetone. Chlorophyll a concentrations reported here were measured using the standard fluorometric method [*Strickland and Parsons*, 1972], although the pigment

concentrations in each sample were also measured using the HPLC method. Fluorometric chlorophyll a concentrations generally overestimated the HPLC concentration. The two measures are related by the regression equation Chl(fluorometric) = 0.025 + 1.115 Chl(HPLC) ($r^2 = 0.934$).

2.3.3 In Situ Absorption Measurements

2.3.3.1 *Reflecting Tube Absorption Meter (RTAM)*

The RTAM uses a collimated beam light source and encloses the sample in a reflective tube. The reflective tube collects the near forward scattered light so that the radiant flux lost due to absorption may be estimated [*Zaneveld et al.*, 1990]. These instruments actually measure the absorption coefficient plus a small portion of the scattering coefficient associated with the uncollected scattered light. The uncorrected absorption coefficient a_u is obtained using:

$$a_u = -\frac{1}{L}\ln\left(\frac{V_{samp}}{V_{pw}}\right), \tag{2.1}$$

where L is the pathlength of the instrument, V_{samp} is the signal voltage for the sample, and V_{pw} is the signal voltage for pure water. Note that this is essentially the same approach as is used in a spectrophotometer. Rather than using a reference cell, the meter is calibrated in the laboratory. Algorithms using simultaneous measurements of the beam attenuation coefficient are then applied to remove the portion of the

scattering coefficient included in the signal [*Zaneveld et al.*, 1992]. We used the "standard" correction scheme described by *Zaneveld et al.* [1992],

$$a_{total} = a_u + 0.13b + a_{water}, \tag{2.2}$$

where b is the total scattering coefficient. In order to determine the total absorption coefficient we used the pure water absorption coefficients of *Smith and Baker* [1981].

Three RTAMs were used to determine absorption coefficients at wavelengths of 456, 488 and 532 nm during the closure experiment. Each of these instruments, manufactured by Sea Tech, Inc., measures absorption over a 25 cm pathlength at a single wavelength. The RTAMs were sampled at a frequency of one Hertz and were lowered and raised at a rate to measure vertical absorption profiles with approximately 0.2 m resolution.

2.3.3.2 *Gershun's Equation*

Several of the in situ methods for determining the spectral absorption coefficient are based on the following relationship, due to *Gershun* [1939];

$$-\nabla \cdot E(r) = a(r)E_0(r), \tag{2.3}$$

where E is the vector irradiance and E_0 is the scalar irradiance. The steady-state plane parallel approximation to Eq. 2.3 can be written as:

$$a(\lambda,z) = K(\lambda,z)\overline{\mu}(\lambda,z), \tag{2.4}$$

where $K = -\frac{1}{E}\frac{dE}{dz}$ and $\bar{\mu} = \frac{E}{E_0}$. Vertical profiles of the vector and scalar irradiance are used to determine K and $\bar{\mu}$. Several methods have been used to measure E and E_0. Vertical profiles of the radiance distribution can be integrated to obtain vertical profiles of E and E_0 and hence K and $\bar{\mu}$ [e.g. *Tyler*, 1960, also in Lake Pend Oreille]. Vector and scalar irradiance fields can be determined more directly from direct measures of their upwelling and downwelling components using calibrated detectors equipped with cosine response and spherical irradiance collectors.. A third approach, proposed by *Gershun* [1939] and first implemented by *Højerslev* [1975], uses two detectors equipped with spherical irradiance collectors oriented in opposing directions, masked so that they each collect light over one hemisphere. When the detectors are aligned in the vertical direction, the upper collector measures a combined hemispherical irradiance given by

$$E_{ht} \propto 0.5(E_0 + E) \tag{2.5}$$

and the lower hemispherical collector measures a hemispherical irradiance of

$$E_{hl} \propto 0.5(E_0 - E). \tag{2.6}$$

Assuming only a relative calibration of the two detectors, values proportional to the vector and scalar irradiances can then be determined by solving equations (2.5) and (2.6). When the absorption coefficient is determined from these quantities using equation (2.3), the proportionality constants cancel (along with any absolute calibration error).

The next three sections describe in water measurement techniques that use some form of Gershun's equation.

2.3.3.3 *Tethered Optical Profiling System (TOPS)*

Vertical profiles of spectral vector and scalar irradiance and radiance, as well as c(660,z) and chlorophyll-a fluorescence F(z), were measured from a buoyant multiple radiometer package, called the Tethered Optical Profiling System (TOPS). The TOPS instrument suite was mounted on an inverted triangular frame (flat edge parallel to the water surface) with each side approximately 3 m long. A line attached to the frame was passed through a block mounted on a mooring anchor at approximately 200 m depth and up to a winch on the barge. This arrangement allowed downward profiles to be obtained by pulling the platform down in the water column. Upward profiles were obtained by floating the positively buoyant system to the surface of the lake. The frame was ballasted to provide proper orientation of the radiometers throughout the profile.

A MER1032 radiometer was attached to one end of the top bar to measure $E_d(\lambda,z)$, $E_u(\lambda,z)$, and $L_u(\lambda,z)$. At the other end of the bar, a MER2040 equipped with spherical collectors was mounted to measure the scalar irradiances $E_{od}(\lambda,z)$ and $E_{ou}(\lambda,z)$.

The MER1032 and MER2040 are commercially available, underwater profiling, multichannel filter radiometers manufactured by Biospherical Instruments, Inc.

Surface irradiance measurements were made high in the barge superstructure using a 5-channel radiometer.

The TOPS $E_d(\lambda,z)$, $E_u(\lambda,z)$, $L_u(\lambda,z)$, and $E_o(\lambda,z)$ profiles were analyzed to determine $K(\lambda,z)$ and the value of each parameter just below the water surface using the integral least-squares finite element method of *Mueller* [1991]. The data were then applied to equation (2.4) in order to obtain estimates of the absorption coefficient.

The estimation of scalar irradiance from the MER2040 with glass spherical diffusers was not straightforward. The optical configurations of the uplooking and downlooking collector assemblies differed from each other, and the collector surfaces were converted to hemispheres (using opaque plastic tape to mask the lower half of the globe) on May 5. Only the uplooking collector measurements were used for the present analysis.

The uplooking collector was configured by placing the glass diffuser globe directly over the MER2040's cosine collector. In this configuration, the unit has relatively uniform directional response to incident irradiance, except for the cone blocked by the instrument body itself (approximately a 1.83 sr solid angle centered on nadir). Assuming the radiance is constant over the blocked cone, we may use the upwelling radiance measured by the MER1032 to correct for the blocked portion of the light field

$$E_o(\lambda,z) = E_{od}(\lambda,z) + 1.8302\, L_u(\lambda,z). \tag{2.7}$$

When the uplooking collector was configured as a hemisphere, its response was that given by equation 2.5. Using $E(\lambda,z)$ measured with the MER1032, scalar irradiance may be computed as

$$E_o(\lambda,z) = 2E_{ht}(\lambda,z) - E(\lambda,z), \tag{2.8}$$

where $E_{ht}(\lambda,z)$ is the measured irradiance using the hemispherical configuration of the uplooking collector.

The MER1032, MER2040 and 5-channel surface irradiance radiometers were calibrated and characterized using the methods described in *Mueller and Austin* [1992]. The internal uncertainty in the radiometric irradiance/radiance responsivities of the MER1032 and 5-channel surface radiometers, based on pre-, intermediate, and post-experiment calibrations and internal consistency checks during individual calibrations, is <2% in all channels. Due to electronic noise in the MER2040, the internal calibration uncertainty for the channels of this instrument ranged from 5% to 7%. This electronic noise was subsequently traced to a floating ground in the electronic boards of this particular MER2040.

To characterize the directional response of the hemispherical E_{hd} collectors, the MER-2040 was illuminated by an FEL spectral irradiance standard at a distance of 150 cm. The instrument was rotated in 10 degree zenith increments from vertical to horizontal illumination. At each zenith angle, 6 readings were obtained by rotating the instrument through 60 degree increments in azimuth. Standard deviations in these samples were typically 7% of the mean response, which is attributed to the electrical noise discussed in the previous paragraph. The variations in the instrument's relative

response followed (1+cos(θ))/2 to within ± 5% (average of the 490 and 532 channels - there was insufficient flux at 456 nm for this laboratory test). The directional response of this collector was not determined for the E_{od} configuration, and we have assumed that uncertainty is similar to the for E_{hd}.

The MER2040 was post-calibrated with the spherical collectors filled with water filtered by a reverse osmosis system. In the field at Lake Pend Oreille, we attempted to fill the globes with reverse osmosis filtered water, but unfortunately, small amounts of lake water leaked into the globes during each of three TOPS system reconfigurations and redeployments on April 29, May 1, and 5 May 1992. Absorption by chlorophyll, other particulates, and dissolved organic material therefore reduced the radiometric responsivities of the MER2040 spherical and hemispherical irradiance channels by some amount during each deployment period. To estimate a minimum adjustment to the E_{0d} (and E_{hd}) channels, we assumed that the mean cosine just beneath the sea surface should be constrained to be less than or equal to the cosine of the refracted solar zenith angle. For each deployment period, we extracted smoothed surface values and computed the E_{0d} (or E_{hd}) adjustment factors at (456, 488, and 532 nm) required to satisfy this mean cosine constraint and averaged to obtain [1.29 (0.09), 1.21 (0.07), and 1.12 (0.07)] for 29 and 30 April E_{0d} measurements, [1.17 (0.08), 1.11 (0.07), and 1.05 (0.08)] for 1 through 5 May 1992 E_{0d} measurements, and [1.22 (0.08), 1.19 (0.09), and 1.14 (0.08)] for 5 through 7 May E_{hd} measurements. E_{0d} or E_{hd} were multiplied by these factors prior to using equations (2.7) or (2.8), respectively, to compute scalar irradiance E_0 at each wavelength. The standard deviations of each

scale factor (given in parentheses) are consistent with the approximately 7% internal uncertainty in the radiometric calibration of the MER2040 channels.

2.3.3.4 *Isotropic Point Source (IPS)*

The isotropic point source (IPS) technique for measuring the in situ absorption coefficient was first proposed by *Sorenson and Honey* [1968]. Basically, they argued that the attenuation of irradiance E from an isotropic source should decay with distance approximately as

$$E(r) \propto \frac{e^{-ar}}{r^2}, \tag{2.9}$$

where a is the absorption coefficient and r is the radial distance from the source. Thus by measuring the irradiance from the source as a function of r, the absorption coefficient could be determined. The error in this result is the approximation that the pathlength in the exponent is the geometrical radial distance r, when in fact scattering increases the mean path by δr so that the expression should properly be

$$E(r) \propto \frac{e^{-a(r+\delta r)}}{r^2}. \tag{2.10}$$

If $\delta r << r$, the error will be small.

The vector irradiance (more precisely the radial component of the vector irradiance) from an isotropic source was rigorously derived from the steady-state radiative transfer equation without internal sources by *Maffione et al.* [1993]. Their result is

$$E(r) = \frac{\Phi_0}{4\pi r^2} \exp\left(-a\int_0^r \frac{dr'}{\overline{\mu}}\right), \tag{2.11}$$

where Φ_0 is the radiant flux emitted by the source, and $\overline{\mu}$ is the average cosine of the light field from the source. The only assumption implicit in equation (2.11) is that the water column within which E(r) is measured is homogeneous. Equation (2.11) can be solved for the absorption coefficient giving

$$a = \overline{\mu}\left(-\frac{1}{E}\frac{dE}{dr} - \frac{2}{r}\right) \tag{2.12}$$

$$= \overline{\mu}\left(K_E - \frac{2}{r}\right),$$

where K_E is the diffuse attenuation coefficient for irradiance.

The similarity of equation (2.12) with the plane-parallel approximation of Gershun's equation, $a = \overline{\mu}K_E$, is no coincidence. In fact, Gershun's equation is a special case of the more general result, equation (2.12). In other words, Gershun's equation can be obtained from equation (2.12) in the far field, where $r \to \infty$ and the light field from an isotropic source (e.g. the sun) becomes plane parallel. Thus methods which use Gershun's equation to determine the absorption coefficient and the IPS method are similar. Both measure a large volume, "integrated" value of a. But the IPS method allows the source to be controlled and measurements can be made in both the near and far field. Furthermore, to a good approximation, measurements of $\overline{\mu}$ in the near field are not needed because $\overline{\mu}$ will be approximately equal to one [*Maffione and*

Jaffe, 1995]. Thus a can be estimated from measurements of the vector irradiance E alone [*Maffione et al.*, 1991, 1993].

Details of the current implementation of the IPS method can be found in *Maffione et al.* [1991, 1993]. To avoid errors due to ambient background light, IPS measurements were made either at night or deep in the water column. To determine the absorption coefficient, irradiance is measured at several distances from an isotropic source. A regression fit to the equation

$$\ln\left[r^2 E(r)\right] = k - ar, \tag{2.13}$$

which is derived from the approximate result given by equation (2.9) yields the absorption coefficient a as the slope of the regression. An example of the regressions from the data taken at Lake Pend Oreille, is shown in Figure 2.3. Because the IPS method is a variable pathlength technique (as are all of the large volume methods), the relative error in the estimate of the absorption coefficient can be accurately calculated. This error is shown in the legend of Figure 2.3 and represents the standard error of the estimate of the slope.

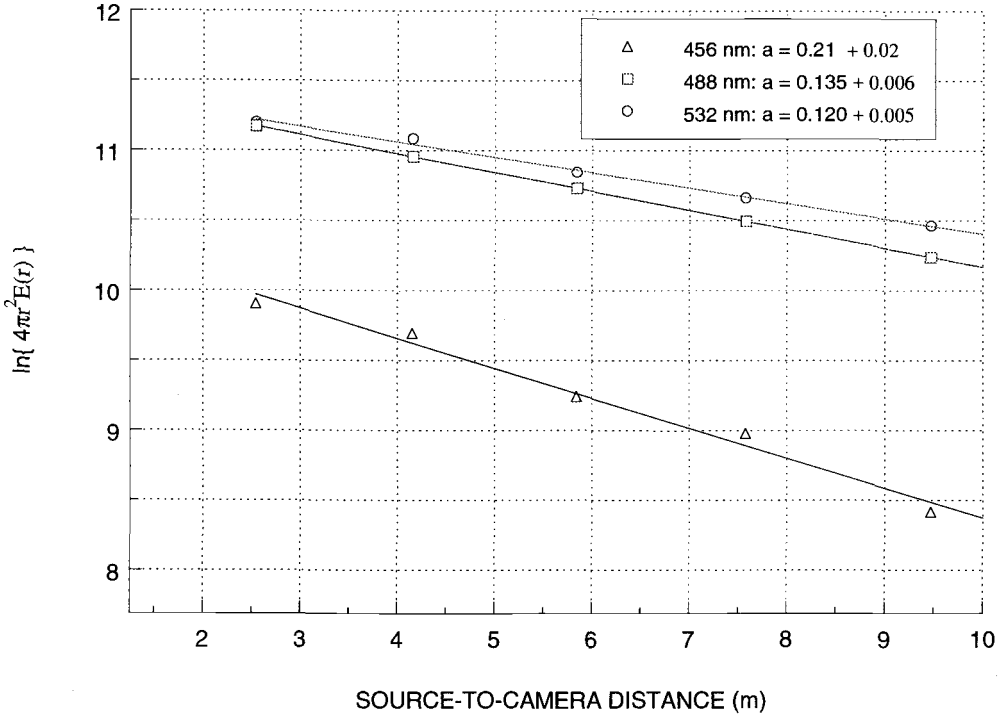

Figure 2.3. Regression fit to attenuation of irradiance from the isotropic source. Slope of the line fit gives the absorption coefficient. Data from May 6; depth range 40 - 50 m.

2.3.3.5 *Compound Radiometer (CR)*

The CR estimates the absorption coefficient by measuring the moments of a Legendre polynomial expansion of a radiance distribution. The absorption coefficient is determined by applying the measured moments to a form of Gershun's equation [*Zaneveld and Pak,* 1972; *Wells,* 1983]. This device uses a series of reflectors to measure the integral moments of the radiance distribution at a number of zenith angles

[*Doss and Wells,* 1992]. The radiance distribution is then deduced from a linear combination of the measured moments. The moments are symmetrical about the vertical axis and optimized to facilitate computation of inherent optical properties in the form of the A_n series as functions of depth, i.e. $A_n(z)$ [*Doss and Wells,* 1992]. The zero-th order moment (A_0) is the absorption coefficient, A_∞ is the beam attenuation coefficient, and the intermediate A_n describe moments of the volume scattering function.

The CR used during this experiment was built and operated by Tetra Tech., Inc. The instrument used at Lake Pend Oreille made measurements on the natural light field, but this instrument can also be used with an artificial light source [*Doss and Wells,* 1992].

2.3.4 Laboratory Methods

2.3.4.1 *Integrating Cavity Absorption Meter (ICAM)*

The integrating cavity spectral absorption meter is a benchtop instrument for the determination of $a(\lambda)$. Samples of 670 ml each are introduced into a quartz cell within the integrating cavity for measurement. The samples were obtained using the Niskin bottles closed at several depths during each CTD cast in the well.

The theoretical basis of the instrument was developed from an idea put forth by Elterman [1970] who built an instrument to measure the absorption of samples of quartz. The theory and a description of the instrumentation is given in Fry et al.

[1992]. The integrating cavity used at Lake Pend Oreille was of the Texas A&M University design [*Fry et al.,* 1992].

Fry et al. [1992] developed a different analysis and calibration scheme than was used for this data set. The calibration scheme and analysis method used for this data set was developed at NRL [Kennedy, 1992]. The algorithm developed by NRL calculates an 'effective path length' for the cavity. The effective path length is critically dependent on the geometry of the cavity, the refractive index of the sample, and the field of view of the detector [*Kennedy,* 1992]. The measurement is better thought of as a measurement of the change in energy density within the cavity due to the presence of a sample of known volume. Four central assumptions of this measurement are;

1) The light field within the cavity is isotropic. Although this cannot be true it is sufficient that any anisotropy be small, localized, and the same when the cavity is empty.

2) The light field within the sample is isotropic. This assumption breaks down for large absorption values and establishes an upper limit on the cavity's performance. This assumption is valid for all samples taken at Lake Pend Oreille.

3) The change in energy density is due solely to the absorptance of the sample.

4) The absorptance of the empty cavity is zero. However, humid air present during the measurement of the "empty" cavity may cause an offset..

When an empty cavity reading is used as the zero absorptance value, the absorption coefficient can be determined from:

$$a = \frac{1}{effective\ path\ length\ (m)} \ln\left(\frac{empty}{sample}\right). \qquad (2.14)$$

When used in this way, the integrating cavity absorption meter does not require standardization either by measuring known calibration samples with a spectrophotometer, or by measuring absorption of 'clean' water to determine the total absorption coefficient of the sample. Due to the long integration times required, the ICAM was not operated in the full spectral mode but at the nine wavelengths given in Table 2.1.

2.3.4.2 *Spectrophotometer*

Water samples from the Niskin bottles were analyzed using a spectrophotometer. The spectrophotometer was used to separately measure the particulate and the gelbstoff absorption coefficients. The total absorption coefficient was determined by summing the component contributions with the absorption coefficient of pure water.

The low concentration and absorption signal of suspended particles in the water column requires that the particles be concentrated before their absorption spectrum can be measured in a spectrophotometer [*Yentsch,* 1962]. Water samples (500 to 1130 ml) were filtered through Whatman GF/F (effective pore size 0.7 μm) glass-fiber filters. Optical density spectra (400 to 750 nm) of concentrated particles on the glass-fiber filter ($OD_{filt}(\lambda)$) were measured in a Kontron Uvikon 860 dual beam scanning spectrophotometer at 4 nm spectral bandwidth using a wet GF/F filter as a blank.

Optical density at 750 nm was subtracted from optical density at all other wavelengths. Corrections for pathlength amplification on the glass-fiber filter and calculations of optical densities for suspensions ($OD_{susp}(\lambda)$) were carried out as described in *Cleveland and Weidemann* [1993], using the empirical equation

$$OD_{susp}(\lambda) = 0.378\ OD_{filt}(\lambda) + 0.523\ OD_{filt}(\lambda)^2. \quad (2.15)$$

Absorption (in m^{-1}) was calculated from optical density as:

$$a_{part}(\lambda) = \frac{A}{V} 2.303 OD_{susp}(\lambda), \quad (2.16)$$

where V is the volume filtered (in m^3) and A is the clearance area of the filter (in m^2).

Dissolved substances (gelbstoff) are typically defined as those materials passing through a 0.45 μm filter. However, since particles are defined as the materials collected by a 0.7 μm filter (described above), this definition of dissolved substances ignores material between 0.45 and 0.7 μm in size. In order to include all size classes, gelbstoff is defined here as the material passing through a GF/F filter. *Bricaud et al.* [1981] showed that nonlinearity in logarithmic absorption spectra indicates scattering by particles in the dissolved sample; no nonlinearity is seen in these logarithmic absorption spectra. *Bricaud et al.* [1981] used GF/C glass fiber filters, which have an effective pore size of 1.5 μm. This larger pore size may account for the differences in scattering contamination of dissolved samples.

Filtrate from the concentration of particles on GF/F filters was collected for analysis of absorption by dissolved substances. Optical density spectra (300 to 800 nm) for gelbstoff were measured in 10 cm quartz cuvettes in the Kontron

spectrophotometer at 4 nm spectral resolution using a blank consisting of water purified by reverse osmosis. Absorption ($a_{gelb}(\lambda)$) was calculated as:

$$a_{gelb}(\lambda) = 2.303\ OD(\lambda)/l\ , \tag{2.17}$$

where l is the pathlength (in m).

No baseline adjustments or zero-corrections were made to the spectra. The exponential slope for each spectrum was calculated from absorption between 300 and 450 nm. The mean of these slopes was -0.017 (n = 26, standard deviation = 0.0013, coefficient of variation 7.6%). Exponential slopes of this magnitude are common in fresh water and coastal waters. Spectral absorption values for all samples were calculated from this slope and the measured absorption at 300 nm:

$$a_{gelb}(\lambda) = a_{gelb}(300)\ \exp(-0.017(\lambda-300)). \tag{2.18}$$

The total absorption coefficient was calculated at the 3 wavelengths of interest as:

$$a_t(\lambda) = a_{part}(\lambda) + a_{gelb}(\lambda) + a_w(\lambda), \tag{2.19}$$

where values of $a_w(\lambda)$ were obtained by interpolation of the results of *Smith and Baker* [1981] to the wavelengths of interest here.

2.3.5 Instrumental Errors

2.3.5.1 *RTAM error analysis*

The inherent error in the RTAM approach is due to the undetected scattered light. Various approaches can be used to estimate this undetected light [*Zaneveld,*

1994]. If simultaneous measurements of the spectral absorption and beam attenuation coefficient are made it can be shown that the error is less than 1% of b [*Zaneveld,* 1994]. The spectral information needed to use these algorithms was not available at Lake Pend Oreille, so that the simpler and less accurate correction scheme of equation (2.2) was used. Use of this procedure provides a possible error of ± 5% of the scattering coefficient. The precision of the instruments was approximately 0.003 m^{-1}, so that the details in the vertical structure are well described using this method.

Two problems were encountered in the calibration of this particular set of reflecting tube absorption meters at Lake Pend Oreille. The first is that they displayed some instrumental drift that could not be entirely removed using pure water calibrations. The second problem was cavitation in the flow tubes of the instruments. While both problems degraded the accuracy of the measurements made at Lake Pend Oreille they were problems with the particular set of instruments and not the method as such. By looking at the deep water (z = 80 m) and correcting for long term trends using the fluorometer data it was concluded that the drift yielded an error with a standard deviation of 0.018 m^{-1}. Another source of bias, common to all systems that use a pure water reference, is the possibility of contaminated "pure" water used in the calibration and is impossible to estimate.

2.3.5.2 *TOPS Error Analysis*

Gershun's equation (2.4) is used with TOPS irradiance profiles to calculate absorption coefficients with an estimated uncertainty of approximately 10%. The dominant uncertainty in TOPS irradiance measurements is an approximately 8% uncertainty in downwelling irradiances measured with the MER2040, either E_{od} with the spherical collector, or E_{ht} with the hemispherical collector. This uncertainty includes up to 7% instrument noise observed during the instrument's characterization and calibration, which contributes significantly to the approximately 8% scatter in the "maximum surface mean cosine" adjustments we determined to account for the unknown amounts of lake water which leaked into the collector globe on each of three occasions when the instrument was reconfigured on the mooring. For determining the lake water corrections, TOPS surface irradiances were limited to cases when the solar zenith angle in air ranged between 30 and 50 degrees. Therefore, neglect of skylight in our estimates of the maximum surface mean cosine contributed < 2% scatter, and no significant bias [*Morel,* 1991, his Fig. 3], to the mean correction coefficients calculated for the MER2040 channels.

Uncertainty in the MER1032 E_d and E_u calibrations, and therefore in E, is < 2%. Because a single working standard source of spectral irradiance was used to calibrate all irradiance channels on both radiometers, any systematic errors in absolute spectral irradiance responsivity cancel when absorption is computed with Gershun's equation (2.4) (K is independent of an instrument's absolute radiometric responsivity).

The 5% uncertainty in directional response of the E_{hd} collector on the MER2040 (and by assumption of the E_o collector also) is less than the 7% electrical noise of the instrument (as observed during responsivity calibration). We conclude that, for this particular instrument, errors in E_{hd} due to this effect are indistinguishable from responsivity noise using normal laboratory sources.

With the E_{od} configuration, the excluded integrated solid angle would include 20% to 50% of upward scalar irradiance E_{ou}, which is < 3% of scalar irradiance [*Voss*, 1989]. We have partially corrected for this discrepancy using radiance measured over a 25 degree zenith cone with the MER-1032, and assuming uniform radiance over a 40 degree cone. Even assuming this estimate is in error by as much as 30%, this uncertainty contributes < 1% uncertainty to scalar irradiance estimated from the MER-2040 E_{od} measurements.

Deck cell records show no significant variability due to cloud shadows, and surface wave induced variations were confined to the top 2 m of the water column. Therefore, the integral smoothing and K profile analysis [*Mueller,* 1991] should contribute < 1% uncertainty in irradiance profiles or K for features in vertical profiles with scales of 4 to 5 m or greater.

2.3.5.3 *IPS Error Analysis*

Errors in the IPS method arise from several sources and all of these errors, except for the assumption of water homogeneity, are due to the particular instrumental

implementation and optical conditions in the lake during the experiment. The largest sources of error were, (1) the assumption of constant radiant output of the isotropic source during each light flash since a reference detector was not used; (2) variable alignment of the source and detectors due to the variability in water movement; and (3) the assumption that $\overline{\mu} = 1$ since only vector irradiance, and not also scalar irradiance, was measured. Errors from (1) and (2) should be random and therefore quantified in the standard error of the regression fit. Errors from (2) can also be systematic if instrument misalignment remains constant during a measurement. The error from the assumption that $\overline{\mu} = 1$ is, however, systematic and more difficult to quantify. One thing that can be determined for certain about this systematic error is that it will always lead to an overestimate of a. To see this, consider equation (2.12) in the form

$$\hat{a} \equiv \frac{a}{\overline{\mu}} = \left(K_E - \frac{2}{r} \right) \tag{2.20}$$

where $\hat{a}$ is the estimated value of a from the regression fit. The right hand side of this equation is determined from the vector irradiance measurements alone and used to determine $\hat{a}$, the estimate of a. Since $\overline{\mu} \leq 1$, it is clear that $\hat{a} \geq a$. A Monte Carlo study by *Maffione and Jaffe* [1995] shows that under a wide range of oceanic conditions, $\overline{\mu}$ is nearly always greater than 0.9 up to 10 attenuation lengths from the source. Thus the largest systematic error to be expected in this approximation is about 10%.

Due to the stratified water above 30 m, absorption values from the IPS method in this region were highly variable and often lower than the other methods. Below this depth, the IPS system operated well except for occasional misalignments between the

source and detectors caused by the variable water currents. The error bars on the IPS values in Figures 2.7-2.9 represent plus or minus one standard deviation in the estimate of the slope from the regression fit described in the Methods section. This is a relative error which accounts for random measurement errors but does not take into account systematic error such as a constant misalignment during a measurement run. Nonetheless, some interesting comparisons can be made with the other methods and the error bars provide an objective indication of the lowest standard deviation in the measurements.

2.3.5.4 *CR Error Analysis*

The CR errors depend in a complicated way on the intercalibration of the instrument's 10 optical and detector elements, and on the positions of nulls in the spherical harmonics on which the underlying theory is based [*Miles and Wells*, 1993]. In view of this, the best estimates of errors are indirect. The CR measures not only absorption but also 8 integral moments of the scattering function, A_0 through A_8, as defined by *Wells* [1983] and repeated by *Doss and Wells* [1992]. The A_n series is known from fundamental principles to be a smooth function of n, and so the deviation of calculated $a = A_0$ from a smooth fit provides the best estimate of error, as shown by *Miles and Wells* [1993; their Fig. 1]. Their results predict an uncertainty of ≈ 0.01 m^{-1} in the depth range of 12 to 18 meters. This is the range in which the radiometer works best. Performance deteriorates in deep water due to lack of light, and also in very

shallow water. The reason for increased CR error in shallow water is probably failure, due to the nearby shadow of the barge, of an underlying assumption of plane-wave illumination.

2.3.5.5 *ICAM Error Analysis*

This method does not require standardization with a spectrophotometer or the need of 'clean' water to return the total absorption coefficient of the sample. Equation (2.14) does not include a small term for the absorption which occurs directly in front of the detector. This term can be shown to be about 1% of the a(532) value calculated from equation (2.14). Due to the geometry of the cavity used at Lake Pend Oreille, this term could not be accurately determined and was therefore not included [*Kennedy*, 1992]. The values reported should be viewed as probably low, by about 1%, due to this error. An additional error arises from the assumption that absorption in an air filled cavity is zero. The assumption of an isotropic field within the cavity sets the upper limit on the absorption coefficient which can be determined. A simple linear analysis, based on the product of the absorption coefficient and the path through the sample, shows that when this product is greater than 0.05 the field at that point will be decreased by about 2%. When the product is 0.01 the field is decreased by less than 0.01% [*Kennedy*, 1992]. The distance from the center of the sample to the outer edge is nominally 0.05 meters. If an anisotropy of less than 2% is acceptable, then absorption coefficients of 1.0 m^{-1} or less can be achieved. An improved geometry for

the cavity and sample could reduce all of the errors discussed here. Additional error sources, albeit in an earlier configuration of this instrument, are described by *Cleveland and Weidemann* [1993].

2.3.5.6 *Spectrophotometer Error Analysis*

Errors in total absorption coefficients estimated from spectrophotometric measurements arise from several sources. The first is the unknown error in values of water spectral absorption obtained from *Smith and Baker* [1981]. Additional errors are associated with separate spectrophotometric determinations of absorption due to suspended particles and that due to dissolved organic material (gelbstoff).

Calculation of particulate absorption from optical density relies on an empirical algorithm for pathlength amplification; relative uncertainty associated with this source is approximately 2% for the particular algorithm and spectrophotometer used here [*Cleveland and Weidemann*, 1993]. Potential uncertainty resulting from variability in filtration and inhomogeneous distributions of particles on the filters can be assessed by filtering and measuring replicate samples from each water bottle, but time did not permit adequate sample replication to determine such an estimate during the Lake Pend Oreille optical closure experiment. From other oceanic experiments where replicate filter samples were measured [*Cleveland*, unpublished data], replicability of particulate field samples is approximately 6%. Together, these two sources contribute

approximately 6.5% uncertainty (in a mean square sense) to spectrophotometric particle absorption coefficients.

Unfortunately, it is not possible to concentrate gelbstoff, which contributes a low net absorptance at visible wavelengths over the path defined by a 10 cm cuvette. Therefore, the resolution limits of the particular instrument used become an important source of uncertainty in spectrophotometric estimates of gelbstoff absorption. The resolution of the Kontron Uvikon 860 spectrophotometer is approximately 0.001 optical density units. For the 10 cm cuvette used here, this instrument resolution yields a resolution of 0.02 m^{-1} in absorption units. The overall mean gelbstoff absorption coefficient at 456 nm is 0.132 m^{-1} for this data set. Therefore, the 0.02 m^{-1} resolution limit represents 15% of the mean gelbstoff absorption. Sample replicability in gelbstoff absorption, measured during a different experiment [*Cleveland*, unpublished data], was approximately 5%. Combining these two error sources would give a mean square relative uncertainty of approximately 16% in the spectrophotometric gelbstoff absorption coefficients at 456 nm presented here; relative measurement errors in the gelbstoff component of absorption would be progressively larger at 488 and 532 nm, due to the exponential decrease in gelbstoff absorption with wavelength.

2.4 RESULTS

2.4.1 Meteorological and Limnological Setting

Unusually warm conditions prevailed during the spring of 1992, so that by 21 April, when we began our measurements, the lake surface temperature was slightly greater than 6 deg. C, and thermal stratification extended to approximately 50 m. Strong winds on 29 and 30 April 1992 produced strong easterly currents (as indicated by surface drift and instrument wire angles) and upwelling in the vicinity of the barge and throughout Scenic Bay (Figure 2.1). In this paper, we present optical measurements over the period of 30 April through 7 May. The period of strong wind forcing ended 30 April, and associated upwelling reduced the near-surface thermal stratification by the morning of 1 May. The surface temperature was reduced from 7.5° C on 30 April to 5.5° C on 1 May, and the base of the overall thermocline was depressed to depths between 80 and 100 m. The near surface mixed layer began to reform on 1 May, and the warming trend continued unabated until 7 May when the surface temperature was 10.5° C. Throughout this period, a diurnal thermocline was usually present between 10 and 30 m throughout much of the day. The base of the upper portion of the thermocline defining the daily mixed layer was found at the 5° C isotherm, which deepened from approximately 10 m on 1 May to 50 m by 7 May. These characteristics were common to the temperature profiles measured with a CTD in the well and with the temperature probe on the TOPS package.

Fluorometers and 660 nm transmissometers were attached to both the CTD and TOPS platforms. The daily averaged profiles of $c_p(660)$ from the two platforms are significantly different only in the upper 5 m of the lake. Comparisons among measurements carried out within the well of the barge and measurements made outside of the barge should then be possible with the exception of the very near surface waters. Since the CTD operated to greater depths than the TOPS profiler and the differences in the ancillary measurements are confined to the near surface waters we will present $c_p(660)$ and fluorometer voltage results only from the instruments mounted on the CTD.

The day-to-day changes in the mean $c_p(660)$ profiles are illustrated in Figure 2.4a and the within-day variability is shown in Figure 2.4b. The transmissometer record indicated that there was a significant amount of natural variability on all time scales. The clearest water measured was on May 1. By May 4 a particle maximum had formed in the upper 20 m. This particle maximum became larger and more sharply peaked over the last three days of the experiment. Changes in its depth and magnitude appear in the $c_p(660)$ coefficient of deviation (standard deviation divided by the mean) profile as a local maximum between 10 and 15m (Fig. 2.4b). The increase in the coefficient of deviation on May 5 and 7 at depths greater than 70 m is caused by the standard deviation remaining constant while the mean value decreased to very small values. Otherwise, the $c_p(660)$ coefficient of deviation remained under 8% for waters greater than 30 m in depth and often it was less than 5%.

To estimate the magnitude of short term variability in particle concentration, we examined the brief time series made at depths where Niskin bottles were attached and removed from the wire during the CTD casts; the longest of these time series, obtained at 65 m on April 30, is illustrated in Figure 2.5. The maximum amplitude of variability in this 7.5 minute time series is one third of the overall variability measured at 65 m throughout the day on 30 April; the coefficient of variation for this short time series is approximately 1.5%, compared to a 4% (approximately) daily coefficient of variation (Figure 2.4b).

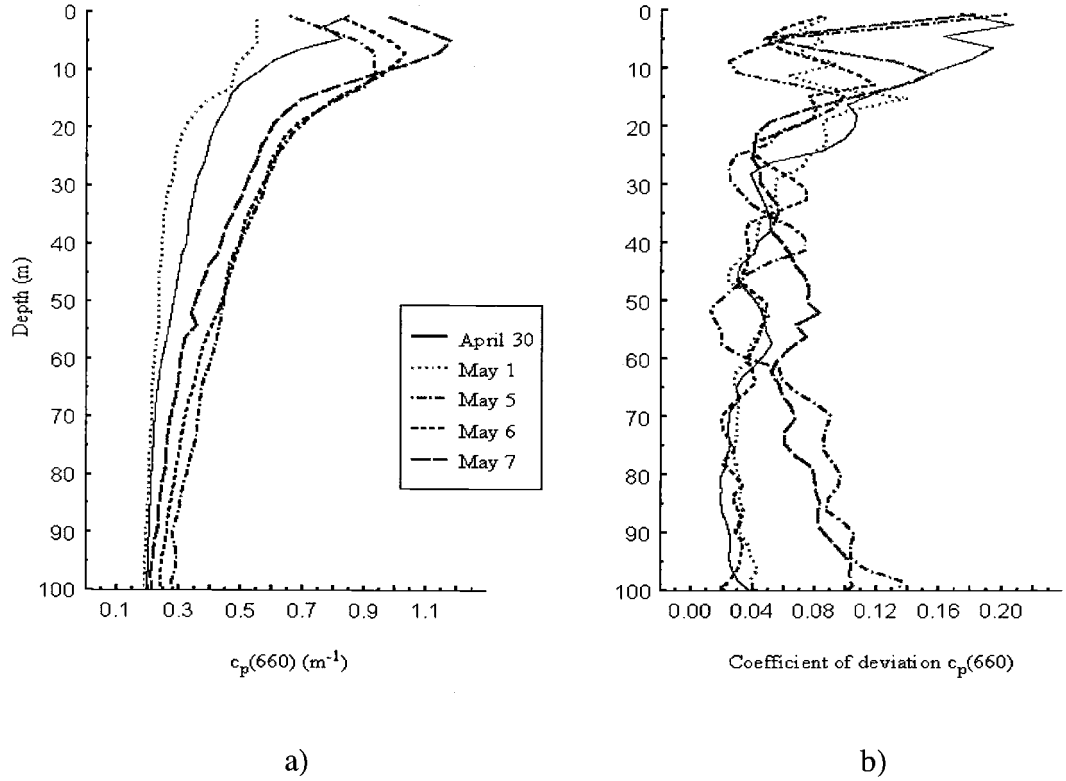

Figure 2.4. a) The daily averaged $c_p(660)$ values for the time period covered in this paper. b) The coefficient of deviation (standard deviation divided by the mean) of the $c_p(660)$ measurements shown in 2.4a.

Profiles of the daily averaged fluorescence voltage (Figure 2.6a) show similar shapes and trends as those seen in the $c_p(660)$ profiles (Figure 2.4a). The coefficients of deviation of the fluorometer voltage profiles (Figure 2.6b) are larger than those associated with the $c_p(660)$ profiles (Figure 2.4b).

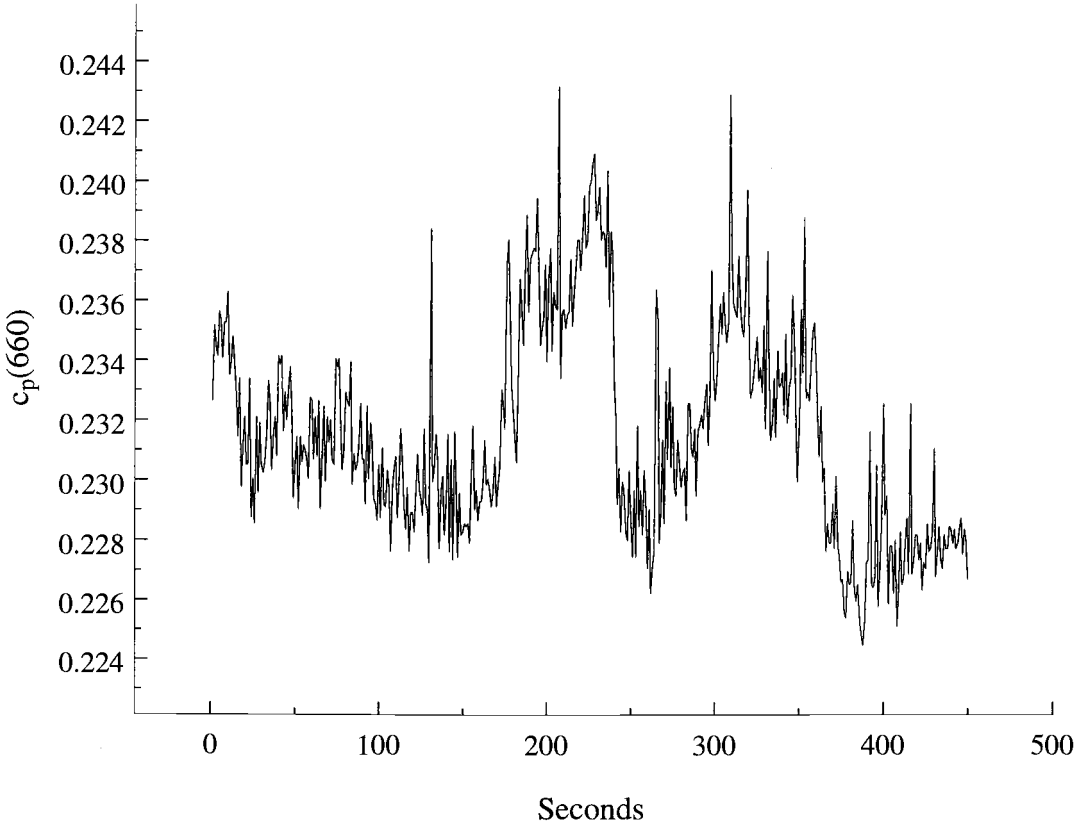

Figure 2.5. A 7.5 minute time series of $c_p(660)$ for indication of short time scale particulate variability.

Vertical profiles of $c_p(660)$, in situ fluorometer voltage, and chlorophyll-a concentration, obtained from analysis of discrete samples, are used as indicators of the natural variability in particle-related bio-optical properties. Analysis of long term

trends in the above parameters indicate that an obvious sub-diurnal trend in particle properties occurred on only one day of the experiment, 30 April, when strong winds drove surface waters offshore and produced upwelling throughout much of Scenic Bay. On other days variability was more random in nature. In the surface waters on April 30, the chlorophyll-a concentration was 7.58 mg/m^3 at 11 AM (PDT) (2 m depth), 5.20 mg/m^3 (5 m) at 4 PM, and 3.25 mg/m^3 (5 m) at 7 PM. This trend of decreasing particle concentration is also seen in the transmissometer and fluorometer records, where there was evidence of a decrease down to depths of 30 m.

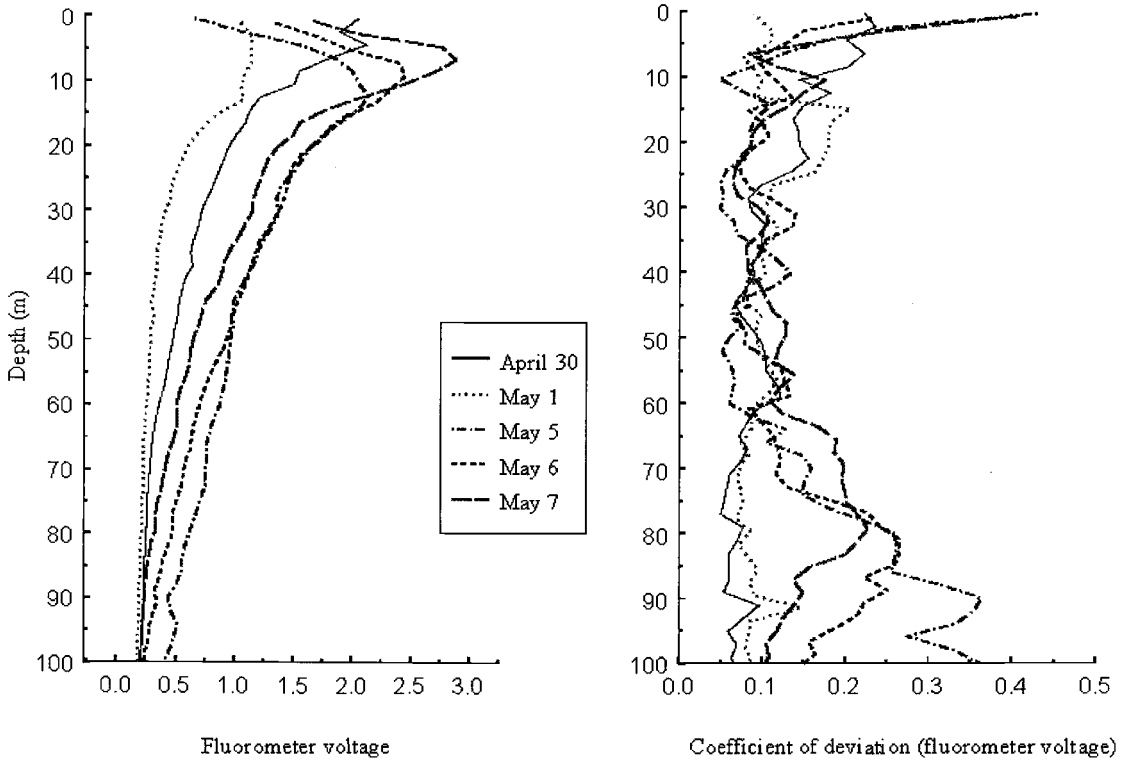

Figure 2.6. a) The daily averaged fluorometer voltage for the days covered. b) The coefficient of deviation for the daily averaged fluorometer voltage.

2.4.2 Vertical Profiles of Absorption

Vertical profiles of absorption determined by all instruments are illustrated in Figures 2.7, 2.8 and 2.9 for wavelengths of 456, 488 and 532 nm, respectively. Panels a through e in each represent profiles for 30 April, 1,5,6 and 7 May, respectively. The temporal trends in the optical properties observed on April 30 make the time sequence of the different absorption measurements on that date (Table 2.2) an important consideration in their interpretation (Figures 2.7a, 2.8a and 2.9a). On the other dates considered here, bio-optical variability was more random and showed no obvious temporal tendencies throughout the day, so that the methods can be compared using the daily mean profiles. Of course, observed spatial and temporal bio-optical variability will contribute significantly to differences in the separately determined means at any given depth. Except for 30 April (Figures 2.7a, 2.8a and 2.9a), therefore, TOPS and RTAM profiles are shown only as the daily average. Measurements by the IPS (with estimated error bars), spectrophotometer, ICAM, and CR are shown as individual values at discrete depths throughout the day. Refer to Table 2.1 for a summary of which instrument and wavelength combinations were used on each day.

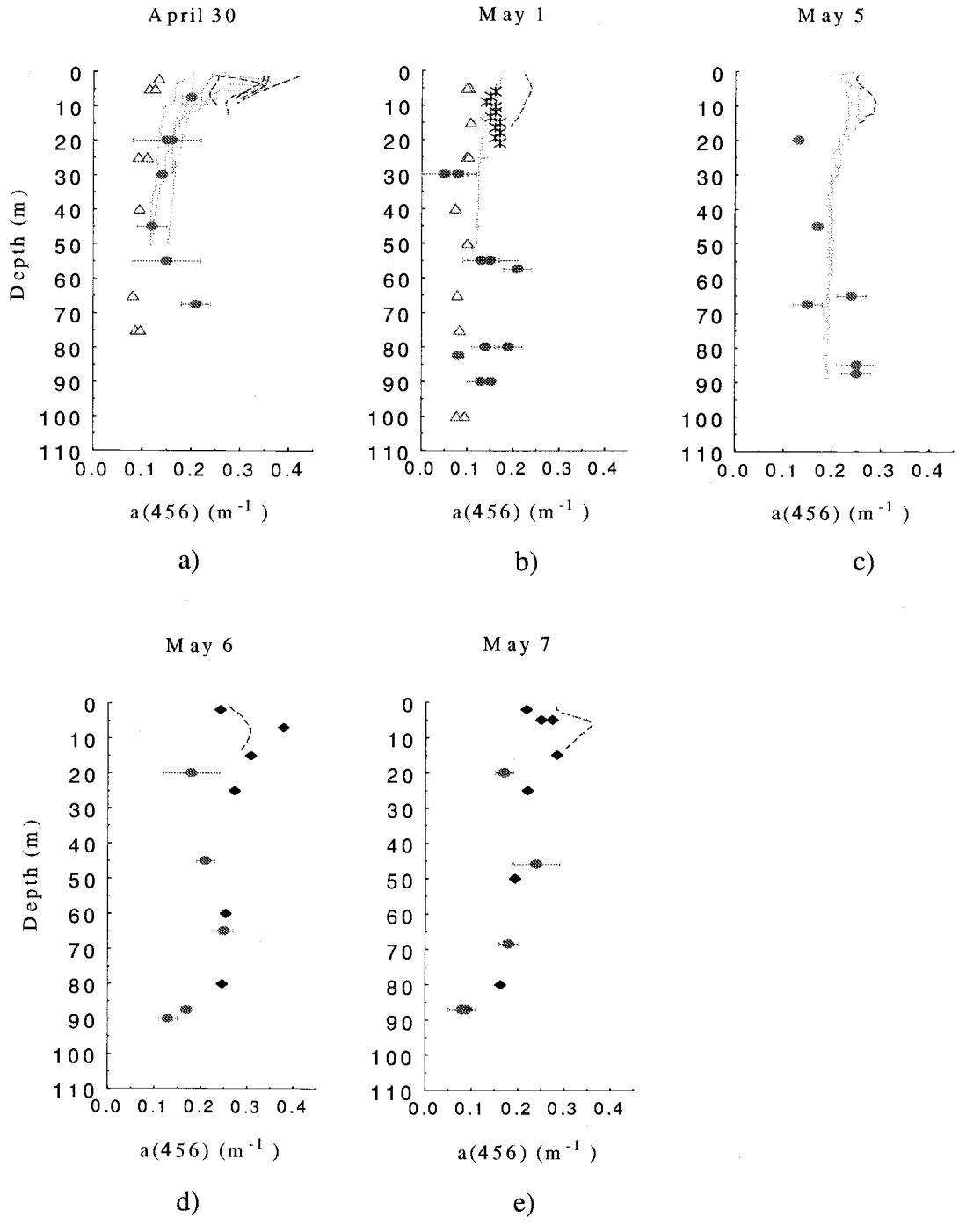

Figure 2.7. a) Measurements of a(456) made on April 30 by the RTAM (—), TOPS (- -), IPS (● with 1 sd error bars), spectrophotometer (◆), ICAM (Δ). b) The same as 7a except the date is May 1. The (⋈) are the compound radiometer. c) The same as 7a except the date is May 5. d) The same as 7a except the date is May 6. e) The same as 7a except the date is May 7.

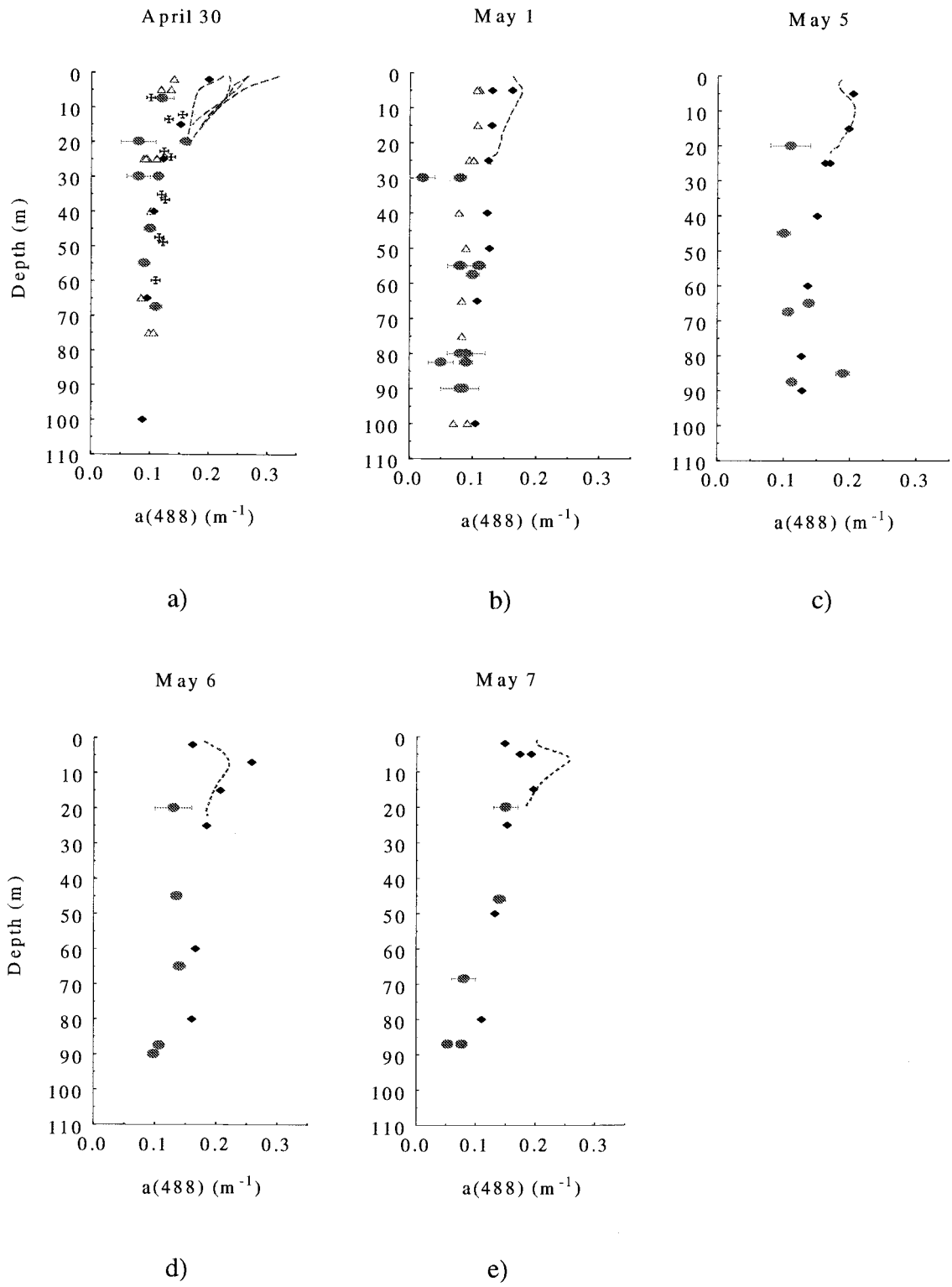

Figure 2.8. a-e) The same as Figure 2.7a-e for a(488). The Maltese cross symbols on 30 April are the data from Tyler (1960).

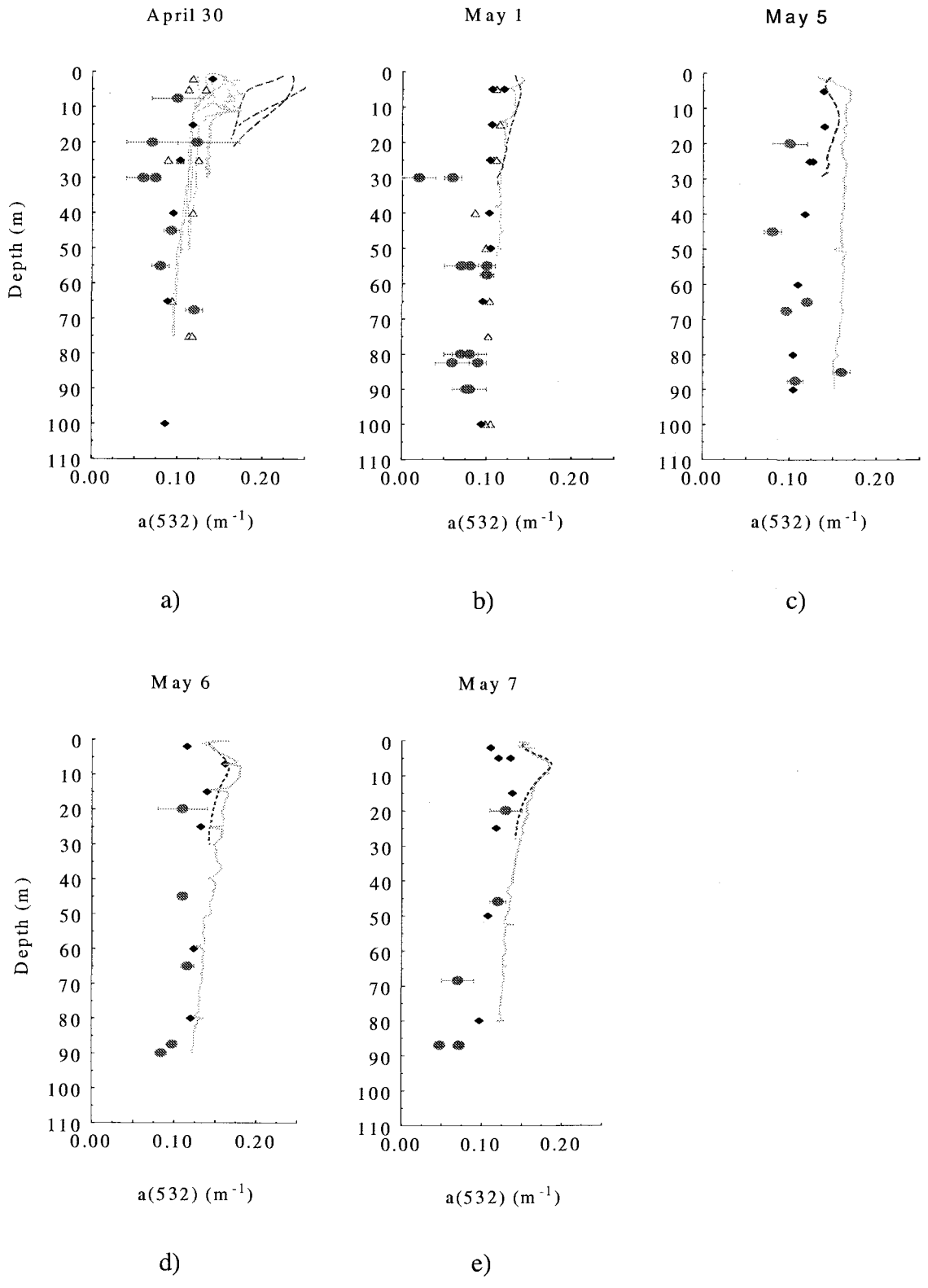

Figure 2.9. The same as Figure 2.7 for a(532).

Table 2.2. Sequence of absorption measurements taken on 30 April, 1992.

Time	Measurement
1100	water samples at 2, 15, 25, 40, 65, and 100 m for the spectrophotometer, ICAM used water from 2, 40, and 65 m, TOPS casts made
1130	TOPS cast
1200	IPS at 15-25, 25-35, 40-50, and 60-75 m
1220	water sample at 25 m for ICAM
1550	RTAM to 30 m
1610	water samples at 5, 25, 75 m for ICAM
1650	RTAM to 75 m
1900	IPS at 5-10, 15-25, 25-35, and 50-60 m, water samples at 5, 25, and 75m for ICAM
2130	RTAM to 50 m

The only historical data with which we may compare our absorption coefficients from Lake Pend Oreille are those determined using *Tyler*'s [1960] radiance distribution measurements which were made 34 years previous to the present Lake Pend Oreille experiment. The measured radiance distribution were integrated to obtain the vector and scalar irradiance profiles, and vector K, needed to compute absorption from Gershun's equation (2.4). *Tyler*'s [1960] a(488) values are compared with our own for 30 April in Figure 2.8a. Tyler's measurements fall within the range of temporal and spatial variabilities observed during the present experiment.

Figure 2.10 illustrates one example of the comparative profiles of chlorophyll a concentration and absorption coefficients for particles and gelbstoff at 456 nm taken from the same set of sampling bottles. The absorption coefficients for particulates and gelbstoff presented were measured using the spectrophotometer. These profiles

illustrate that the particulate fractions of absorption and chlorophyll a concentration (the primary absorbing material in phytoplankton) follow similarly shaped vertical profiles, which closely mimic those seen in the total absorption profiles measured using most of the methods considered here. Furthermore, the gelbstoff absorption measurements do not follow a profile similar to any of the particle related optical measurements, and there is no evidence in the data to suggest that the dissolved organic concentrations are correlated with suspended particle concentrations. The gelbstoff contribution to the total absorption coefficient increases with depth because of the decrease in particulate absorption.

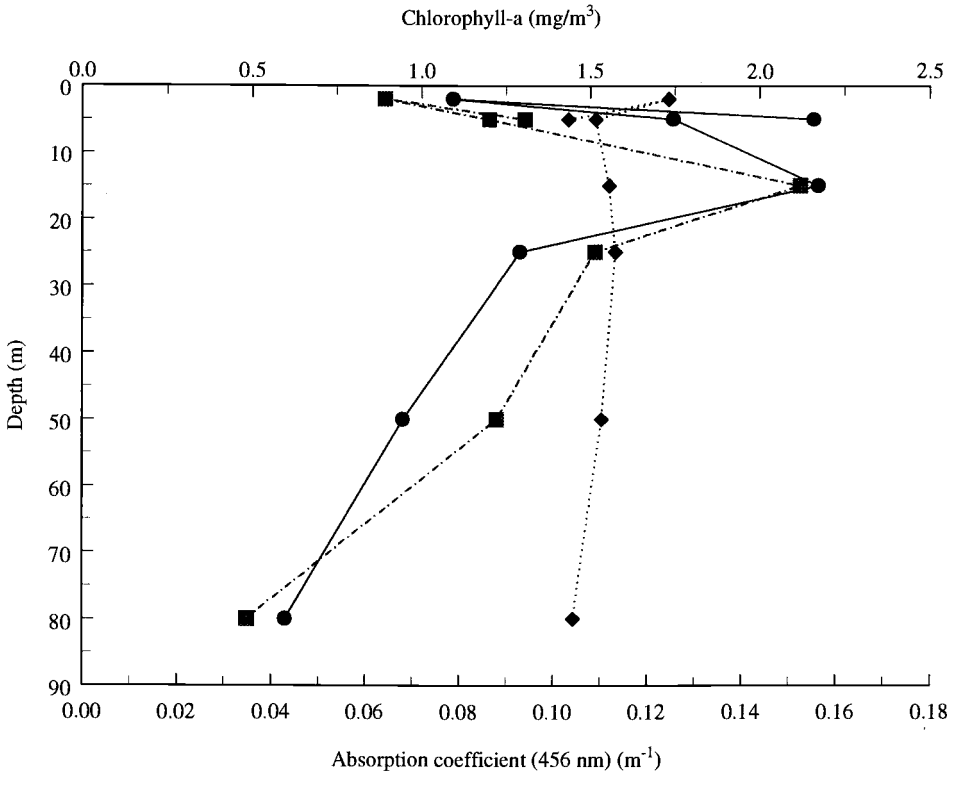

Figure 2.10. The absorption coefficients for the particulate (●) and gelbstoff (◆) components measured using the spectrophotometer and the chlorophyll-a concentrations (■) from the same sample bottles.

Data from the ICAM are presented in this paper for 30 April and 1 May (Figures 2.7, 2.8 and 2.9, panels a and b). ICAM and spectrophotometer samples were obtained from the same Niskin bottles. Absorption values at 456 nm measured with the ICAM were 75% (std. dev. 12%) lower than those measured with the spectrophotometer. The difference in a(456) between the two laboratory measurements increased with increasing particulate absorption as measured using the spectrophotometer. Agreement between the two laboratory methods improved at 488 nm [48% (sd 7%)] and differences were essentially unbiased with much smaller scatter at 532 nm. Similar spectral differences were found in a previous comparison between ICAM and spectrophotometer absorption values [*Cleveland, et al.,* 1990].

Daily average absorption coefficients for May 1 at 15 and 50 m for the spectrophotometer, ICAM, RTAM, TOPS, IPS and CR are compared in Table 2.3. Relative to averages over all instruments at each depth, at 456 nm the spectrophotometer is 20% to 36% high, ICAM is 46% to 53% low, RTAM is 12% to 17% high, TOPS is 22% high, IPS is 9% high, and CR is 3% high. At 532 nm, the spectrophotometer is 1% to 17% low, the ICAM is 1% high, RTAM ranges from < 1% low to 6% high, TOPS is 13% high and IPS is 5% low. This does not imply that the average value is the correct value. It merely highlights potential systematic differences.

Table 2.3. The averaged absorption coefficients measured at 15 and 50 m on May 1. The IPS measurements start at 50m and extend to 60 m.

	spectrophotometer	ICAM	RTAM	TOPS	IPS	CR
a(456)						
15 m	0.190	0.107	0.140	0.200	•••	0.170
50 m	0.193	0.100	0.118	•••	0.160	•••
a(488)						
15 m	0.129	0.107	•••	0.152	•••	•••
50 m	0.126	0.089	•••	•••	0.088	•••
a(532)						
15 m	0.108	0.115	0.123	0.129	•••	•••
50 m	0.104	0.099	0.113	•••	0.093	•••

Table 2.4. Mean biases and RMS deviations of Tops spectral absorption coefficients relative to those of the RTAM's. Mean absorption coefficients are those of RTAM.

λ	$\bar{a}$	Bias	RMS
456*	0.246	0.011	0.020
532	0.149	-0.004	0.009

* May 1 and 5 only

Sufficient numbers of paired measurements were made at common depths on 1 through 7 May to allow direct comparisons of overall deviations in absorption (at all wavelengths) between the TOPS and RTAMs (Figure 2.11a), and between the spectrophotometer and TOPS (Figure 2.11b), the RTAMs (Figure 2.11c), and the IPS and RTAM (Figure 2.11d). The numbers of absorption pairs measured at common depths on the same days were too few to allow this type of comparison between the

other instrument combinations. Mean biases and Root-Mean-Square (RMS) deviations of the TOPS absorption coefficients relative to those of the RTAMs are listed in Table 2.4 for 456 (6 and 7 May only) and 532 (1, 6 and 7 May) nm. At these two wavelengths respectively, TOPS absorption coefficients are biased high by 7% and 4%, and RMS deviations are 6% and 8%, of the associated subsample mean RTAM absorption coefficients; were we to include the 1 May 456 nm subsample, in which the two instruments are obviously biased apart by a fixed 0.05 m^{-1} (Figure 2.11a), the combined 456 nm mean bias and RMS would increase to 16% and 21%, respectively, of the RTAM mean. Mean biases and RMS deviations, relative to the spectrophotometer spectral absorption coefficients, for the IPS, TOPS and RTAMs are listed in Table 2.5. Relative to the spectrophotometer subsample means, at 456 nm IPS is biased 12% low (25% RMS deviation), TOPS is unbiased (19% RMS deviation), and RTAM is biased 17% low (20% RMS deviation). At 488 nm IPS is biased 18% low (25% RMS deviation) and TOPS is biased 8% high (19% RMS deviation). At 532 nm IPS is unbiased (22% RMS deviation), TOPS is 26% high (32% RMS deviation) and RTAM is 19% high (22% RMS deviation). The bias and RMS comparisons in Table 2.5 are all referenced to the spectrophotometer estimates simply because it is the only instrument which has enough paired observations (same days and depths) with all three of the others to form a common basis for intercomparisons; we do not suggest that the spectrophotometer absorption estimates should be regarded as a standard.

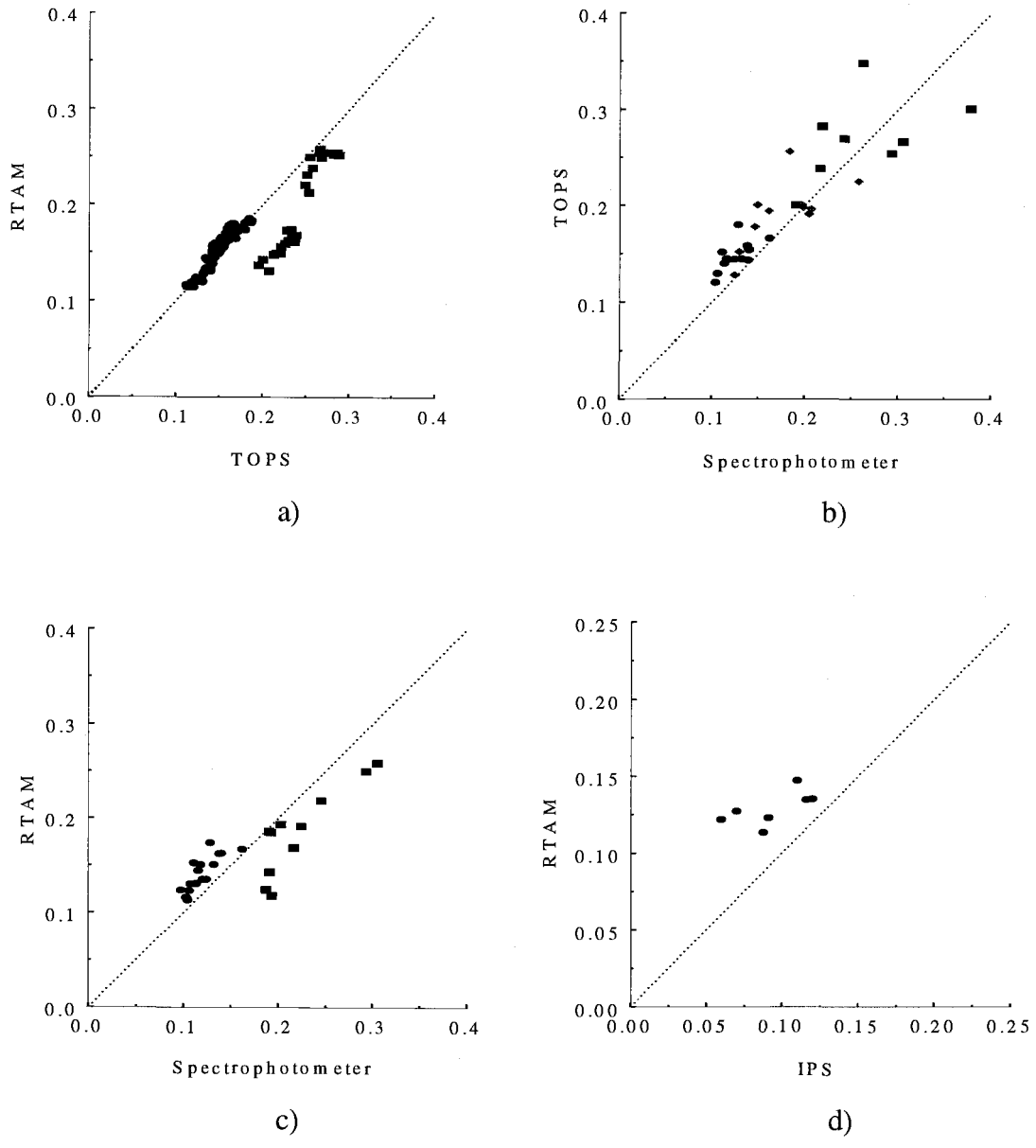

Figure 2.11 a) Scatterplot of RTAM vs TOPS data for the absorption coefficient at 456 nm (■) and 532 nm (●). The 456 nm data is for May 1, 6, and 7. b) Scatterplot of TOPS vs spectrophotometer data for the absorption coefficient at 456 nm (■), 488 nm (◆), and 532 nm (●). The data were taken on May 1,5,6, and 7. c) Scatterplot of RTAM vs spectrophotometer data for the absorption coefficient. Symbols for wavelength and observation dates same as in a). d) Scatterplot of RTAM vs IPS dat for the absorption coefficient at 532 nm. IPS data from below 30 m. Data was taken on May 1,6, and 7.

Table 2.5. Mean biases and RMS deviations of IPS, TOPS and RTAMs absorption coefficients relative to those of the spectrophotometer*. Mean absorption coefficients are those of the spectrophotometer.

	IPS			TOPS			RTAMs		
λ	$\bar{a}$	Bias	RMS	$\bar{a}$	Bias	RMS	$\bar{a}$	Bias	RMS
456	0.203	-0.019	0.052	0.263	-0.007	0.052	0.219	-0.039	0.045
488	0.135	-0.024	0.034	0.178	0.015	0.033	•••	•••	•••
532	0.109	-0.009	0.022	0.126	0.021	0.037	0.119	0.021	0.024

* This is not to imply that the spectrophotometer is a reference value. It is chosen because it has the most data in common with all the other instruments.

2.5 DISCUSSION

2.5.1 Temporal Variability of Bio-Optical Properties

The magnitudes of our absorption values agree remarkably well with those measured by *Tyler* [1960] 34 years earlier (Figure 2.8a), suggesting that springtime optical properties of Lake Pend Oreille have not changed significantly in the interim. However, Tyler's early April 1958 optical and temperature profiles in March-April 1958 are representative of a vertically well mixed, and horizontally homogeneous, water column. In contrast to the strong thermal stratification we found in the upper 50 m, Tyler measured a constant temperature of 3.6 ° C from the surface to 137 m with a diurnal mixed layer increasing to 4.5 ° C in the top 1.25 m as late as 29 April. Even a casual inspection of the results presented above shows clearly how the vertical

structure of optical properties in the lake were strongly affected by the thermally stratified surface layer.

The existence and evolution of the thermally stratified surface mixed layer in Lake Pend Oreille profoundly affected the vertical profile of bio-optical properties during the optical closure experiment. A relatively intense phytoplankton bloom produced strong vertical structure in vertical profiles of particle and pigment concentrations, as documented here by profiles of $c_p(660)$, chlorophyll-a fluorescence and extracted chlorophyll a concentrations (Figures 2.4a, 2.6a and 2.10). Profiles of all of these variables show an increase from the surface to a strong maximum in the top 15 m, a decrease with depth below the maximum to approximately surface values between 30 and 50 m, and a continued decrease (approximately exponentially) to constant background values at depths > 100 m. The near surface maxima in daily averages of both $c_p(660)$ and chlorophyll a fluorescence initially decreased on 1 May, following the 30 April wind event, and then increased monotonically between 1 and 7 May by overall factors of 2.2 and 2.5, respectively (Figures 2.4a and 2.6a); the depths of the maxima became progressively shallower each day, from 15 m on 1 May to 5 m on 7 May. Chlorophyll a concentrations measured in the top 30 m also increased on a daily basis throughout the period. In the water column below 30 m, $c_p(660)$ and fluorescence initially increased after 1 May, reached a maximum at all depths between 30 and 100 m on 5 May, and then decrease progressively through 6 and 7 May (Figures 2.4a and 2.6a). We interpret these sequences as symptomatic of a spring bloom in the top 60 m, which was briefly interrupted by a strong wind event which flushed the

surface layer out of Scenic Bay and replaced it with deeper water between 30 April and 1 May. This was followed by a period of more rapid warming and phytoplankton growth through 7 May, which became progressively more confined to the upper 20 to 30 m. Near the end of the period, the increased optical density of the surface layer shaded the deeper water column, where reduced productivity levels and sinking combined to produce progressively decreasing particle and chlorophyll a concentrations.

Significant variability of particulate properties is also evident on time scales ranging from diurnal down to a few minutes. Within a given day, $c_p(660)$ and chlorophyll a fluorescence in the water column vary from ±10% to ±> 20% in the shallow maxima, and in the range of ±4% to ±10% in the water column below 30 m (Figures 2.4b and 2.6b). We interpret this diurnal variability as symptomatic of phytoplankton growth and particle sinking associated with the bloom cycle described above, coupled with advective displacements of spatially varying bio-optical profiles in the vicinity of the instrument locations. Short term variability estimated from time series measurements of $c_p(660)$ at 65 m on 30 April (Figure 2.5) is approximately 1.5%, which is approximately one-third of the corresponding diurnal variability (Figure 2.4b). Inspection of the CTD cast from which the data for Figure 2.5 were extracted shows that the base of the seasonal thermocline was at 65 m, and that the vertical gradient of $c_p(660)$ at that depth is such that a 3 m random displacement (e.g. due to internal waves) is sufficient to explain the amplitude of the variability in Figure 2.5. Assuming that a similar mechanism is primarily responsible for short term variability

in the top 30 m, where vertical gradients of bio-optical properties are much larger (Figures 2.4a and 2.5a), we may assume that the magnitude of short term relative variability increases approximately in proportion to diurnal variability (i.e. 3% to 7% in the near-surface maxima).

The time lapse between the ancillary measurements and individual absorption measurements with different methods was often as large as hours (Table 2.2), and the measurements were separated horizontally by 10's to 100's of m. Diurnal and short term variability clearly contributes significantly to deviations between "daily average" absorption coefficients measured by any pair of instruments. This is especially true in cases where one (or both) of the "averages" being differenced is actually a single observation separated by several hours from the paired "average" measurements; on 1 May for example, the spectrophotometer absorption coefficients were measured from samples taken at 1138 PDT, the CR measurements were made between 1045 and 1340 PDT, the TOPS profiles were measured between 1700 and 1900 PDT, RTAM casts were distributed from 1445 to 2100 PDT and IPS casts were made at 1100 and 1350 PDT.

Profiles of absorption measured in situ with the TOPS and RTAMs are both characterized by vertical structure and spatio-temporal variabilities on weekly, daily and diurnal time scales (Figures 2.7-2.9) similar to those occurring in the $c_p(660)$ and chlorophyll a fluorescence profiles. Absorption measurements at fixed depths by the other in situ and laboratory instruments are also consistent with these characteristics of particulate bio-optical profiles (Figures 2.7-2.10), but do not resolve the shapes of the

vertical profile, nor are the full magnitudes of the shallow maximum usually determined.

2.5.2 Vertical Profiles

2.5.2.1 *Spectrophotometer and ICAM*

On most occasions the vertical profiles of the absorption coefficient provided by the spectrophotometer are similar in shape to the $c_p(660)$ and fluorescence profiles with the differences being caused by gelbstoff absorption. The spectrophotometer estimates of the total absorption coefficient did not reproduce the day-to-day variability seen in the fluorescence or $c_p(660)$ profiles. This is in part due to the vertical resolution not being fine enough to see the changes in the shape of the particle maximum near the surface and in part due to the measured gelbstoff absorption changing independently of the particulate absorption.

Since the GF/F filters pass all particles smaller than 0.7 um, the gelbstoff absorption estimates obtained with the spectrophotometer from the filtrate probably include some particulate absorption and scattering.

The ICAM a(456) data does not display a significant reduction as seen in the $c_p(660)$, fluorometer voltage, and chl-a concentrations seen over the day in the surface waters on April 30 even though it would be expected that a(456) would change with the general reduction of particle concentration observed in the ancillary measurements.

Direct comparisons of the ICAM results with spectrophotometer measurements made using water from the same sampling bottle were presented earlier in this paper.

2.5.2.2 *RTAM*

The RTAM measurements provided continuous profiles of the depth structure of the absorption coefficient at 456 and 532 nm. Except for April 30 the RTAM data are presented as a mean profile for the measurements taken throughout the day. The a(456) values determined using the RTAM are within the range provided by the other methods. The large and small scale temporal and spatial variations observed agree well with the $c_p(660)$ and fluorometer voltage variations. Only on May 5 does the RTAM show a flatter profile than the other parameters. Cavitation in the particular set of instruments used at Lake Pend Oreille may have been the cause of this. The RTAM and spectrophotometer estimates of a(532) differ by 0.015 to 0.025 m^{-1} throughout the experiment. This shows that the structure of the profiles compares very well (to ± 0.005 m^{-1}) but that a bias of approximately 0.02 m^{-1} was present. The bias is probably associated with pure water calibrations for the ac-9 and purity of reference cell water for the spectrophotometer.

2.5.2.3 *TOPS*

The absorption coefficients determined using the TOPS data are presented as a mean profile for each day except on April 30. At all three wavelengths the TOPS

measurements are similar in shape to the profiles of $c_p(660)$ and fluorometer voltage. TOPS also reproduced the day to day changes in $c_p(660)$ and fluorescence. At 488 nm there is good agreement between the TOPS and the spectrophotometer measurements. The shape and magnitude of the TOPS a(532) profile agree well with the RTAM profiles on most occasions. Except for April 30 the TOPS a(532) measurements are about 10% higher than the spectrophotometer measurements. The a(532) coefficients of deviation are smaller in magnitude than the $c_p(660)$ coefficients of deviation.

2.5.2.4 *IPS*

At 456 nm on April 30, IPS values compare closely with RTAM except for an anomolously high value at 70 m which was traced to instrument misalignment. Except for the 70 m data point, the IPS values for this day and wavelength fall between the spectrophotometer and ICAM values. On the other days shown in Figures 2.7a-e, the IPS system yielded absorption values that varied by as much as a factor of two, indicating a high degree of instrumental error at this wavelength. This is not surprising because the lowest signal-to-noise and fewest measurements for the regression fits were at this wavelength. One would therefore expect less variability and better agreement with the other methods at the two longer wavelengths where signals were higher and this is indeed found to be the case. At 488 nm on April 30 and May 1 there is remarkable agreement among the IPS, spectrophotometer, and ICAM values below about 30 m (Figure 2.8a). Above 30 m there is still good

agreement, but the highly stratified water resulted in an increase in the variability of the measurements. On May 6 and 7, the IPS values tend to be consistently lower than those measured with the spectrophotometer (Figures 2.8d and e).

2.5.2.5 *CR*

The compound radiometer was only compared with the other absorption measurements during one set of casts. The CR was deployed only on May 1 when clear skies and a calm lake surface made for ideal measurement conditions. In the depth range between 12 and 18 m, where the CR error analysis predicts accurate operation, its absorption coefficients agreed very closely with the mean of the others (Table 2.3). The CR appeared to measure low absorption values near the surface and high values below 18 m, which is counter to the trends measured by the other in situ instruments (Fig. 2.8a); in absolute magnitude, nevertheless, these values fell well within the range determined by the other instruments for that day.

2.5.3 Intercomparisons

Comparisons between magnitudes of daily average spectral absorption coefficients measured using the several methods were most complete for the spectrophotometer, RTAMs, IPS, and TOPS. Limited numbers of observations make the comparisons of absorption coefficients measured with the ICAM and CR more anecdotal in nature.

The spectrophotometer measurements provide a convenient common basis for intercomparing the IPS, TOPS and RTAMS (Figures 2.11b-d and Table 2.5). In general, all of the in situ measurements demonstrate comparable RMS deviations ranging from 17% to 30% relative to the spectrophotometer, with in many cases a mean bias accounting for a large fraction of the deviations. The dominant source of these deviations is the 16% uncertainty in the gelbstoff component of the absorption coefficient determined by the spectrophotometer. All of the other methods measured total absorption, and only the spectrophotometer was used to separate the particulate and dissolved components; unfortunately, its uncertainty in the gelbstoff component is by far the largest instrumental error contribution in this set. The in situ and spectrophotometer particle absorption measurement uncertainties are all $\leq$ 10%, as is the uncertainty associated with environmental variability.

The direct comparisons between TOPS and RTAM absorption coefficients show agreement within 8%, if 1 May a(456) data (which are obviously biased by a fixed offset) are excluded (Fig. 2.11a, Table 2.4). This agreement is better than the 10% instrumental uncertainty associated separately with each technique.

2.5.4 The Scale Hypothesis and Other Potential Sources of Error

The "scale hypothesis" of ocean optics asserts that profile measurements of IOP measured over scales of 10's of cm and representative of volumes ranging from < 1 liter to several liters, can be used in radiative transfer models to predict AOP's

measured over pathlength scales of m to 10's of m. In terms of Gershun's Equation (2.4), the scale hypothesis states that profiles of absorption measured using small pathlength (volume) IOP measurements (in this case using the RTAM's, spectrophotometer and ICAM) are not significantly different from absorption profiles determined using profiles of irradiance measured with instruments having effective pathlengths ranging from meters to 10s of m.

Each of the instruments used during the optical closure experiment measures absorption over a different working volume of (or pathlength in) water. The ICAM and spectrophotometer measure samples representative of 10 l of water collected in a Niskin bottle (assuming that the water in the bottle is well mixed before subsamples are removed), even though each uses smaller sub-sample volumes. The RTAM measures absorption over a 25 cm pathlength (volume is approximately 20 ml), but water is pumped continuously through its tube while the instrument traverses approximately 20 cm vertically during each sample. It thus had a vertical resolution of 0.2 m^{-1}. The working pathlengths of the IPS, TOPS and CR are determined by the minimum distance over which each can accurately determine the gradient of vector irradiance. The IPS integrates absorption over a 10 m path, in which the water properties are assumed to be homogeneous. Under reasonably stable surface illumination, the TOPS system resolves K and a over a few m, and can generally resolve sharp features with vertical scales of approximately 5 m or greater. The CR has a similar working volume to TOPS, but only performs accurately in the narrow depth range between 12 and 18 m.

At the levels of uncertainty in the present absorption comparisons (e.g. <8% for TOPS and RTAM, with similar uncertainties in more anecdotal comparisons between other combinations of instruments) there is no evidence of any systematic deviation between large and small volume absorption measurements which would contradict the scale hypothesis.

There is also no evidence of systematic differences which might be traced to the 2 to 4 nm differences in center wavelengths and spectral bandpass characteristics between instruments at some nominal wavelengths.

The spectrophotometer and RTAM were both calibrated using "pure" water filtered by reverse osmosis. The assumed absorption values for the "pure" water were those of *Smith and Baker* [1981]. Values of the spectral absorption coefficients for pure water have a range of values depending on what source is used [*Tam and Patel,* 1979; *Smith and Baker,* 1981; *Pope,* 1993]. These differences are most pronounced at shorter wavelengths. Systematic biases would be expected were either instrument calibrated using impure reference water, or if the assumed absorption values are incorrect. The calibrations of the TOPS and IPS systems are both purely radiometric, and therefore, are independent of this possible error source. The 8% agreement between TOPS and RTAM (Table 2.4) is well within the uncertainty of both instrument's error budget, and the 10% uncertainty of assumed pure water absorption. Likewise, the 20% to 30% uncertainties in comparisons between the spectrophotometer and both TOPS and IPS absorption (Table 2.5) are well within the combined instrumental uncertainties, which are dominated by 15% uncertainty (at 456

nm, and perhaps 40% uncertainty at 532 nm) in the spectrophotometric gelbstoff absorption estimate. The results do not support a conclusion that impure reference water contributed a significant bias to absorption coefficients measured using either the spectrophotometer or the RTAMs.

Separate measurements of gelbstoff and particulate absorption coefficients were obtained using the spectrophotometer. Since the spectrophotometer measured the particulate component this component can be compared with the ancillary measurements which provide indications of changes in particle properties. The shape of the particulate absorption profile was similar to the chlorophyll-a concentrations (Figure 2.10), $c_p(660)$ and fluorometer voltage. The profiles of gelbstoff absorption, as may be expected, were not related to any of the ancillary measurements. The gelbstoff absorption becomes increasingly important at greater depths because of the decrease in particulate absorption.

The measurements of $c_p(660)$, fluorescence voltage, and chlorophyll-a concentrations do not provide any information about the variability of the gelbstoff concentrations in the water. There is no evidence to indicate that the gelbstoff concentration should be proportional to the particle concentration or that the variability in gelbstoff concentration has the same magnitude or the same time and space scales as the particulate variability. Concentrations of gelbstoff were determined with the spectrophotometer and indicated that gelbstoff absorption was not correlated with particulate absorption. There are only three occasions where measurements of gelbstoff absorption were made twice in a day at the same depth. In these three cases

the largest percent change in absorption by gelbstoff was 12.1% for samples taken at 5 m on May 1. The other two cases (May 5, 25 m and May 7, 5 m) showed changes in gelbstoff absorption of 6%. The day-to-day variability in the absorption coefficient attributed to changes in gelbstoff concentration by the spectrophotometer are not always evident in the total absorption coefficients of the other techniques.

2.6 CONCLUSIONS

The different techniques for the measurement of the absorption coefficient agreed within ±25% at 532 nm with decreased agreement at shorter wavelengths, but with far better comparisons between certain methods. When the pure water absorption values are subtracted from all of the measurements at the three wavelengths the margin of error is roughly constant. The reason is that pure water absorption is a larger fraction of the total absorption at longer wavelengths where better agreement was found. In a purely absorbing medium the methods would likely agree nearly perfectly. Due to different geometries the addition of scatterers affects the instruments differently. In the blue part of the spectrum light sources have smaller outputs and detectors are less sensitive. Therefore, comparisons of absorption methodologies (as opposed to specific instrumentation) are best carried out in the green part of the spectrum where purely instrumental problems are smaller. Future comparisons should thus start by making observations at 532 nm. At this wavelength there is sufficient penetration of solar radiation for the techniques that require a natural light field, long

pathlengths for the isotropic point source, and better signal to noise ratios for the reflecting tube absorption meter. This does not imply that other wavelengths should be ignored. An understanding of the differences in measurement techniques is needed at all wavelengths to compare measurements by investigators using a variety of equipment.

One of the more interesting results is the generally good agreement between the large volume and small volume techniques as well as agreement between in-situ measurements and laboratory measurements. There is generally good agreement, on all days and at all three comparable wavelengths, between the IPS method, an in-situ large volume measurement, and the spectrophotometer, a benchtop system that uses water samples. On May 1 and 7 there is also good agreement at 532 nm between the RTAM, a small volume technique, and TOPS, a large volume technique.

Comparison of the measurements at Lake Pend Oreille is complicated by the natural variability of the lake. The natural variability observed also highlights the difficulty in reporting optical properties of a given water mass. A single or even several profiles are not sufficient to properly define the optical properties of a water mass. For making comparisons of measurements made in a natural environment the variability of that environment must be taken into account. It is important to be able to track the variability in both particle and gelbstoff properties. Future comparisons of absorption measurements should include some method of providing an inter-calibrated reference measurement, on all of the absorption measurement platforms, capable of detecting changes in particle and gelbstoff properties. Time series measurements from

scales of minutes to days are necessary to properly define the optical properties of a water mass and could also be useful in interpreting the possible effects of natural variability on the different absorption measurements. If the short time scale variability is large however, the use of a time series to remove the natural variability from measurements by different techniques will be difficult unless the spatial scale between the location of the measurements is small. We thus recommend that in the future instruments should be located as much as possible on the same instrument platform.

To improve the comparisons of instruments and the ability to measure the natural variability new methods will need to be developed that can be used to measure the contributions of the individual components to the total absorption coefficient both in the laboratory and in situ. As the spectral resolution of the different methods improve it may be possible to apply inversion techniques to the data in order to identify contributions of the components to the absorption coefficient. It is also possible to filter the input of the RTAM providing a separation of the components in a manner similar to laboratory techniques. The ability to differentiate the components of the total absorption coefficient will provide methods to check results from the spectrophotometer and help to isolate problem areas of individual measurement techniques. Measurement of component contributions using techniques of all volume scales will improve our understanding of the possible differences that may be associated with use of different sampling volumes.

It should be remembered that it is not possible to make simultaneous measurements on a single volume of water using all of the different methods available

because of the differences in sampling volume and time required to obtain a measurement using the different instruments. If all methods are to be compared during a single experiment then it would be desirable to have waters with little natural variability. Future experiments do not need to include all instrumentation to be in the water at the same time. Comparisons of large scale techniques, comparison of large versus small volume measurements, as well as comparisons between laboratory and in water techniques will all improve the understanding of the capabilities of the instrumentation and move us a step closer towards providing comparable measurements of the absorption coefficient by a variety of methods.

Many of the systems used at Lake Pend Oreille were relatively new and the comparison among systems has shown areas where individual techniques required improvement in design or application (e.g. reduction of cavitation in the reflecting tubes, addition of a reference detector to the IPS, improved geometry for the ICAM). Data analysis techniques were also improved as a result of the experiment. Modifications to the instrumentation and analysis techniques since the Lake Pend Oreille experiment have improved our ability to provide precise, accurate, and dependable measurements of the absorption coefficient with the various techniques.

The Optical Closure Experiment at Lake Pend Oreille provides a benchmark for the measurement of the absorption coefficient of natural waters. Therefore this paper provides a review of most of the available methodologies for the measurement of absorption. Many of the instruments used in this experiment were of relatively new design. This comparison has also highlighted areas where the instrumentation or

analysis techniques required improvement. Many of the instruments have been modified in the past two years to incorporate changes made obvious by this work. Because of this we can expect much greater convergence of results at all wavelengths in the near future.

2.7 REFERENCES

Bennett, G. T., E. S. Fry, and F. M. Sogandares, Photothermal measurements of the absorption coefficient of water at 590 nm. in *Ocean Optics VIII*, M. A. Blizard, ed., Proc. Soc. Photo-Opt. Inst. Eng., 637, 172-180, 1986.

Bricaud, A., A. Morel and L. Prieur, Absorption by dissolved organic matter of the sea (yellow substance) in the UV and visible domains. *Limnol. Oceanogr.*, **26**, 43-53, 1981.

Cleveland, J. S., R. M. Pope, and E. S. Fry, Spectral absorption coefficients measured with an integrating cavity absorption meter, in *Ocean Optics X*, R. W. Spinrad, ed., Proc. Soc. Photo-Opt. Instr. Eng., 1302, 176-186, 1990.

Cleveland, J. S., and A. D. Weidemann, Quantifying absorption by aquatic particles: A multiple scattering correction for glass-fiber filters, *Limnol. Oceanogr.*, 38, 1321-1327, 1993.

Doss, W., and W. Wells, Undersea compound radiometer, *Appl. Opt.*, 31, 4268-4274, 1992.

Elterman, P., Integrating cavity spectroscopy, *Appl. Opt.*, 9, 2141-2142, 1970.

Fry, E. S., G. W. Kattawar, and R. M. Pope, Integrating cavity absorption meter, *Appl. Opt.*, 31, 2055-2065, 1992.

Gershun, A., The Light Field, *J. Math. Phys.*, 18, 51-151, 1939.

Højerslev, N., A spectral light absorption meter for measurements in the sea, *Limnol. Oceanogr.*, 20, 1024-1034, 1975.

Jerlov, N. G., *Marine Optics* Elsevier, Amsterdam, 1976.

Kennedy, C. D., Integrating cavity spectral absorption meter, Masters Thesis, December 1992, Long Memorial Library, University of New Orleans, New Orleans, La.

Kiefer, D. A. and J. B. Soohoo, Spectral absorption by marine particles of coastal waters of Baja California. *Limnol. Oceanogr.*, 27, 492-499, 1982.

Maffione, R. A., and J. S. Jaffe, The average cosine due to an isotropic light source in the ocean, *J. Geophys. Res.*, 100, 13,179-13,192, 1995.

Maffione, R. A., R. C. Honey, and R. A. Brown, Experiment for testing the closure property in ocean optics, Proc. Soc. Photo-Opt. Instr. Eng., 1537, 115-126, 1991.

Maffione, R. A., K. J. Voss, and R. C. Honey, Measurement of the spectral absorption coefficient in the ocean with an isotropic source, *Appl. Opt.*, 32, 1993.

Miles, E., and W. H. Wells, Revised results from the underwater compound radiometer, Report to ONR under contract N 00014-88-C-0715, Dec. 1993. (available from Tetra Tech. Data Systems Inc. 2451a Impala Dr. Carlsbad, CA 92008)

Moore, C., J. R. V. Zaneveld, and J. C. Kitchen, Preliminary results from an *in situ* spectral absorption meter, in *Ocean Optics XI*, G. D. Gilbert, ed., Proc. Soc. Photo-Opt. Instrum. Eng., 1750, 330-337, 1992.

Morel, A., Light and marine photosynthesis: a spectral model with geochemical and climatological implications, *Prog. Oceanog.*, 26: 263-306, 1991.

Mueller, J. L., Integral method for irradiance profile analysis, *CHORS Tech. Memo.* 007-91, San Diego, CA., 1991.

Mueller, J. L. and R. W. Austin, Ocean optics protocols for SeaWiFS validation, SeaWiFS Technical Report Series, Vol. 5. (Hooker, S.B. and E.R. Firestone, eds), NASA TM-104566, Vol. 5, NASA Goddard Space Flight Center, Greenbelt, MD. 43pp, 1992.

Pope, R. M., Optical absorption of pure water and sea water using the integrating cavity absorption meter, Ph. D. Thesis, Texas A&M University, December 1993.

Roesler, C. S., M. J. Perry, and K. L. Carder, Modeling in situ phytoplankton absorption from total absorption spectra in productive inland marine waters, *Limnol. Oceanogr.*, 34, 1510-1523, 1989.

Sathyendranath, S., L. Lazzara, and L. Prieur, Variations in the spectral values of specific absorption of phytoplankton, *Limnol. Oceanogr.*, 32, 403-415, 1987.

Smith, R. C., and K. S. Baker, Optical properties of the clearest natural waters (200-800 nm), *App. Opt.*, 20, 177-184, 1981.

Sorenson, G., and R. C. Honey, Instrumentation for measuring visibility-limiting characteristics of sea water, *Proc. Soc. Photo-Opt. Instr. Eng.*, 12, 115-122, 1968.

Spitzer, D., and M. R. Wernand, *In situ* measurements of absorption spectra in the sea, *Deep-Sea Res.*, 28A, 165-174, 1981.

Tam, A. C., and C. K. N. Patel, Optical absorptions of light and heavy water by laser optoacoustic spectroscopy, *Appl. Opt.*, 18, 3348-3358, 1979.

Trees, C. C., and K. J. Voss, Optoacoustic spectroscopy and its application to molecular and particle absorption, in *Ocean Optics X*, R. W. Spinrad, ed., Proc. Soc. Photo_Opt. Instr. Eng., 1302, 149-156, 1990.

Tyler, J. E., Radiance distribution as a function of depth in an underwater environment, *Bull. Scripps Inst. Oceanogr. Univ. Calif.,* **7**, 363-412, 1960.

Voss, K. J., Use of the radiance distribution to measure the optical absorption coefficient in the ocean, *Limnol. Oceanogr.*, 34(8), 1614-1622, 1989.

Voss, K. J., and A. L. Chapin, Next generation in-water radiance distribution camera system, in *Ocean Optics XI*, G. D. Gilbert, ed., *Proc. Soc. Photo-Opt. Instr. Eng.,* 1750, 384-387, 1992.

Wells, W. H., Techniques for measuring radiance in sea and air, *Appl. Opt.*, 22, 2313-2321, 1983.

Yentsch, C. S., Measurement of visible light absorption by particulate matter in the ocean, *Limnol. Oceanogr.*, 7, 207-217, 1962.

Zaneveld, J. R. V., The scattering error correction of reflecting-tube absorption meters, in *Ocean Optics XII,* J. Jaffe, ed., Proc. Soc. Photo-Opt. Instrum. Eng., 1994

Zaneveld, J. R. V., R. Bartz, J. C. Kitchen, Reflective-tube absorption meter, in *Ocean Optics X*, R. W. Spinrad, ed., Proc. Soc. Photo-Opt. Instrum. Eng., 1302, 124-136, 1990.

Zaneveld, J. R. V., J. C. Kitchen, A. Bricaud, and C. Moore, Analysis of *in situ* spectral absorption meter data, in *Ocean Optics XI*, G. D. Gilbert, ed., Proc. Soc. Photo-Opt. Instr. Eng., 1750, 187-200, 1992.

Zaneveld, J. R. V., and H. Pak, Some aspects of the axially symmetric submarine daylight field, *J. Geophy. Res.*, 77, 2677-2680, 1972.

CHAPTER 3

TOWARDS CLOSURE OF THE INHERENT OPTICAL PROPERTIES OF NATURAL WATERS

W. Scott Pegau, J. Ronald V. Zaneveld, and Kenneth J. Voss

Published in *Journal of Geophysical Research*
July 15, 1995, 7 pages

3.1 ABSTRACT

A fundamental relationship of inherent optical properties (IOP) is that the beam attenuation coefficient is the sum of the volume absorption and scattering coefficients ($c = a + b$). A relative calibration of a set of instruments can be provided using this IOP closure equation. Measurement of the true beam attenuation coefficient c is not practical as all attenuation instruments have some finite acceptance angle in which scattered light is collected. We provide a theoretical framework for measuring the attenuation and scattering coefficients in a consistent manner. Using this framework we provide a practical version of the IOP closure equation. We apply the practical IOP closure equation to measurements made at Lake Pend Oreille, Idaho in the spring of 1992. Results of this IOP closure indicate that the practical closure equation is a useful approach. Closure was achieved during some measurement sets, but not at others. The intermittent lack of closure may be due to the method of determining the scattering coefficient from the general angle scattering meter or that the calibration of at least one of the instruments drifted during the time of the experiment.

3.2 INTRODUCTION

Several new techniques and devices for the measurement of the optical properties of water have recently been developed. Along with the new measurement techniques, methods for verification and testing of these new ideas and instruments must be developed. Closure of the inherent optical properties provides an important

method of checking the performance of instrumentation. Closure is simply "the simultaneous verification of a mathematical relationship and a set of parameters by means of the independent measurement of the parameters" [*Zaneveld,* 1994]. The inherent optical properties (IOP) are those properties of a water column that are independent of the radiance distribution [*Jerlov,* 1976]. They include the absorption coefficient, a, and the volume scattering function, $\beta(\theta,\phi)$. Integration of the volume scattering function over all angles provides the scattering coefficient b:

$$b = \int_0^{2\pi}\int_0^{\pi} \beta(\theta,\phi)\sin(\theta)\,d\theta\,d\phi\,. \tag{3.1}$$

Another IOP, the beam attenuation coefficient, c, is defined to be the sum of the absorption and scattering coefficients:

$$c \equiv a + b. \tag{3.2}$$

Equation (3.2) provides the basis for closure of the inherent optical properties. Since equation (3.2) is exact, IOP closure is a test of the instrumentation only and does not test the mathematical relationship.

An important aspect of closure is that it provides a method to check the consistency of individual IOP measurements. No such check is available when comparing measurements of a single or even two components of equation (3.2). For example, when multiple measurements of a single property, such as the absorption coefficient, are made in a natural water column there presently is no way to know the exact value of the absorption coefficient so that it is difficult to resolve which system provides the best measure of a. Measurement of the attenuation coefficient will help

bound the possible values of a but the true value of a remains unknown. With closure of the IOP we are able to determine if the measurements of a, b, and c are consistent with each other. When IOP closure cannot be accomplished, equation (3.2) cannot be used to determine which of the properties measured has an erroneous value. Other measurements or relationships must be used in order to isolate improper measurements. Even with IOP closure it is possible, but unlikely, that all the measurements are in error by the same percentage.

Although IOP closure provides a method to check the performance of instrumentation there have only been a few times when all three parameters have been measured [*Højerslev,* 1973; *Højerslev,* 1974]. During the closure cruises of Højerslev it was not possible to measure all three IOPs simultaneously. The temporal and spatial variability between measurements affected the ability to obtain closure at some of the stations. Another interfering factor in Højerslev's measurements is that the absorption coefficient was measured at a different wavelength than the attenuation and scattering coefficients. The results of Højerslev's IOP closure showed agreement from 3 to 40% between a+b and c. Since the work of Højerslev there has been little progress towards providing IOP closure. Maffione et al. [1991] describe instrumentation that may be able to provide IOP closure on large volumes of water.

During the optical experiment conducted in 1992 at Lake Pend Oreille, Idaho we measured a, c, and the scattering function from 10 to 170° [$\beta(10 \rightarrow 170°)$] using separate instruments. We will use these measurements in order to determine the

present status of calibration and accuracy in the closure of the inherent optical properties.

Phytoplankton and dissolved organics were the dominant optical materials in the measurement region. A phytoplankton maximum was located between 10 and 20 meters depth. The chlorophyll-a levels associated with the phytoplankton maximum were over 3 mg/m^3. The chlorophyll-a levels remained above 1 mg/m^3 down to depths of nearly 60 m. The dissolved organics became an increasingly important component of the absorption coefficient at depths below the phytoplankton maximum.

3.3 THEORY

By definition:

$$c = a + \int_0^{2\pi}\int_0^{\pi} \beta(\theta,\phi)\sin\theta d\theta d\phi \ . \tag{3.3}$$

Equation (3.3) requires that the instrumentation used to measure the attenuation coefficient reject all scattered light, however all transmissometers accept some portion of the forward scattered light depending on the transmissometer design [*Voss and Austin,* 1993]. For the collimated beam transmissometer used in these measurements the measured c can be written as:

$$c_{measured} = c_{\Omega m} = a + \int_{\Omega_m}^{4\pi} \beta(\Omega)d\Omega \ = a + b_{\Omega m} \tag{3.4}$$

where Ωm is the solid angle of the instrument, Ω is the solid angle and $d\Omega = \sin\theta d\theta d\varphi$. Equation (3.4) is a pragmatic IOP closure equation. We have redefined c to include

the scattered light collected by the non-zero diameter aperture. This redefined c is designated $c_{\Omega m}$. At the same time we have redefined b as $b_{\Omega m}$ which does not include the same amount of scattered light. The equation thus continues to be balanced. To ensure that all scattered light is accounted for once and only once the measurement of b must include light at angles up to, but not less than, the acceptance angle of the attenuation measurement.

In choosing an acceptance angle many factors must be accounted for. The first and foremost consideration is the application of the measurements. One common application of the inherent optical properties is in the computation of irradiances and the radiance field using the radiative transfer equation. For irradiance level calculations the IOPs as presented in equation (3.4) have been used with success in schemes such as Gordon's [1973] quasi-single scattering model. Recent work by Gordon [1993] indicates that irradiance level radiative transfer can be accomplished disregarding scattering in the first 15 degrees. Other schemes such as the Delta-M method [*Wiscombe,* 1977] are used in order to truncate the highly forward peaked scattering function found in hydrological environments. This truncation reduces the number of terms in the Legendre polynomial expansion of the scattering function and allows radiative transfer models like the discrete ordinate model (Stamnes et al. 1988) to be used to rapidly and accurately calculate the irradiance levels. Radiance level calculations can also use the IOPs as given in equation (3.4). The equation of radiative

transfer in a homogeneous plane parallel medium without internal sources and transspectral effects is given by:

$$\cos\theta \frac{dL(\Omega)}{dz} = -cL(\Omega) + \int_0^{4\pi} \beta(\Omega,\Omega')\, L(\Omega')d\Omega' \tag{3.5}$$

where Ω is the solid angle and $d\Omega = \sin\theta d\theta d\varphi$. Similar to the instrumentation all radiative transfer models have some minimum $\Delta\Omega$ used in the integration of equation (3.5) [*Mobley et al.,* 1993]. The $\Delta\Omega$ in numerical integration is thus similar to the Ω_m in a measurement scheme. Both represent a minimum solid angle over which the radiance must, for practical reasons, be considered constant. Equation (3.5) can then be rewritten as:

$$\cos\theta \frac{dL(\Omega)}{dz} = -[c - \int_{\Omega_m} \beta(\Omega,\Omega')d\Omega']L(\Omega) + \int_{\Omega_m}^{4\pi} \beta(\Omega,\Omega')\, L(\Omega')\, d\Omega' \tag{3.6}$$

where Ω_m is of the same form as in (3.4) and the portion in the brackets is similar to the value of $c_{\Omega m}$ given in equation (3.4). The resolution of the radiance distribution in the model sets the maximum allowable acceptance angle for the attenuation measurements. In the modeling comparison of Mobley et al. [1993] the radiance field was divided into "quads" with a $\Delta\phi$ of 15° and a $\Delta(\cos\theta)$ of 0.1. Modeling can be done with smaller solid angles at the expense of increased computing time. A practical constraint on the models is the resolution of radiance measurements that can be used to validate the models. The early radiance detector used by Tyler [1960] had a solid

angle of 0.01sr. Newer camera type systems have reduced the solid angle to approximately 2×10^{-4} sr [*Voss*, 1989].

Use of the measured c in other radiative transfer problems depends on the application. Imaging applications are probably the most stringent and here the required measurement depends on the specific field of view and instrumentation. At very small angles a beam is refracted at density inhomogeneities associated with turbulent flow. These density inhomogeneities are non-stationary and lead to a non-stationary scattering function. The simple radiative transfer equations (Eq. 3.5) no longer applies and so a time averaged or time dependent radiative transfer equation must be used. For a very narrow beam in a turbulent medium (natural turbulence or instrument induced turbulence) there is a very small probability that the beam will propagate without an interaction at a density interface. Scattering from non-stationary interfaces then cause the time averaged scattering function and attenuation coefficients to become very large. We thus arrive at something akin to an uncertainty principle: The smaller the detection angle of a "perfect" beam attenuation meter is, the larger the time-averaged beam attenuation coefficient becomes. Fortunately there are few applications in which very narrow angle forward scattering is important.

It is thus necessary to arrive at a practical approach towards the measurement of the beam attenuation coefficient and the volume scattering function. For IOP closure and radiative transfer it is important that the instruments for the measurement of the beam attenuation and scattering coefficient be matched in order to ensure the

accounting of all scattered light while ensuring that there are no overlapping regions where scattered light is accounted for a second time. The application determines the appropriate solid angle. In all cases, the attenuation coefficient should be reported with the instrument's acceptance angle. The scattering coefficient or volume scattering function should also be reported with the range of angles covered by the instrumentation. The angular resolution of these measurements must be appropriate for the comparison of measurements and in creating a matched set of IOPs to be used in closure or radiative transfer modeling.

3.4 METHODS

We made measurements of c and a using Sea Tech, Inc., transmissometers and single wavelength reflecting tube absorption meters [*Zaneveld et al.,* 1990]. The filters used in the transmissometers and absorption meters had nominal wavelengths of 456 and 532 nm and a 10 nm full width half max bandpass. The acceptance angle of the transmissometers is 1.0 degrees. The measurements of $\beta(\theta)$ were made using the general angle scattering meter (GASM) [*Petzold,* 1972] at nominal wavelengths of 440, 490, 520, 550, 610, and 670 nm. Data was collected with all instruments during three days of the experiment (May 4, 6, and 7, 1992).

Measurements were made from a barge operated by the Navy's David Taylor Research Facility in Bayview, Idaho. The barge was anchored in water over two hundred meters deep at the southern end of Lake Pend Oreille. Physically all

measurements were made close together with the a and c meters located within a meter of each other on a single instrument platform and the GASM instrument located approximately 10 m away. Simultaneous measurements were made with all instruments at the same depth on May 4. On May 6 and 7 the c and a measurements were made within one hour of the $\beta(\theta)$ measurements.

Using the pragmatic definition of c given in equation (3.4) there is no need to make scattering corrections to the attenuation coefficient. A scattering correction must be applied to the reflecting tube absorption meters however, since they do not collect all of the scattered light. The first order correction to the absorption measurements is given by:

$$a = a_m - \zeta b_\Omega \tag{3.7}$$

with

$$b_\Omega = \frac{c_m - a_m}{1 - \zeta} \tag{3.8}$$

where the m subscript indicates the measured value which includes the pure water value (Zaneveld and Bartz 1984). The value of ζ is the proportion of the scattering coefficient that is the error for the absorption meter. Mie scattering models indicate that the value of ζ ranges from 0.09 to 0.19 depending on the size distribution of the scattering particles. For this work we have used $\zeta = 0.13$ [*Zaneveld et al.,* 1992] which was determined by Monte Carlo simulations using the scattering functions of Petzold [1972] [*Kirk,* 1992].

We estimate the maximum error in the scattering coefficient as determined by the difference of the attenuation and absorption coefficients to be $\pm 0.1\ m^{-1}$. This estimate is based on the range of possible values of ζ and drift in the instrument calibrations during the experiment. The major sources of error were the instrument's electronic stability and changes in the calibration caused by the flow characteristics of the instrumentation.

The general angle scattering meter measures the scattering function with one degree resolution from 10 to 170°. However, to create a matched set of parameters as is required by equations (3.4) or (3.6) we must extend the measured scattering function to include scattering from 1.0 to 180°. One method to estimate the scattering coefficient was given by Jerlov (1976). He suggested that the total scattering coefficient is approximately 32 times $\beta(45°)$. Applying this formula to the data of Petzold [1972] we found that this method gives the value of b to within a factor of 2. This method lacked the desired accuracy and also did not provide a matched data set. An alternate technique is to extrapolate the near forward portion of the scattering function from the measured region. We used linear and second order polynomial fits to the data from 10 to 100° in log log coordinates in order to extrapolate the missing portion of the volume scattering function. Application of these extrapolation methods to Petzold's data indicated that there was no one method or range of angles that provided a good fit to all the volume scattering function curves. Therefore, the extrapolation methods proved unsuitable for our purposes.

In order to estimate the small angle scattering and arrive at an estimate of the value of b_1 (where 1.0 is the aperture angle of the instrument which defines the instruments solid angle for this set of measurements) we choose to fit the scattering function measured by the GASM in the 10 to 100 degree range to the family of scattering functions provided by Petzold [1972]. In doing this we are assuming that the shapes of the Lake Pend Oreille scattering functions are bounded by those provided by Petzold. The shape of the scattering function depends on the particle size distribution, the complex index of refraction of the particles, the shape of the particles, and the wavelength of light used. Since Petzold's data includes data from the Tongue of the Ocean and San Diego Harbor we feel that his family of scattering functions contains the extremes of particle size distributions and that the Lake Pend Oreille scattering functions are contained within those given by Petzold. The measured scattering functions indicated that there is little change in the shape of the scattering function for the different wavelengths (Figure 3.1) especially in the near forward direction. This allowed us to use Petzold's single wavelength measurement for all six wavelengths. Extrapolation of the scattering function from 170 to 180° is less critical than the near forward extrapolation because $\beta(\theta,\phi)$is small in this region.

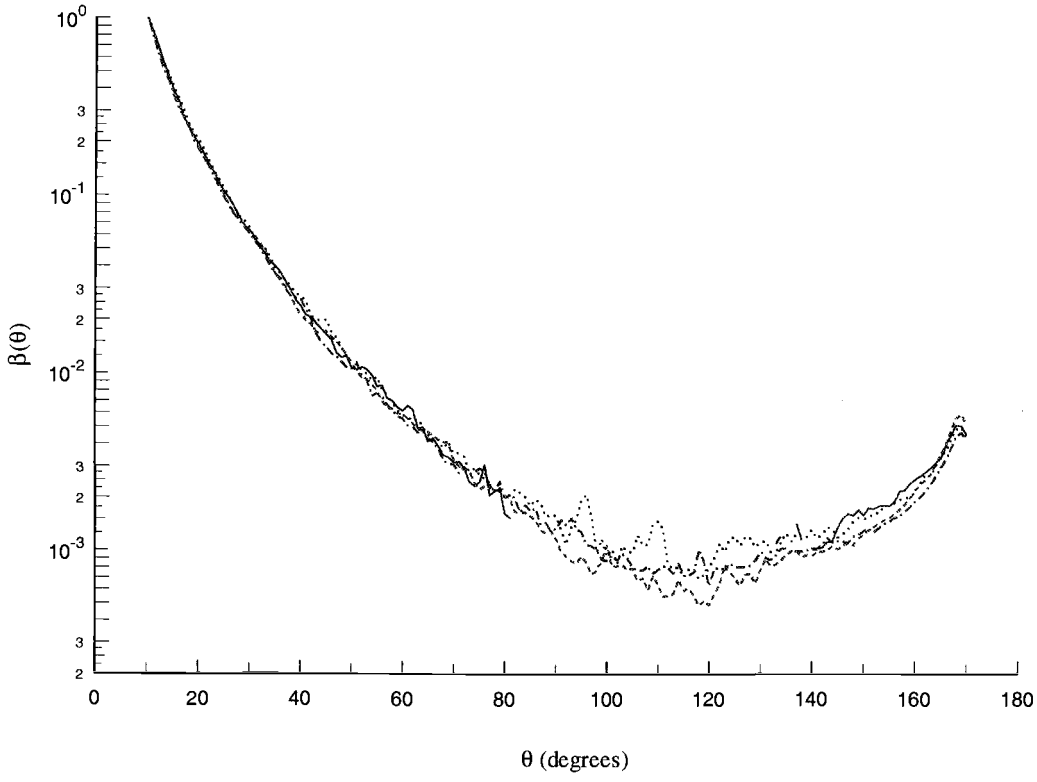

Figure 3.1 Scattering functions at 440, 490, 550, and 670 nm as measured by the general angle scattering meter (GASM) on May 6, 1992, at 15 m depth. The scattering functions are normalized to the value at 10° in order to remove changes in magnitude.

The GASM data was noisy due to the small scattering volume and fluctuations in the number of large particles in the volume. There were also missing points in the scattering minimum normally located just beyond 100° so we chose to use 100° as a cutoff point. The cutoff of 100° simplified the analysis procedure and provided the same results as the regressions to 170°. Petzold's data is given in 5° increments, so that using the 100° cutoff provided 15 data points for the curve fitting. The fitting

method used was a linear least squares regression without a constant. This provided a single multiplier χ such that:

$$\beta_{GASM}(\theta) = \chi\beta_{Petzold}(\theta). \tag{3.9}$$

Since the value of b is determined by Eq. (1) the estimate of b_{GASM} is simply $\chi b_{Petzold}$. We will provide two estimates of b_1 from the fitting method. The first value, b_{1best}, is the estimate of b_1 provided by the curve of Petzold that produced the best fit to the measured curve as determined by the adjusted r^2 value. The second value, b_{1ave}, is the average of b_1 value estimates determined for curves that had an r^2 value >0.99. For the fits with $r^2 > 0.99$ the standard deviation of the b_{1ave} estimates as well as minimum and maximum values of b_1 are used in order to assess the possible range of b_1. In most cases b_{1best} is within one standard deviation of b_{1ave}. The standard deviation determined for b_{1ave} provides an estimate of the error margin of the fitting method, although it does not include the errors associated with the GASM instrument itself. Note that the extrapolation contains approximately 65 % of the total b_1 providing a large possible source of error.

3.5 RESULTS

Since the GASM measurements were made at different wavelengths than the c and a measurements, the first problem is to determine the spectral shape of the scattering function in order to estimate b at the desired wavelengths. A regression was done at each depth for each day to determine if there was a λ^{-n} relationship to the scattering coefficient. Only on May 7 at 60 m was there an n value that was significantly different from 0.0 [n = -1.3 (0.3)]. Since to first order b showed no spectral dependence we will compare values of b(440) to b(456) nm and b(550) to b(532) nm without making any corrections for wavelength dependence. For the case with an observed spectral dependence (May 7, 60 m) we will interpolate the 550 value to that at 532 nm.

Measurements using a Sea Tech, Inc., 660 nm transmissometer indicated that during the experiment there was an attenuation maximum in the upper 20 m of the water column. Below the maximum the value of $c_p(660)$ decreased slowly with depth ($\approx$0.005 m^{-1}/m). Over the three days the value of $c_p(660)$ at the greater depths also decreased slightly. The coefficient of variation for waters deeper than 20 m is 7.5%. In the upper 20 m there are much larger changes as the magnitude and position of the particle maximum changed during each day as well as between days of the experiment.

On May 4 measurements of all three parameters were made simultaneously at 50 m depth. In Table 3.1 the estimated values of b_1 are given as well as the standard deviation, minimum, and maximum values. The estimates of $b_1(456)$ are within the

0.1 m^{-1} estimated error for the c_1-a estimate of b_1. The same is not true at 532nm, however. On the sixth of May the c(532) and a(532) measurements were made one hour prior to the GASM measurements. Near 15 m the transmissometer indicated an attenuation maximum that increased in magnitude and depth throughout the day. The agreement between the two methods is good (Table 3.1 and Figure 3.2).

On May 7 the c(532) and a(532) profiles were obtained half an hour before and after the GASM measurements. Data from both profiles is used to estimate b(532) at the time of the GASM measurements (Table 3.1 and Figure 3.2). As on May 4 the $b_1(532)$ determined by c_1-a is higher than the value of b_1 determined using the GASM data.

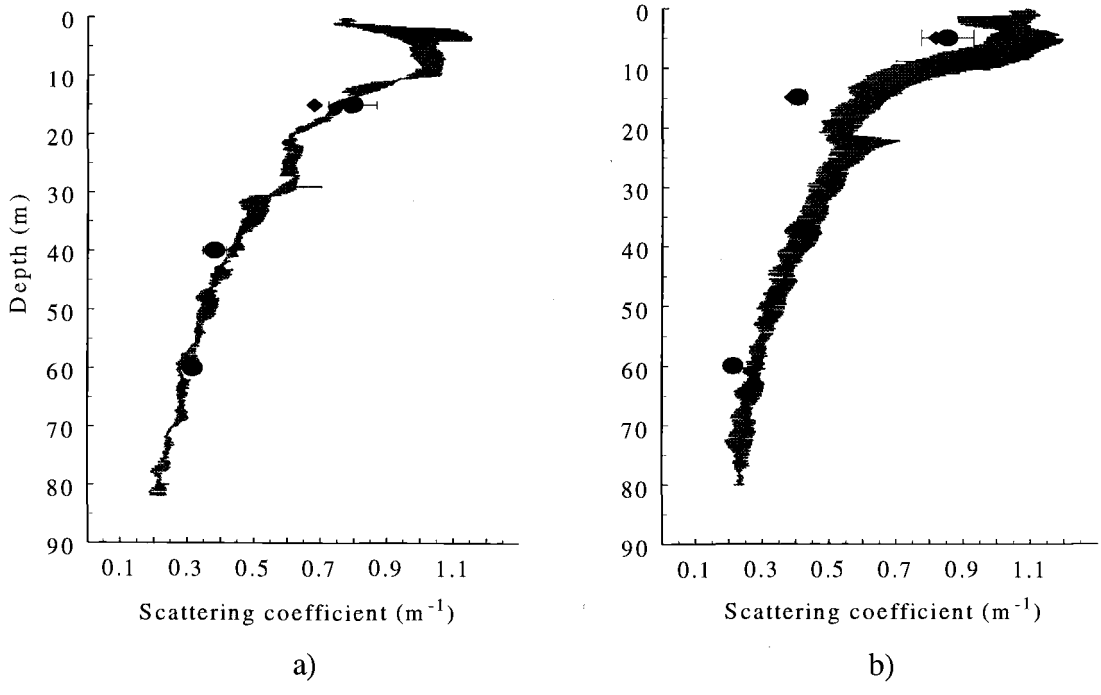

Figure 3.2 Depth profiles of the estimates of $b_1(532)$ from GASM (b_{best}, diamonds, and b_{ave} , circles, plus 1 standard deviation error bars) and $c_1(532)$ - a(532) (solid line) for (a) May 6 and (b) May 7.

Table 3.1 Scattering coefficient determined from the GASM data (440 and 550 nm) and the associated c_1-a measurements (456 and 532 nm). The c_1-a estimates of b_1 are based on an average value for a two meter depth interval centered on the reported depth. The standard deviation reported for the c_1-a measurement is the standard deviation of the two meter interval. The estimated systematic error in the c_1-a measurement is $\pm$ 0.1 m^{-1}.

Date May 4/92	Depth 50m					
instrument	GASM	c_1-a	GASM	c_1-a		
wavelength	440	456	550	532		
b_{1best}	0.343	•••	0.350	•••		
b_{1ave}	0.37	0.446	0.35	0.500		
$sd(b_{1ave})$	0.02	0.004	0.02	0.007		
minimum	0.34	•••	0.32	•••		
maximum	0.39	•••	0.38	•••		
Date May 6/92	Depth 15m		Depth 40m		Depth 60m	
wavelength	550	532	550	532	550	532
b_{1best}	0.68	•••	0.37	•••	0.31	•••
b_{1ave}	0.80	0.75	0.38	0.44	0.32	0.31
$sd(b_{1ave})$	0.07	0.02	0.03	0.02	0.03	0.02
minimum	0.68	•••	0.33	•••	0.27	•••
maximum	0.90	•••	0.43	•••	0.36	•••
Date May 7/92	Depth 5m		Depth 15m		Depth 60m	
wavelength	550	532	550	532	550	532
b_{1best}	0.82	•••	0.39	•••	0.21	•••
b_{1ave}	0.85	1.10	0.41	0.624	0.21	0.28
$sd(b_{1ave})$	0.08	0.08	0.02	0.052	0.02	0.02
minimum	0.72	•••	0.37	•••	0.17	•••
maximum	0.97	•••	0.45	•••	0.23	•••

Since the measurements on the fourth were made simultaneously it is unlikely that a source of error in the comparison can be attributed to natural variability. A 15 minute long time series of the c and a measurements was obtained during the time that

the GASM measurements were made and the time series did not indicate large variability over the short time period of the measurements. If the difference in b_1 estimates cannot be attributed to natural variability then either the method of determining b_1 from the GASM data is at fault or at least one of the instruments was improperly calibrated. If the extrapolation was at fault we would expect consistent differences in the estimates of b_1 for the three days because the particulate properties did not appear to change significantly from day to day. Since the extrapolated portion of the scattering coefficient is so large, small errors in the extrapolation can create large changes in b_1. It is also possible that there may have been some drift in the calibration of the instrumentation over time. In order to determine if one set of instrumentation was more stable over the measurement period we compare the estimates of b_1 to the daily averaged attenuation values measured by a Sea Tech. Inc., transmissometer minus the contribution by pure water [$c_{1p}(660)$]. The attenuation measurements were made at a different location within the well and at different times than the other instruments. Results of the comparison are given in Table 3.2. The c-a estimate at 532 nm on the fourth of May is higher than what appears to be normal. On May 6 the b_{1ave} from GASM appears higher than on the other two days. On average the GASM estimates of b_1 are consistently lower than the c_1 - a estimates which may indicate an error in the extrapolation or in the instrument calibrations.

Table 3.2. The relationships between the b_1 estimates and the measured value of $cp_1(660)$.

Date	Wavelength	Depth	$cp_1(660)$	GASM $b_{Ave}/cp_1(660)$	c_1-a $b_1/cp_1(660)$
May 4/92	456	50 m	0.498	0.74	0.90
	532	50 m	0.498	0.70	1.00
May 6/92	532	15 m	0.797	1.00	0.94
	532	40 m	0.495	0.77	0.89
	532	60 m	0.366	0.87	0.83
May 7/92	532	5 m	1.183	0.72	0.93
	532	15 m	0.684	0.6	0.91
	532	60 m	0.306	0.70	0.90

3.6 CONCLUSIONS

The differences in the estimates of b_1 are not consistent over the three days. On May 6, at two of the three depths, it appears that closure was achieved whereas, on May 4 and 7 it does not appear that closure was achieved. Spatial and temporal variability may account for a portion of the differences in determining b_1 by the two techniques. The significant proportion of the scattering coefficient that must be determined by fitting the measured phase functions to those of Petzold provides a large source of possible error in determining the scattering coefficient from the GASM measurements. It is also possible that one or more of the instruments had calibration drift during the experiment. It is possible that the estimates of b_1 using the GASM data are too low on May 4 and 7 or it could be that the c-a estimate of b_1 was too high on all three days and on May 6 GASM overestimated the value of b_1.

The measurements taken at Lake Pend Oreille do take some steps forward in providing closure of the IOP when compared to the previous closure experiments of Højerslev [1973, 1974]. The instrumentation used at Lake Pend Oreille provided simultaneous measurements of a and c. In one case there were simultaneous measurements of $\beta(\theta)$ and in all cases the measurements of a, c, and $\beta(\theta)$ were made within an hour of each other. Thus, we have reduced the temporal and spatial scales between the individual measurements. We have also provided measurements made on approximately the same spatial scale allowing comparisons to be made without worrying about possible differences in the IOP with scale. Even when closure was not obtained the percentage difference in the estimate of the scattering coefficient is within those observed by Højerslev.

There are still areas for improvement in providing IOP closure. One simple step is to carry out all three measurements at the same wavelength band. Although this step seems obvious it has not been done for any of the three attempts at closure. The small differences in wavelengths in this closure attempt can be worked around but provide an additional and unnecessary source of errors. Two other areas that the errors could be reduced are by measuring the forward scattering component and more frequent calibration of the instrumentation. Measurement of the scattering function between 10° and the acceptance angle of the transmissometer is required in order to remove errors associated with the fitting methods. Improvements in our ability to measure the volume scattering function are essential if we expect to obtain IOP closure. Calibration of the instrumentation during the experiment in addition to the pre

and post-experiment calibrations is needed to remove the possibility of calibration drifts during the experiment.

It is also necessary to improve our scattering correction schemes for the absorption meter. Presently a single correction factor is used although the scattering correction varies with wavelength, particle size distribution, and the optical properties of the particles. Better methods of correcting for scattering errors include using measurements of the absorption coefficient at long wavelengths [*Zaneveld,* 1992]. Such schemes would be able to account for changes in the particle size distribution that the present correction methods do not.

The time and space scales between measurements of the individual IOPs should be reduced further by mounting all of the instruments onto a single platform. Minimizing the distance between measurements will reduce errors in closure that are associated with the natural variability of the water being measured.

Closure of the IOPs does not provide absolute calibration but does indicate whether the devices are producing consistent results. The quality of this relative calibration depends on the temporal or spatial variability of the water column as applied to the measurement sequence. In this paper we have provided a solid theoretical framework for the consistent measurement of the beam attenuation and scattering coefficients based on a practical definition. It is imperative that all radiant energy be accounted for either as being considered directly transmitted or as scattered energy. This allows for closure of the equation of radiative transfer without the need to approach the absolute value of c (which is impossible to measure in any case) or $\beta(\theta,\phi)$

down to zero degrees. For most applications it is desirable to improve our measurement capabilities so that the volume scattering function can be measured to the same angles as the acceptance angle of the attenuation meters.

3.7 REFERENCES

Gordon, H. R., Simple calculation of the diffuse reflectance of the ocean, *Appl. Opt.*, **12**, 2803-2804, 1973.

Gordon, H. R., Sensitivity of radiative transfer to small-angle scattering in the ocean: Quantitative assessment, *Appl. Opt.*, **32**, 7505-7511, 1993.

Højerslev, N. K., Inherent and apparent optical properties of the Western Mediterranean and the Hardagerfjord, *Report 21,* 23 pp, Institut for Fysisk Oceanografi, Københavens Universitet, Copenhagen, Denmark, 1973.

Højerslev, N. K., Inherent and apparent optical properties of the Baltic, *Report 23,* 41 pp, Institut for Fysisk Oceanografi, Københavens Universitet, Copenhagen, Denmark, 1974.

Jerlov, N. G., *Marine Optics,* Elsevier Oceanography Series, 14, Amsterdam, 231 pp., 1976.

Kirk, J. T. O., Monte Carlo modeling of the performance of a reflective tube absorption meter, *Appl. Opt.*, **31**, 6463-6468, 1992.

Maffione, F. A., R. C. Honey, and R. A. Brown, Experiment for testing the closure property in ocean optics, *Proc. SPIE, Int. Soc. Opt. Eng.,* **1537**, 115-126, 1991.

Mobley, C. D., B. Gentili, H. R. Gordon, Z. Jin, G. W. Kattawar, A. Morel, P. Reinersman, K. Stamnes, and R. H. Stavn, Comparison of numerical models for computing underwater light fields, *Appl. Opt.*, **36**, 7484-7504, 1993.

Petzold, T. J., Volume scattering functions for selected ocean waters, *SIO Ref. 72-78,* 79 pp, Scripps Inst. of Oceanogr., La Jolla, Calif., 1972.

Stamnes, K, S.-C. Tsay, W. Wiscombe, and K. Jayaweera, Numerically stable algorithm for discrete-ordinate-method radiative transfer in multiple scattering and emitting layered media, *Appl. Opt.*, **27**, 2502-2509, 1988.

Tyler, J. E., Radiance distribution as a function of depth in an underwater environment, *Bull. Scripps Inst. Oceanogr. Univ. Calif.*, **7**, 363-412, 1960.

Voss, K. J., Electro-optic camera system for measurement of theunderwater radiance distribution, *Optical Engineer.*, **28**, 241-247, 1989.

Voss, K. J., and R. W. Austin, Beam-attenuation measurement error due to small-angle scattering acceptance, *J. Atmosph. and Oceanic Technol.*, **10**, 113-121, 1993.

Wiscombe, W. J., The Delta-M method: rapid yet accurate radiative flux calculations for strongly asymmetric phase functions, *J. Atmos. Sci.* **34**, 1408-1422, 1977.

Zaneveld, J. R. V., Optical closure: from theory to measurement, *in Ocean Optics,* R. W. Spinrad, K. L. Carder, and M. J. Perry editors, Oxford University Press, New York, 283 pp, 1994.

Zaneveld, J. R. V., and R. Bartz, Beam attenuation and absorption meters, *Proc SPIE, Int. Soc. Opt. Eng.,* **489**, 318-324, 1984.

Zaneveld, J. R. V., R. Bartz, and J. C. Kitchen, A reflective-tube absorption meter, *Proc SPIE, Int. Soc. Opt. Eng.,* **1302**, 124-136, 1990.

Zaneveld, J. R. V., J. C. Kitchen, and A. Bricaud, Analysis of in situ absorption meter data, *Proc. SPIE, Int. Soc. Opt. Eng.,* **1750**, 187-200, 1992.

CHAPTER 4

TEMPERATURE-DEPENDENT ABSORPTION OF WATER IN THE RED AND NEAR-INFRARED PORTIONS OF THE SPECTRUM

W. Scott Pegau and J. Ronald V. Zaneveld

Published in *Limnology and Oceanography*
January 1993, 5 pages

4.1 ABSTRACT

The absorption of light by water is important in many studies of hydrologic optics. In this study we looked at the influence of temperature and salinity on the absorption coefficient of water with emphasis on the red and near infrared portions of the spectrum. The absorption coefficient of pure water was found to have a strong dependence on temperature and little dependence on salinity near the harmonics of the O-H bond stretching frequency. Using in situ and laboratory data we found an increase in the absorption coefficient of 0.009 m^{-1} $°C^{-1}$ at 750 nm, and 0.0015 m^{-1} $°C^{-1}$ at 600 nm. In order to properly interpret measurements of optical properties we must understand how environmental parameters, such as temperature and salinity, affect those measurements.

4.2 INTRODUCTION

The absorption of water is a fundamental property that influences the passage of light through the water column. Changes in the absorption coefficient will alter measured light properties such as irradiance and reflectance. It has long been known that temperature affects the absorption coefficient of water at the harmonics of the stretching of the O-H bond (Collins 1925, Luck 1963, Tam and Patel 1979). Effects of salinity on the O-H bond are manifested in the reflectance (Hirschfeld 1985) and Raman scattering (Georgiev et al. 1984). Sullivan (1963) showed that salinity affects the absorption of water in the near-infrared. The influence of temperature and salinity

on the absorption of water in regions of the harmonics are related to formation of tetrahedral-shaped hydrogen bonded macromolecules of water (Walrafen 1967; Whetsel 1968). Increasing temperature and salinity break up the hydrogen bonded water macromolecules. Changes in the proportion of the water macromolecules with temperature or salinity are then seen as changes in the absorption of water at harmonics of the O-H bond stretching frequency. Although it has been understood that environmental parameters modify the absorption of water, there has been little effort to quantify the modification.

The role of temperature in determining the absorption properties of water has recently been reexamined. Højerslev and Trabjerg (1990) recently reported a Δa of $+0.003\ m^{-1}\ °C^{-1}$ from 10 to 30 °C for wavelengths between 400 and 600 nm. Apparent changes, as a function of temperature, of the in situ absorption coefficient measured at 750 nm using a reflecting tube absorption meter developed by Sea Tech, Inc. prompted our study of temperature effects on the absorption coefficient at longer wavelengths.

Our study combines shipboard and laboratory experimental data to investigate the dependence of the absorption coefficient on variations in temperature and salinity. Using our results and interpreting the results of other authors (Collins 1925; Højerslev and Trabjerg 1990), we estimate the size of the change in absorption at the 750 nm absorption maximum and the 600 nm absorption shoulder. We also identify other regions of the spectrum that may have variations in absorption with changes in environmental parameters.

4.3 METHODS

In situ absorption was measured using a reflecting tube absorption meter developed by Sea Tech, Inc. (Zaneveld et al. 1990). The filter used in the absorption meter had a peak value of 750 nm ± 2 nm and a full width half maximum bandpass of 10 nm. A Sea Tech, Inc. transmissometer was used to measure beam attenuation at 660 nm in conjunction with the absorption measurements. These measurements were made from the eastern boundary of the central gyre of the North Pacific Ocean to the Oregon coastal region.

In the laboratory we used a dual beam Cary 118 spectrophotometer to carry out investigations of the temperature and salinity dependence of the absorption spectrum of water. The spectrophotometer was modified to allow a computer to control the scanning wavelengths and to record the measurements. The computer was programmed to measure the transmittance in 1 nm intervals between 800 and 700 nm and in 5 nm intervals from 700 to 405 nm. Samples were placed in one beam and the reference path was left empty. A diffuser plate was placed in front of the photomultiplier tube in order to measure forward scattered light as well as the attenuated direct beam. A nitrogen purge was connected to the sample box to prevent condensation.

Optically clean freshwater was obtained using a reverse osmosis filter. Samples of 400 ml were placed in a covered beaker in a temperature controlled bath. A 10-cm quartz cuvette was then filled with sample water and analyzed using the

spectrophotometer. Another set of samples were obtained by heating the filtered water to near the boiling point and mechanically removing bubbles that formed as the sample cooled. The removal of bubbles in the second set of samples provided filtered water that was not contaminated by gases and microbubbles. Comparisons of the absorption of the two sample waters at identical temperatures showed that microbubbles affected the measured absorption in the blue portion of the spectrum but not in the red. To be able to use both data sets we do not consider the shorter wavelengths in the visible spectrum where effects of microbubble contamination were significant.

A salt water sample with a salinity of approximately 29‰ was prepared using an aquarium salt mix. The artificial seawater sample was passed through a 0.3-mm Nuclepore filter before being placed in the sample cuvette.

Temperature was measured before and after each scan to determine the temperature drift during the sampling period. The spectrophotometer took one minute to scan the 800-700 nm range and another 1.25 minutes to scan the 700-400 nm range. The temperatures listed on all figures are ±0.5°C for measurements at 21°C and ±1.0°C for every ten degrees above or below 21°C.

In order to ensure that changes in absorption measured were not due to changes in the absorption of the sample cuvette we measured the absorption of the empty quartz cuvette at two temperatures. Absorption was measured for a cuvette at room temperature and again after the cuvette had been in a freezer (-10 °C) for 2 hr. The cuvette's absorption coefficient did not display a discernible temperature dependence.

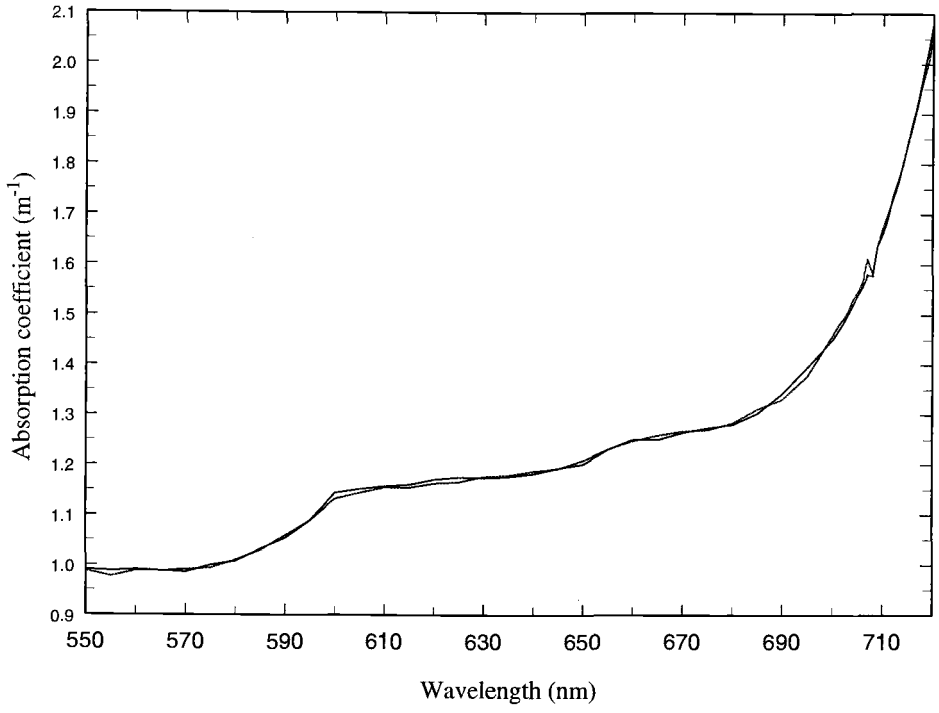

Figure 4.1 Absorption of the sampling system corrected for instrument drift at 21 and 10 °C.

4.4 RESULTS

Højerslev and Trabjerg (1990) suggest that there is a nearly uniform increase in absorption with temperature in the range between 400 and 600 nm. Our results (Fig. 4.1) and previous work (Collins 1925; Tam and Patel 1979) indicate that absorption at 685 nm is invariant with changes in temperature. Since there was no evidence of a uniform increase with temperature, we have adjusted all curves to the value of

absorption at 685 nm as given by Tam and Patel (1979). Correction to this value allows changes in the shape of the curves to be studied easily. It should be noted that we did not determine the absolute value of the absorption coefficient of water. We searched for changes in the absorption coefficient as displayed by changes in the shape of the spectral absorption curve of water. Since there was no evidence that the quartz cuvette was responsible for changes in measured absorption, the changes must be due to changes in the absorption coefficient or index of refraction of water. The changes in the index of refraction would have to be much larger than published values (Austin and Halikas 1976) in order to account for the observed effects. Changes in the index of refraction with wavelength thus contribute very little to the measured changes in absorption.

The apparent correlation between temperature and absorption at 750 nm observed during an oceanographic cruise off Oregon (Fig. 4.2) was the motivation behind this study. The correlation of absorption with temperature indicated a temperature response that was too rapid to be accounted for by temperature drift of the instrumentation. We therefore performed a multiple regression with absorption at 750 nm [a(750)] as the dependent variable with temperature and c(660) (a proxy measure of the scattering error) as the independent variables. At stations in oligotrophic waters the regression analysis gave values of $\Delta a(750)/DT$ ranging from 0.0122 to 0.0142 for regressions with an r^2 value greater than 0.97. For coastal stations the values of $\Delta a(750)/DT$ ranged from 0.0063 to 0.0091 with r^2 values greater than 0.97. The experimental design was not to test the temperature dependence of absorption at 750

nm so we suspect uncontrolled factors caused the differences in the ranges of Δa(750)/DT in the two water types. The consistent and significant dependence of the a(750) measurements on temperature observed at sea prompted the laboratory portion of this study.

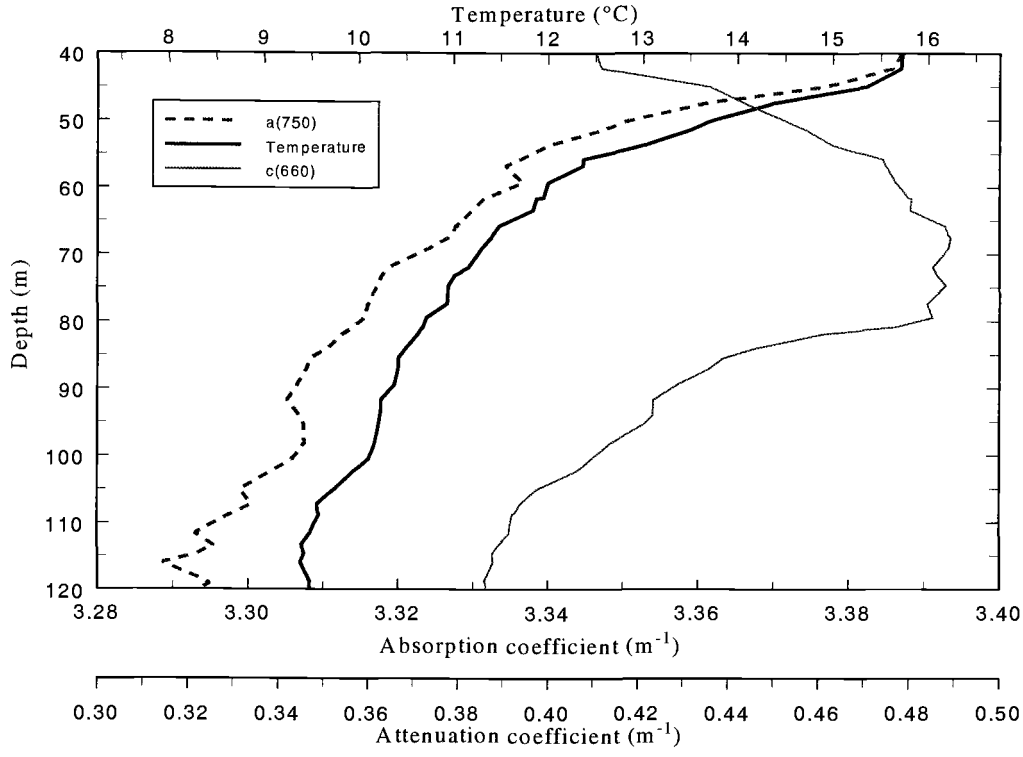

Figure 4.2 Profiles of temperature, a(750), and c(660) from 40 to 120-m depth as measured in the gentral gyre of the North Pacific Ocean.

In laboratory experiments at the 750 nm absorption maximum, absorption increased significantly with temperature (Fig. 4.3). Our results for this region are in good agreement with those of Collins (1925). In both cases the absorption maximum

shifts towards 745 nm with increasing temperatures. In both studies there appears to be a crossover region at approximately 775 nm where there is little or no temperature effect. At wavelengths between 775 and 800 nm an increase in temperature causes a decrease in absorption. At 750 nm both studies show an increase in the absorption coefficient of approximately 0.25 m^{-1} for a 25°C temperature shift within the range of 0° to 30°C, which is the range of oceanographic interest. We found that at a given wavelength the change in the absorption coefficient with temperature is nearly linear (Fig. 4.4). The magnitude of the slope of the linear regression changes with wavelength which represents the shift in the absorption peak.

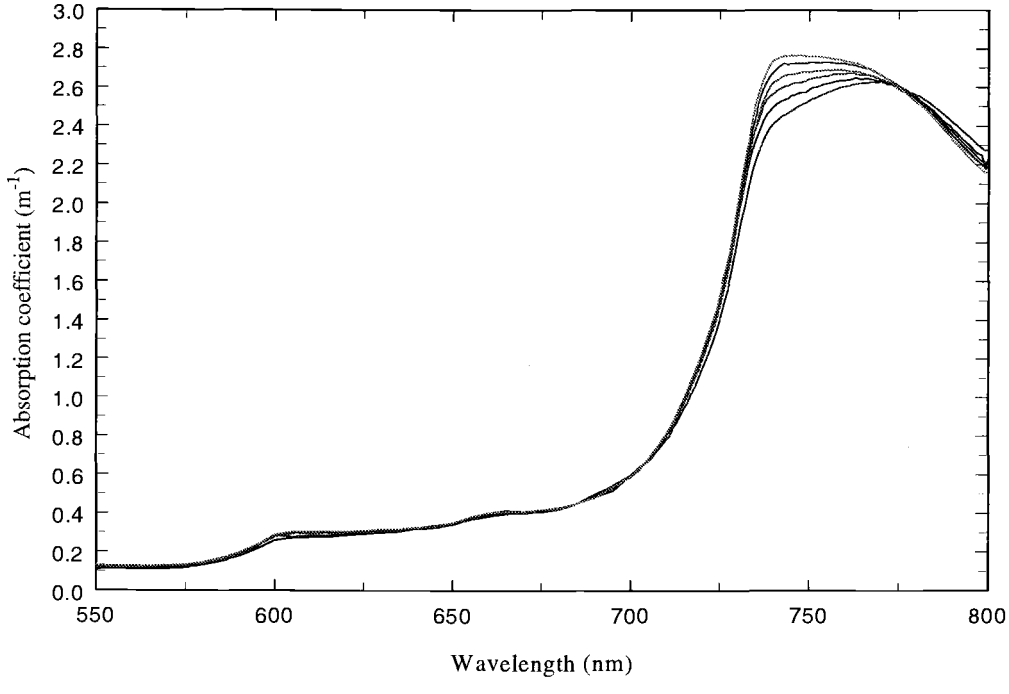

Figure 4.3 Absorption coefficient from 550 to 800 nm adjusted at 685 nm to the value of Tam and Patel (1979). The curves represnt absorption at temperatures of 5, 10, 15, 21, 25, and 30 °C as read from bottom to top at 750 nm.

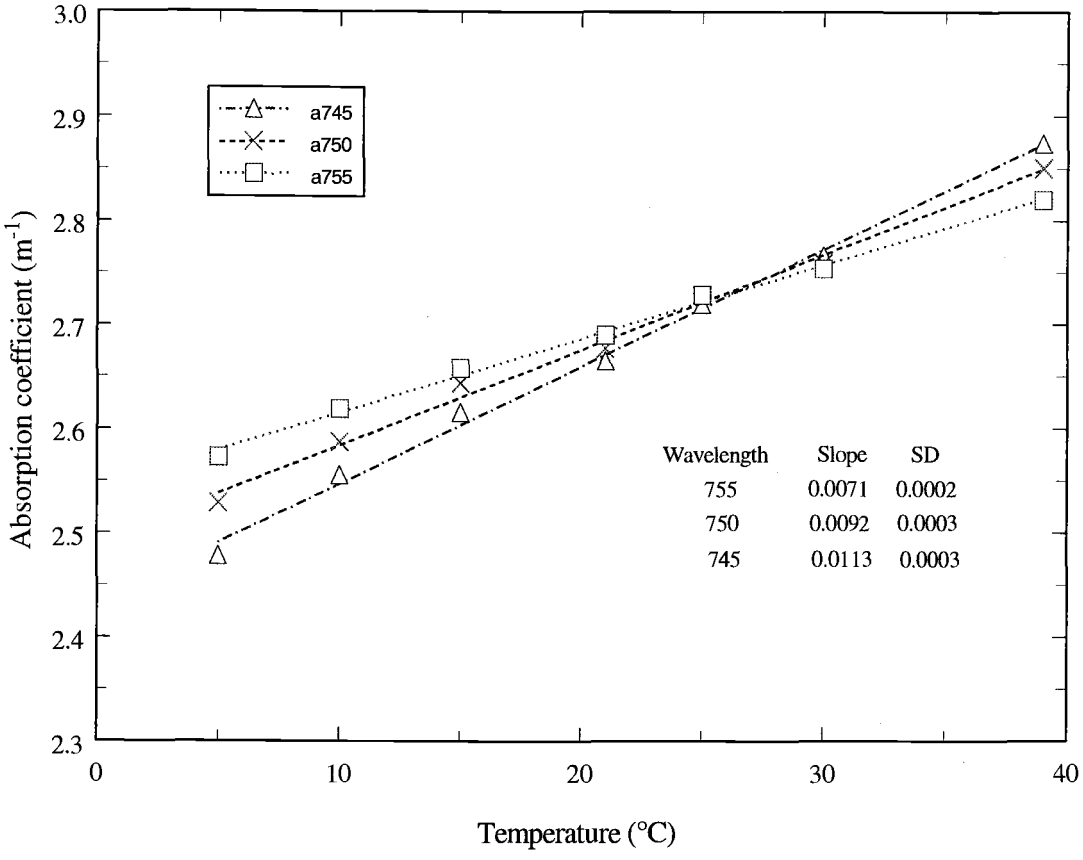

Figure 4.4 Absorption coefficients as a function of temperature. Linear regressions of the absorption coefficients with temperature have r^2 values >0.99 at all wavelengths.

The value of the temperature dependence determined in the laboratory is in good agreement with the in situ values, with the laboratory results ($\Delta a(750)/DT \approx 0.009\ m^{-1}\ °C^{-1}$) being within the range found using the in situ measurements. The $\Delta a(750)/DT$ of 0.009 m^{-1} $°C^{-1}$ implies that for a one degree temperature change there is a 0.36 percent change in the absorption coefficient at 750 nm.

Tam and Patel (1979) report that absorption is temperature dependent at the fifth (600 nm) and sixth (510 nm) harmonics of the O-H bond stretching frequency. Because of scattering by contaminants such as microbubbles it is difficult to observe these lower harmonics with any certainty in our data. Our results do suggest that the absorption shoulder at 600 nm is raised with increasing temperature. There is also a suggestion of a temperature dependent shoulder at 660 nm. The work of Højerslev and Trabjerg (1990) also shows the change in the shape of the curve of the absorption coefficient at 600 nm. Their figure 1 furthermore hints at temperature dependent changes in the shape of the absorption spectrum at 515 and possibly 550 nm. From our measurements and interpretations of figure 1 in Højerslev and Trabjerg we estimate that there is a Δa of 0.01 m^{-1} per 6-7°C at 600 nm, or $\Delta a(600)/DT \approx 0.0015\ m^{-1}\ °C^{-1}$. Using the value of the absorption coefficient from Smith and Baker (1981) at 600 nm (0.245 m^{-1}) gives a 4% change in absorption with a 7°C change in water temperature.

An example of environmental parameters affecting measurements is the apparent negative values of the absorption coefficient for some Gelbstoff measurements. Figure 4.5 is a portion of two Gelbstoff measurements made recently at Lake Pend Oreille, Idaho. For these measurements water samples were collected and filtered through a GFF filter. The filtered water was placed in a dual beam spectrophotometer with a pure water sample in the reference path. The collected water had temperatures as low as four degrees centigrade and the pure water reference was at room temperature. When the Gelbstoff absorption measurements were made the difference in the absorption of water caused an apparent negative absorption of

Gelbstoff in the near infrared. Allowing the Gelbstoff samples to reach room temperature removed the apparent negative absorption. Measurements of Gelbstoff in a water sample is one of the applications of optical measurements in which one needs to take into account the influence of environmental parameters on the measurement itself.

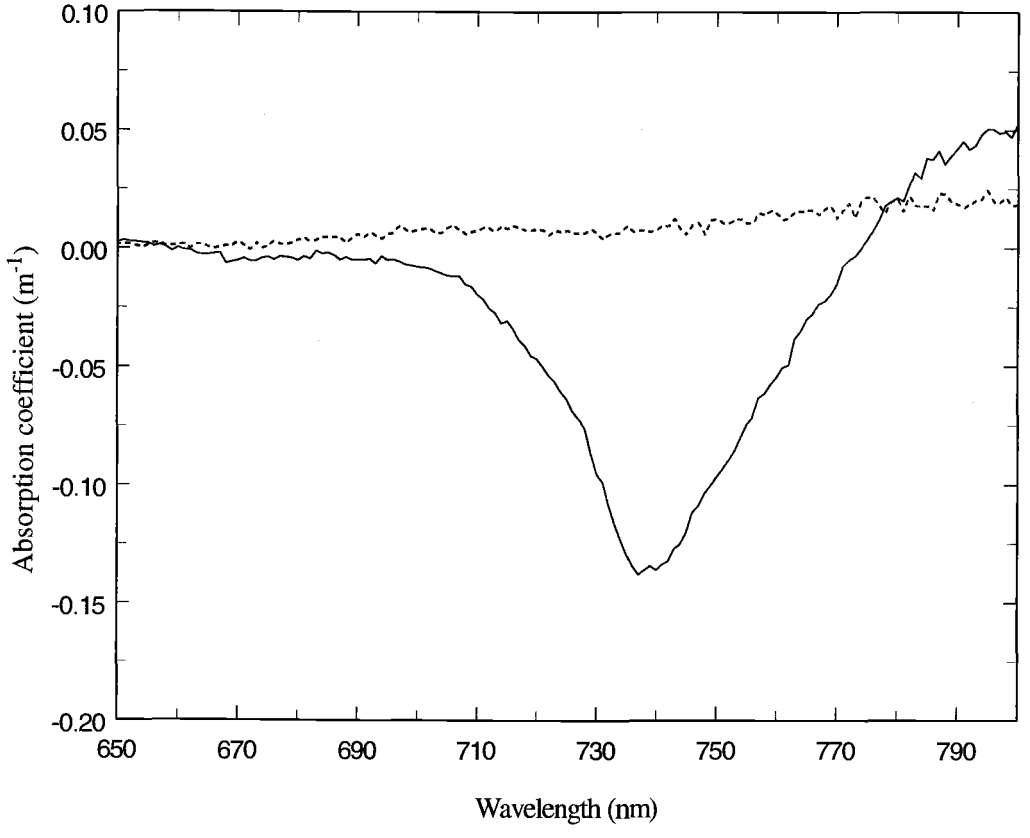

Figure 4.5 A portion of Gelbstoff absorption spectra taken at Lake Pend Oreille. The solid line represents a sample at ~5 °C measured against a warm reference sample in a dual-beam spectrophotometer. This curve implies an apparent negative absorption. The broken line represents a Gelbstoff spectrum when the sample has been allowed to warm to the same temperature as the reference sample.

Sullivan (1963) showed artificial seawater absorbed more strongly than distilled water with a Δa of 0.04 m^{-1} for wavelengths above 735 nm. Our results for the near infrared portion of the spectrum indicated the change in the absorption coefficient between fresh and saline water is about a quarter of that found by Sullivan. Since the artificial seawater that we used was not passed through a reverse osmosis filter we have reason to suspect that there may have been some very small particles in the sample that increased the backscattering error in the measurements at shorter wavelengths preventing us from making observations of the effects of salts in the 600 nm region.

4.5 CONCLUSIONS

The greatest effect of temperature on the absorption coefficient of water occurs at frequencies near the harmonics of the O-H bond stretching frequency. The region of the fourth harmonic's (750 nm) absorption maximum has the largest temperature effect in the portion of the spectrum between 500 and 800 nm. The absorption shoulder in the 600 nm (the fifth harmonic) region also has a significant temperature dependence. Our analysis indicates that temperature may also affect the absorption coefficient at 515 nm, 550 nm, and 660 nm. Our results indicate that the effect of temperature on absorption is much greater than that of salinity.

With the development of in situ measuring devices for absorption and the increased use of remote sensing it becomes imperative that we understand the

influence of environmental properties on absorption in the waters being measured. Our work has been an attempt to identify portions of the spectrum that may be affected by environmental parameters. We have given estimations of the effects of temperature on absorption at the 750 nm absorption peak and 600 nm absorption shoulder. Further research needs to be carried out to identify wavelengths at which the absorption coefficient is influenced by environmental parameters and to quantify the magnitude of these effects. Since the studies of temperature effects on absorption have been restricted to pure water, the effect of temperature on the absorption of saline solutions is still to be studied. When the effects of environmental parameters are understood we will be able to better interpret measurements of absorption and related optical properties.

4.6 REFERENCES

Austin, R., and G. Halikas. 1976. The index of refraction of seawater. Univ. Calif. SIO Ref. 76-1.

Collins, J. R. 1925. Change in the infra-red absorption spectrum of water with temperature. Phys. Rev. **25**: 771-779.

Georgiev, G. M., T. K. Kalkanjiev, V. P. Petrov, and Zh. Nickolov. 1984. Determination of salts in water solutions by a skewing parameter of the water Raman band. Appl. Spectrosc. **38:** 593-595.

Hirschfeld, T. 1985. Salinity determination using NIRA. Appl. Spectrosc. **39:** 740-741.

Højerslev, N. K., and I. Trabjerg. 1990. A new perspective for remote sensing measurements of plankton pigments and water quality. Univ. Copenhagen Inst. Phys. Oceanogr. Rep. 51.

Luck, W. 1963. Beitrag zur assoziation des flüssigen wassers. I die temperaturabhängigkeit der ultrarotbanden des wassers. Ber. Bun. Ges. **67:** 186-189.

Smith, R. C., and K. S. Baker. 1981. Optical properties of the clearest natural waters (200-800 nm). Appl. Opt. **20:** 177-189.

Sullivan, S. A. 1963. Experimental study of the absorption in distilled water, artificial sea water, and heavy water in the visible region of the spectrum. Opt. Soc. Am. J. **53:** 962-968.

Tam, A. C., and C. K. N. Patel. 1979. Optical absorption of light and heavy water by laser optoacoustic spectroscopy. Appl. Opt. **18:** 3348-3357.

Walrafen, G. E. 1967. Raman spectral studies of the effects of temperature on water structure. J. Chem. Phys. **47:** 114-126.

Whetsel, K. B. 1968. Near-infrared spectrophotometry. Appl. Spectrosc. Rev. **2:** 1-67.

Zaneveld, J. R. V., R. Bartz, and J. C. Kitchen. 1990. A reflective-tube absorption meter. *In* Ocean Optics X. SPIE **1302**, p. 124-136.

CHAPTER 5

ABSORPTION OF VISIBLE AND NEAR-INFRARED LIGHT IN WATER: THE DEPENDENCE ON TEMPERATURE AND SALINITY

W. Scott Pegau, Deric Gray, and J. Ronald V. Zaneveld

to be submitted to *Applied Optics*

5.1 ABSTRACT

We have made measurements of the absorption coefficient of pure and salt water at 15 wavelengths in the visible and near infrared regions of the spectrum. The water temperature and salinity were varied to study the effects of these parameters on the absorption coefficient of liquid water. In the near infrared the absorption was found to be highly dependent on temperature. In the visible region the temperature dependence was found to be less than 0.001 $m^{-1}/°C$ except for a small region around 610 nm. The same results were found for the temperature dependence of a salt water solution. In determining the effect of salinity on the absorption coefficient it is important to account for decreasing reflectance at the water-glass interfaces of the instruments with increasing salinity. After accounting for index of refraction effects, the salinity dependence at visible wavelengths is negligble. Salinity does appear to be important in determining the absorption coefficient of water in the near infrared region. At 715 nm, for example, the salinity dependence was -0.00027 m^{-1}/PSU. Field measurements support the temperature and salinity dependencies found in the laboratory both in the near infrared and at shorter wavelengths. To make estimates of the temperature dependence in wavelength regions where we did not make measurements we used a series of Gaussian curves that were fit to the absorption spectrum in the visible region of the spectrum. The spectral dependence on temperature was then estimated based on multiplying the Gaussians by a fitting factor.

5.2 INTRODUCTION

The optical properties of liquid water are the basic building blocks on which hydrologic optics is built. To understand the optical properties of the oceans we must understand the optical properties of liquid water which is the major component of the oceans. The two major mechanisms in which light interacts with water are scattering and absorption. Scattering by water has been studied both theoretically and experimentally. While there are some differences in the estimates of scattering by pure water[1] the connection between theory and experiment is well developed[2]. In contrast, our theoretical and experimental understanding of absorption by water is quite limited. The lack of agreement on the structure of liquid water[3] hampers the task of solving Schrödinger's equation from which we might be able to get a theoretical handle on absorption. Measurement of the absorption coefficient in the visible region (400 to 700 nm) is difficult due to the low absorption values in this region. Contaminants in the water, such as dissolved organics, also interfere with making accurate measurements in the visible region. An illustration of the difficulties in measuring the absorption coefficient of pure water is provided in Figure 5.1. The variability of the measured absorption coefficients shown in the near ultraviolet and blue portions of the spectrum are most likely due to the presence of contaminants. Some of this variability may also be explained by an unaccounted for dependence of the absorption coefficient on temperature. In most studies the water temperature is not reported or accounted for in any way. If a temperature dependence of the order 0.001 $m^{-1}/°C$ throughout the

visible exists[1, 4] it may explain some of the differences between measurements at all wavelengths.

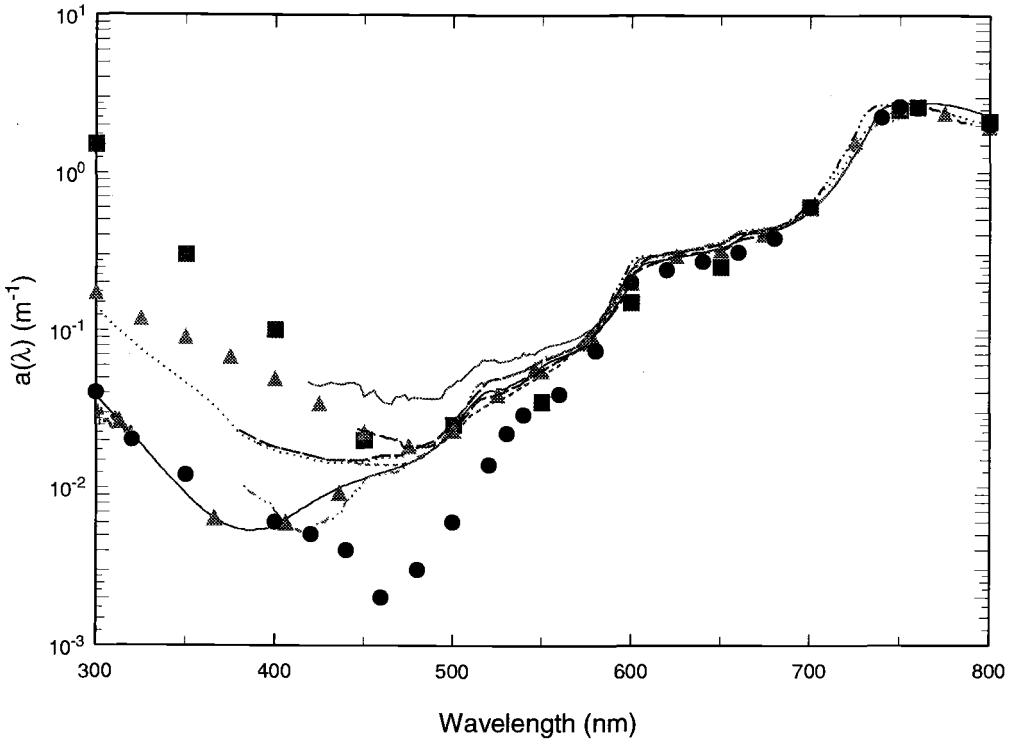

Figure 5.1. The absorption coefficient of pure water as measured or compiled by several investigators [1, 2, 11, 18, 19, 21, 27-33]. The discrepancy in the estimated absorption coefficients is largest at short wavelengths where absorption by organic contaminants is significant. At wavelengths longer than 550 nm the standard deviation of the estimates is between 5 and 10 % of the mean value.

The effects of temperature and salinity are also important in the operation of instruments in which pure water is used as a reference medium[5]. Such instruments include dual beam spectrophotometers and the ac-9 (nine wavelength absorption and attenuation meter). These instruments are used to measure the absorption coefficient

of samples that may have a different temperature or salinity than the reference water. It has been shown that in the near infrared region of the spectrum an apparently negative absorption by dissolved materials may be observed if the temperature difference is not accounted for[6]. In-situ measurements using systems like the ac-9 are made at ambient temperatures and salinities; it is not possible to control the temperature or salinity of the sample. The effect of temperature and salinity on absorption must then be known to interpret the measured absorption values. In either case, when absorption measurements of sea water are compared to a fresh water reference, the salinity effects must be accounted for. Not accounting for the change in the absorption coefficient with temperature or salinity could lead to errors in the measurement of dissolved organic absorption by creating errors in the baseline which have been seen to exist[7]. Measurements of other optical properties, such as remotely sensed reflectance, which depend on the inherent optical properties of water must also account for the possible variability caused by changes in temperature or salinity.

Despite the importance of water in oceanographic studies, the dependence of the absorption coefficient of water on temperature and salinity has not been definitively determined. This is in large part due to the very low absorption coefficients in the visible region, which makes accurate measurements difficult. Højerslev and Trabjerg [4] stimulated the recent interest in the effect of environmental conditions on the absorption coefficient of water. Their work has led to further investigations of the role of temperature on the absorption coefficient of water [1, 6, 8, 9] including the present study. Three of the studies[1, 4, 9] found a constant temperature dependence of order

0.001 $m^{-1}/°C$ throughout the visible region of the spectrum. In our earlier work [6] we were unable to discern such a dependence and the investigation focussed on the change in shape of the absorption spectrum with changing temperature. The constant temperature dependence was not observed in a preliminary study[8]. In the present study we use an increased number of wavelengths and more stable instrumentation to follow up on our preliminary laboratory work.

As was the case with temperature there has been little work done in studying the role of salinity on the optical properties of water at visible wavelengths [10, 11]. In this study we combine the wavelength regions covered in the previous studies to provide a more comprehensive understanding of the effects of dissolved salt on the absorption coefficient. By incrementally changing the concentration of salt we describe how the absorption coefficient depends on salinity over the wide range of naturally occurring salinities.

The absorption coefficient of water has been shown to be dependent on temperature at the overtones of the O-H vibrational frequencies in the infrared and near-infrared portions of the spectrum [6, 12-14]. The absorption by water in the same spectral band has also been shown to depend on salinity [11, 15]. In the present study we use laboratory and field measurements to extend the investigation of the effects of temperature and salinity on the absorption coefficient of water to the visible wavelengths. A goal of this paper is to determine if a linear temperature slope Ψ_T and salinity slope Ψ_S exist so that the absorption coefficient of water can be given as:

$$a_w(\lambda,T,S) = a_w(\lambda,T_r,0) + \Psi_T(T-T_r) + \Psi_S S \qquad (5.1)$$

where T is the temperature, T_r is a reference temperature, and S is the salinity. We furthermore investigate the possibility of a constant temperature dependence at visible wavelengths on the order of 0.001 ($m^{-1}/°C$) as has been reported by other investigators.[1, 4] As a check for possible interactions between temperature and salinity we look for differences in the temperature dependence between pure and saline water solutions. Lastly, we estimate the magnitude of Ψ_T using a series of Gaussians that are fit to the absorption spectrum.

5.3 BACKGROUND

To understand why temperature and salinity should be expected to affect the absorption coefficient of water we review the molecular structure of liquid water.

A water molecule consists of two hydrogen and one oxygen atoms. The two hydrogen atoms are bonded to the oxygen atom at a 104° angle so that water is not a linear molecule. This nonlinearity gives rise to the polar nature of the water molecule that is responsible for many of the unusual properties of liquid water. While these facts are agreed upon, unanimity about the exact structure of liquid water has not been reached[3]. The polar nature of the water molecules allows formation of hydrogen bonds between water molecules creating dimers, trimers, and larger clusters[16]. The strength of the hydrogen bonds is low enough that thermal motion tends to break the clusters apart and thus the number and size of the clusters are dependent on temperature. The addition of ions to water causes larger, more tightly bound clusters, in which the ions

are surrounded by a loose outer shell of water molecules[17]. Both temperature and salinity, therefore, are expected to affect the molecular structure of water which in turn affects the absorption properties of the water.

When light of wavelength longer than 450 nm is absorbed, the energy is transferred to one or more of the vibrational modes of the O-H bond. The three normal vibrational modes are the symmetric stretch, the bend, and the asymmetric stretch. The primary vibrational modes can be seen as peaks in the absorption spectrum of liquid water at 3049, 6079, and 2865 nm, respectively[34]. Higher overtones of the vibrational modes can be seen as peaks and shoulders in the absorption spectrum. Using Pope's measurements of the absorption coefficient of water in the visible region[18] an absorption peak at 740 nm and shoulders at 610, 515, and 450 nm can be seen as shown in Figure 5.2. There are also weak shoulders in the absorption spectrum at 665, and 560 nm. As the water molecules form hydrogen bonds with each other the O-H vibrational frequencies are shifted to longer wavelengths. As the temperature decreases the number of hydrogen bonded molecules increases which causes the absorption peaks to be transferred to longer wavelengths resulting in a decrease in the absorption coefficient at the overtone frequencies.

Light absorption at wavelengths in the ultraviolet is attributed to an electronic transition within the water molecule itself. The peak in the ultraviolet absorption occurs at 147 nm and absorption in the near ultraviolet represents the tail of that absorption maximum[19]. Around 400 nm the absorption tail from the ultraviolet crosses the absorption tail from the infrared and the absorption minimum is located at

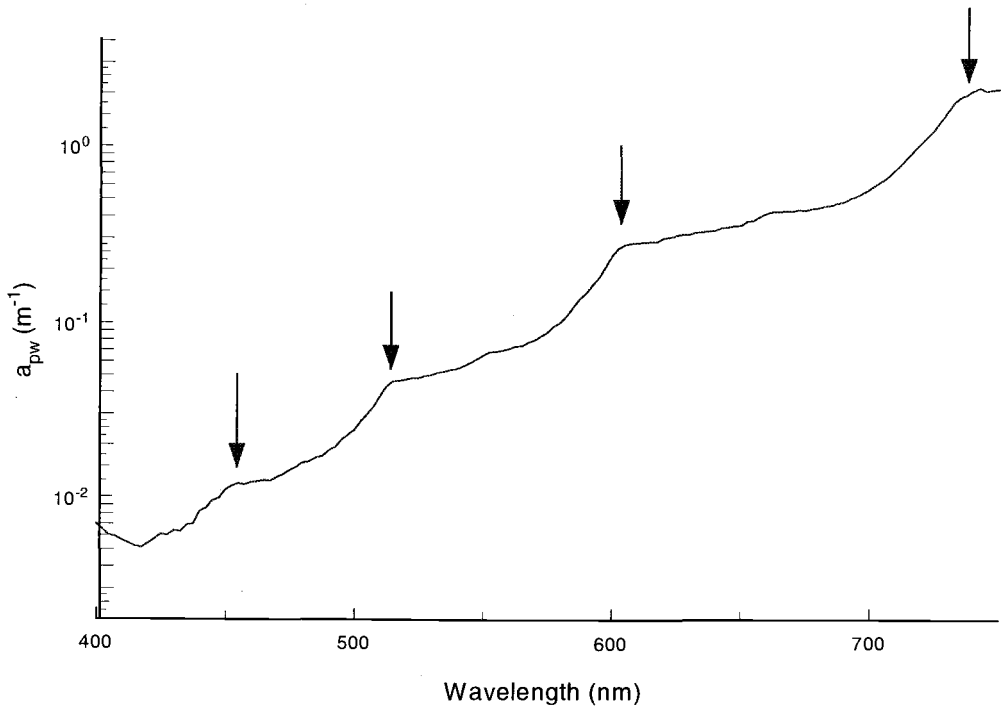

Figure 5.2. The absorption coefficient of pure water as measured by Pope. The arrows point to the major absorption shoulders in the visible and the first absorption peak in the near infrared. Lesser absorption shoulders also exist at 555 and 665 nm.

this junction. At short visible wavelengths it is therefore necessary to consider how the ultraviolet spectrum changes with temperature. There is a dearth of high quality absorption spectrum measurements of water in the ultraviolet with even fewer measurements of the temperature dependence[20]. The results of Halmann and Platzner[20] indicate that the ultraviolet absorption may change by as much as 4% at a reference temperature of 20° for every degree change in water temperature. In the blue portion of the spectrum a maximum expected absorption coefficient[18, 21] of 0.01 m^{-1} would result in a temperature dependence of less than 0.0004 $m^{-1}/°C$.

5.4 METHODS

Measurements of the absorption coefficient were made at discrete wavelengths in the visible and near-infrared using two 25 cm-pathlength WETLabs ac-9s (nine wavelength absorption and attenuation meters) and a 10 cm-pathlength WETLabs a-3 (three wavelength absorption meter) [22]. Temperature and salinity were measured using a SeaBird Electronics SBE-25 CTD. The data streams from the instruments were combined using a WETLabs MODAPS (Modular Ocean Data And Power System) and the combined data was archived on a computer. A time stamp from the MODAPS unit allowed the data streams to be merged based on time which provided a single merged data file.

The wavelengths used in each of the instruments were determined by selection of 10 nm bandpass interference filters. The wavelengths used in the three instruments are given in Table 5.1. Wavelength selection was driven primarily by field use requirements. For example, the a-3 wavelengths were selected to allow measurement of frazil ice crystal concentrations within the water column[23]. The selection of wavelengths however, provides good representation of the blue and green portions of the visible spectrum. Measurements were also made at a few wavelengths in the far red and near infrared regions. The 750 and 975 nm portions represent two of the higher order vibrational overtones in the near infrared.

The plumbing configuration used for the temperature dependence test is shown in Figure 5.3. A reverse osmosis water system was used as the water source. The

water from the reverse osmosis system was then filtered using a 0.2 μm polishing filter before being passed to the temperature control region. To control the temperature the water was fed through a long length of tubing that was immersed in a water bath. The clean water temperature was varied by changing the temperature of the water bath. After passing through the temperature control bath the water was sent to the instruments. The flow tubes of the a-3 and ac-9s were plumbed in series along with the temperature and conductivity sensors of the CTD. Downstream from the conductivity cell outlet a valve was installed to provide backpressure to prevent the formation of bubbles in the tubing. The water flow rate through the system was adjusted to approximately 2 l/min.

Table 5.1. Wavelengths at which the absorption coefficient was measured. The potential error in the central wavelength of these filters is ± 2 nm.

Wavelength	ac-9 117	ac-9 141	a-3 115
412	X	X	
440	X	X	
488	X	X	
510		X	
520	X		
532	X	X	
555		X	
560	X		
650	X	X	
676	X	X	
715		X	
750	X		
850			X
900			X
975			X

The instruments have internal temperature compensation to ensure that changes in the temperature of the electronics do not affect the measurements. We further stabilized the instruments by placing them in a constant temperature bath. This is necessary to ensure that small errors in the temperature compensation of the electronics are not interpreted as variations in the absorption by water.

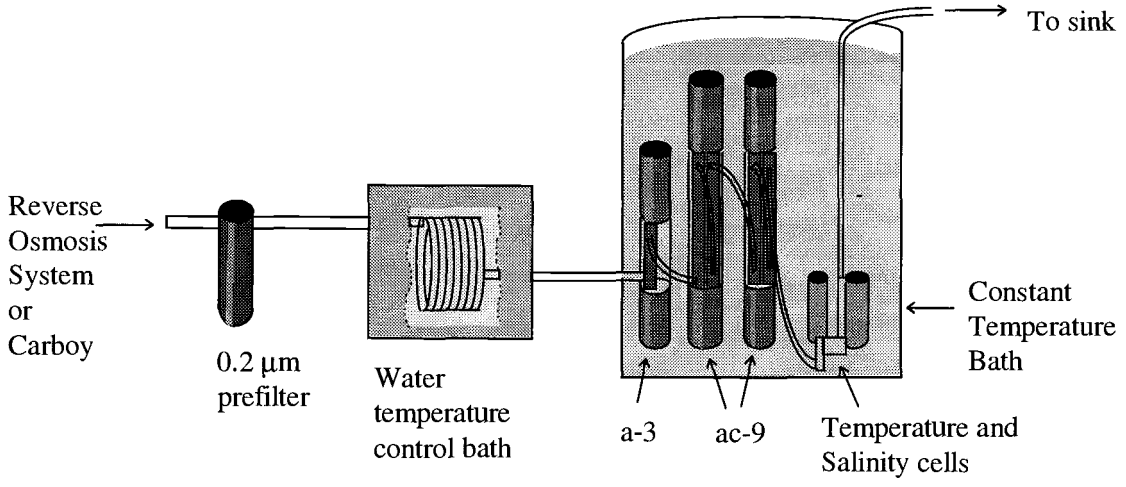

Figure 5.3. A schematic diagram of the plumbing used for this experiment.

For the study of the influence of temperature on absorption measurements, data at a single temperature were collected over a 100 second period. When the data were merged it was necessary to account for the time lag of water reaching the different instruments. At the 2 l/min. flow rate there was a 12.5 second difference between the time a parcel of water reached the first instrument and when it reached the last

instrument. There occasionally was a sharp temperature gradient between water from the cooling coils and residual water left in the lines between runs. This temperature gradient could be observed in at least one channel of each instrument and was used to check the time alignment of the data set. Because the water temperature could vary by a few tenths of a degree during a measurement run, the temperature values were plotted as a function of time to determine a time period in which the temperature had the least variability. A subset of at least 12 seconds of data was collected from the time period with a nearly constant temperature and the absorption and temperature records were averaged over this subset to provide a single data point with a standard deviation. A complete series of data points consisted of such measurements made at eight temperatures between 15 and 30°C. A linear least squares regression was fit to each series of data to provide a slope of the absorption coefficient versus temperature for each wavelength. Five complete series of data and the slopes have been collected to provide an average value of the slopes with a standard deviation.

For tests of the dependence of the absorption coefficient on salinity we used the reverse osmosis water system as a source of water and combined the water with either NaCl or aquarium salts (Coralife scientific grade marine salt). A 20-liter polycarbonate carboy was filled with clean water and salts were added in incremental portions to provide a wide range of salinities. The carboy was pressurized to 10 psi using nitrogen gas. The water from the carboy entered an activated charcoal filter to remove organics and then was sent through the 0.2 μm pore size prefilter and the remainder of the system previously described. A collection carboy was added to allow

the same water to be used in all measurements. By collecting the water we were able to vary the temperature while maintaining a constant salinity. For salinity dependence measurements the collection carboy helped to ensure that the temperature of the saline solution was nearly constant throughout the experiment. Temperature variability throughout an experiment was held to less than 1 °C to minimize the possibility of temperature changes being interpreted as salinity effects. To further reduce the possible temperature effects the measured absorption coefficients were corrected to the mean temperature of each experiment (~21 °C) using the previously determined temperature corrections.

The salinity measurements were made over a longer time period to ensure that there was a complete change of water within the system. The temperature and salinity were plotted to ensure the selection of a time period when the two parameters were stable. A subset of the total data set was again used to provide a single data point.

We used field measurements to verify our laboratory results. The field measurements were made in several locations using the ac-9s. The ac-9s, SBE-25, and MODAPS units were combined on a free-falling platform for profiling. In some instances we installed a 0.2 μm pore size prefilter at the intake of the absorption flow tube of one ac-9. The filter allows us to measure the absorption of the dissolved component directly and allows us to observe changes in the absorption coefficient independent of the influence of particle absorption.

In the field the absorption and attenuation meters were calibrated using water from a Barnstead ® nanopure water system. The water was collected in a 20-liter

polycarbonate carboy. The carboy was then attached to an ac-9 flow tube using teflon tubing. A valve was placed on the outlet of the flow tube to provide back pressure. The carboy was then pressurized to 10 psi using a tank of dry nitrogen and the valve adjusted to provide a flow rate of approximately 1.5 l/min. The data was recorded for the pure water and used as a calibration blank for the instruments. The temperature of the calibration water was also recorded.

When the pure water calibrations are applied to the ac-9s the output of the instruments is the total absorption minus the absorption of the reference medium (i.e. pure water at a given temperature). An error proportional to the scattering coefficient also exists in the measured absorption value:

$$a_m = a_t - a_{wr} + \varepsilon b \tag{5.2}$$

$$a_t = a_p + a_d + a_w \tag{5.3}$$

where a_m is the measured absorption coefficient, a_t is the total absorption coefficient, a_p is the absorption coefficient of the particulate matter, and a_d is the absorption coefficient of the dissolved material, a_{wr} is the absorption coefficient of the reference water, a_w is the absorption coefficient of the water, b is the scattering coefficient, and εb is the scattering error. It is important to remember that a_{wr} is only equal to a_w at one specific temperature and salinity. Thus the measured absorption coefficient can be written as:

$$a_m = a_p + a_d + (a_w - a_{wr}) + \varepsilon b. \tag{5.4}$$

When a 0.2 μm filter is placed on the intake the measured dissolved absorption a_{md} is:

$$a_{md} = a_d + (a_w - a_{wr}). \quad (5.5)$$

In equation 5.5 we have assumed that the scattering by particles passing through the 0.2 μm filter is negligible. Being able to remove the particulate contribution to the measured absorption coefficient makes it easier to study the effects of temperature and salinity on measurements made in the field.

5.5 RESULTS

5.5.1 Laboratory Measurements and Work

5.5.1.1 *Temperature Measurements*

In the laboratory we were able to remove the particulate and dissolved materials allowing us to study the changes in absorption due to water alone. We are also able to maintain the instruments at a constant temperature which removes possible errors due to slight errors in the internal temperature compensation of the instrumentation. We are thus capable of confidently resolving slopes greater than 0.0004 $m^{-1}/°C$. The results of the five temperature dependence tests on pure water and two on salt water are shown in Table 5.2. The results shown in Table 5.2 combine the common wavelengths of the two ac-9s and pool the absorption and attenuation measurements.

It may be expected that the attenuation measurements have a different temperature dependence because the measurements would include the changes in the

Table 5.2. The linear slopes of the temperature dependence of the absorption coefficient measured in the laboratory. For pure water the results of five tests are combined. The results of two tests were combined for the salt water results. The absorption and attenuation meter results have been pooled together as well as pooling the common wavelengths between instruments. The standard deviations of the pooled values are provided.

wavelength	Ψ_T pure water	standard deviation pure water	Ψ_T salt water	standard deviation salt water
412	0.0001	0.0003	0.0003	0.0003
440	0.0000	0.0002	0.0002	0.0002
488	0.0000	0.0002	0.0001	0.0002
510	0.0002	0.0001	0.0003	0.0001
520	0.0001	0.0002	0.0002	0.0002
532	0.0001	0.0002	0.0001	0.0002
555	0.0001	0.0001	0.0002	0.0002
560	0.0000	0.0002	0.0000	0.0002
650	-0.0001	0.0001	-0.0001	0.0001
676	-0.0001	0.0001	-0.0001	0.0002
715	0.0029	0.0001	0.0027	0.0001
750	0.0107	0.0003	0.0106	0.0005
850	-0.0065	0.0001	-0.0068	0.0001
900	-0.0088	0.0001	-0.0090	0.0002
975	0.2272	0.0028	0.2273	0.0009

scattering coefficient with temperature. Morel[2] carried out a thorough analysis of the scattering of pure and salt water based on the Einstein-Smoluchowski equation to obtain the following:

$$\beta_{pw}(90) = \frac{2\pi^2}{\lambda^4} KTn^2 \frac{1}{\beta_T}\left(\frac{\partial n}{\partial P}\right)_T^2 \frac{6+6\delta}{6-7\delta}, \tag{5.6}$$

and

$$b_{pw} = \frac{8\pi}{3}\beta_{pw}(90)\frac{2+\delta}{1+\delta}, \tag{5.7}$$

where $\beta_{pw}(90)$ is the volume scattering function for pure water at 90°, K is the

Boltzmann constant, T is the absolute temperature, β_T is the isothermal compressibility, n is the index of refraction, δ is the depolarization ratio for unpolarized light, and b_{pw} is the scattering coefficient. From equation 5.6 it can be seen that the scattering coefficient is directly proportional to temperature. The index of refraction, its partial derivative with respect to pressure, and the isothermal compressibility are also temperature dependent. There are no measurements of the temperature dependence of the depolarization ratio. Using this equation Buiteveld et al. [1] performed an analysis of the effect of temperature on the scattering coefficient. Their work indicated that between 15 and 30 °C the scattering coefficient decreased by 2.4 percent which translates into a maximum temperature dependence of the scattering coefficient on the order of $-1x10^{-5}$ $m^{-1}/°C$ which is insignificant compared to our observations of the temperature effect on absorption.

Our measured slopes of attenuation versus temperature were between 0.0004 and 0.0001 $m^{-1}/°C$ lower than the absorption versus temperature slopes at the same wavelength. In no case however, was there a statistically significant difference between the absorption slope and attenuation slope. Since there was no evidence that the two measurements should be treated separately we chose to combine the measurements.

Our results indicate that for the measured wavelengths shorter than 700 nm the only wavelength region where there is a possibly statistically significant temperature dependence is at 510 nm (Fig. 5.4). The possible temperature dependence at 510 nm is expected because this wavelength corresponds to the peak of an overtone of the O-H

vibrational frequency. Even if the results at 510 nm are statistically significant, the very small magnitude of the results make the temperature dependence of little practical consequence. The absorption coefficient for wavelengths around 610 nm is also expected to have a significant temperature dependence, but no measurements were made in this wavelength region. For wavelengths longer than 700 nm all measured wavelength bands had a statistically and practically significant temperature dependence.

The results from the present work are combined with the limited number of previous results [1, 6, 8, 9] and displayed in Figure 5.5. Figure 5.5 does not display the spectrally constant temperature dependence in the blue-green portion of the spectrum that is discussed in the works of Højerslev and Trabjerg [4, 9]. The results of this work agree well with our preliminary data[8]. The present work shows slightly higher temperature dependencies at 715 and 750 nm than our 1993 work[6] but agrees well with the earlier results at shorter wavelengths. There is a bias between our results and those of Buiteveld et al.[1] of 0.0011 $m^{-1}/°C$ throughout the visible region. There is also a large difference in the magnitude of the peak temperature dependence in the near-infrared between Buiteveld et al.[1] and other studies [6, 9]. The result reported in Trabjerg and Højerslev [9] that there is a Ψ_T = -0.001 $m^{-1}/°C$ in the blue-green portion of the spectrum is not reproduced in our results. This is most likely due to the fact that our instrumentation does not allow for the long settling times that were required to obtain their result. There is good agreement in the magnitude of Ψ_T between the results of Trabjerg and Højerslev in the yellow and red portions of the spectrum compared to our

present and previous work. The largest difference is in the location of the peak in the temperature dependence with our studies indicating the peak at 740 nm vs. 735 nm reported by Trabjerg and Højerslev. Near the absorption peak at 740 nm Ψ_T changes rapidly, thus small errors in wavelength can create large differences in estimates of Ψ_T. For example, at 715 nm the ±2 nm uncertainty in the central wavelength of the filter creates a range of possible temperature slopes of 0.0023 to 0.0035 $m^{-1}/°C$ depending on the actual central wavelength.

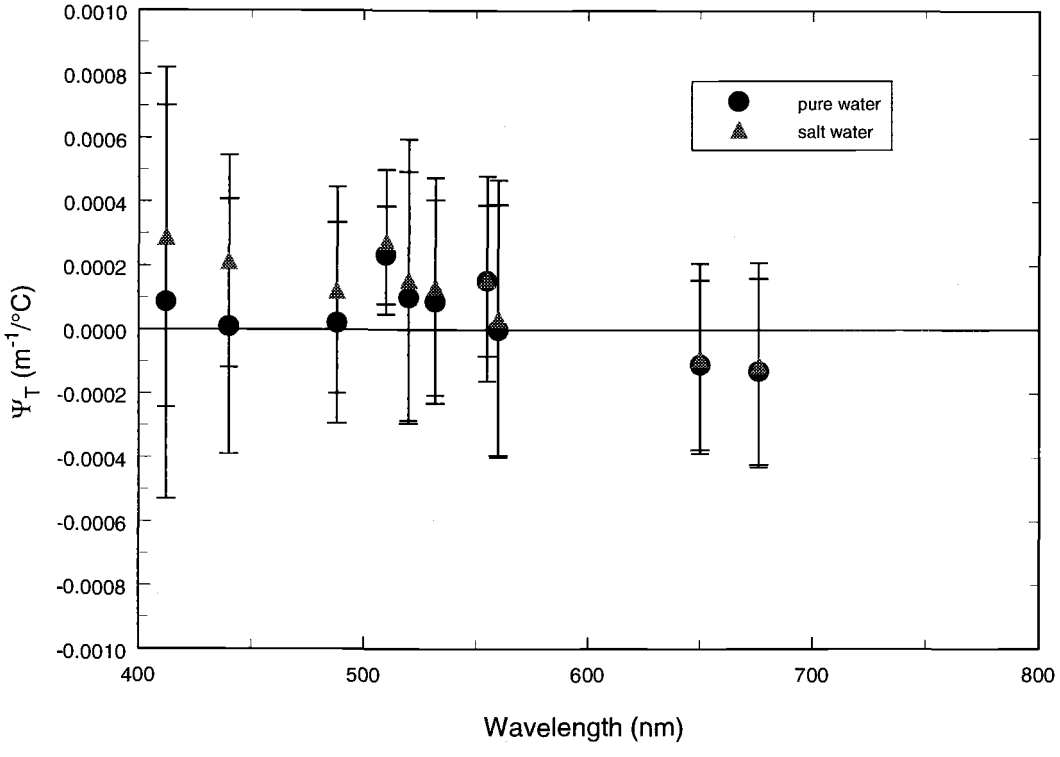

Figure 5.4. The measured temperature slopes (Ψ_T) in the visible. The error bars represent ± two standard deviations of the measurements. There is no significant difference between the values of Ψ_T of pure and saline water.

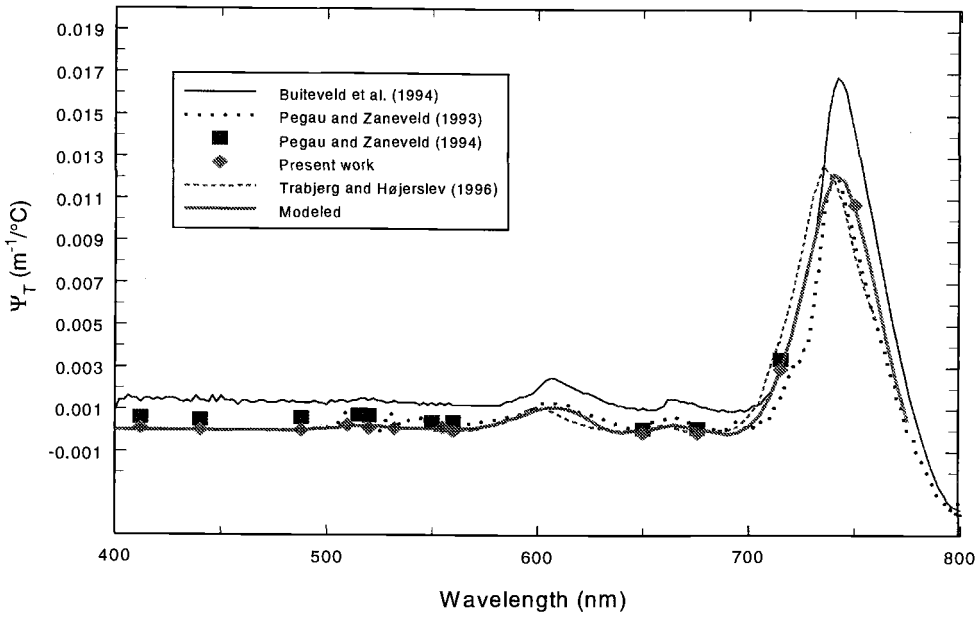

Figure 5.5. A compilation of estimates of Ψ_T. In the visible there is a bias of 0.0011 between the present measurements and those of Buiteveld et al. In regions of the peaks, some of the difference between the measurements may be due to errors in wavelength. When the peaks of Ψ_T are aligned the estimates are more consistent. Included with the measured values is a curve representing an estimate of Ψ_T based on the Gaussians fit to the absorption spectrum. The constant values of Ψ_T (0.003^{4}, -0.001^{9}) reported in the blue and green portions of the spectrum are not provided in this plot.

5.5.1.2 *Temperature Model*

A more complete temperature dependence spectrum can be estimated from a modeled absorption spectrum of water. The absorption spectrum can be simulated by a series of Gaussian curves representing the absorption at the O-H vibrational overtones. It is expected that a continuum of separate Gaussians for each configuration of water molecules would be necessary to properly represent the absorption spectrum. We

found that a good fit to a measured absorption spectrum could be achieved using a single Gaussian for the overtones shorter than 600 nm and a pair of Gaussians for each of the vibrational overtones for longer wavelengths. The pair of Gaussians consisted of one at the absorption shoulder and a second Gaussian at a longer wavelength. The absorption peak at 740 nm required two pairs of Gaussians for a good fit.

To make the temperature dependence spectrum conform to the present and earlier[6] measurements required that the shorter wavelength Gaussian of the pair have a positive dependence on temperature and the longer wavelength Gaussian a negative temperature dependence. This is consistent with the concept that the shorter wavelength Gaussian represented absorption by individual molecules and clusters of a few water molecules. At higher temperatures more molecules would be in smaller clusters and thus the absorption by these molecules would increase with temperature. In contrast, the absorption at the longer wavelength Gaussian would represent absorption by large clusters of water molecules. The number of the larger clusters would decrease with increasing temperature and the absorption would have a negative temperature dependence.

Based on the temperature dependencies measured in this work and in our earlier work [6] in the red and near infrared portion of the spectrum we estimate that the temperature dependence for the Gaussians with peak values in the region of absorption peaks and larger shoulders is approximately 0.5% per degree of the absorption at 20 °C. The smaller absorption shoulders that can be seen in Figure 5.2 at 555 and 665 nm would have a smaller temperature dependence than the more pronounced absorption

maxima and shoulders. Based on our earlier work[6] we estimate the temperature dependence for these shoulders to be 0.2% per degree of the absorption at 20 °C. The small absorption combined with a small temperature dependence prevents us from observing a peak at 555 nm. The measured peaks in the temperature dependence spectrum can be recreated well using the Gaussian curves. The fitted values are shown in Figure 5.5 and in Table 5.3. We estimate that the temperature dependencies obtained from the Gaussian curves are accurate to within ±0.0004 $m^{-1}/°C$ throughout the visible portion of the spectrum.

Table 5.3 The estimates of Ψ_T calculated based on Ψ_T being a percentage of the magnitude of the Gaussian fit to the absorption spectrum of pure water. Outside of the near infrared the only wavelengths with a temperature dependence on the order of 0.001 $m^{-1}/°C$ are near 610 nm. From 400 to 500 nm the value of Ψ_T is <0.0001 $m^{-1}/°C$.

Wavelength	Ψ_T	Wavelength	Ψ_T	Wavelength	Ψ_T
500	0.0001	585	0.0004	670	0.0002
505	0.0001	590	0.0006	675	0.0001
510	0.0002	595	0.0008	680	<0.0001
515	0.0002	600	0.0010	685	-0.0001
520	0.0002	605	0.0011	690	-0.0002
525	0.0002	610	0.0011	695	-0.0001
530	0.0001	615	0.0010	700	0.0002
535	0.0001	620	0.0008	705	0.0007
540	0.0001	625	0.0005	710	0.0016
545	0.0001	630	0.0002	715	0.0029
550	0.0001	635	<0.0001	720	0.0045
555	0.0001	640	-0.0001	725	0.0065
560	0.0001	645	<0.0001	730	0.0087
565	0.0001	650	<0.0001	735	0.0108
570	0.0001	655	0.0001	740	0.0122
575	0.0002	660	0.0002	745	0.0120
580	0.0003	665	0.0002	750	0.0106

5.5.1.3 *Salinity Measurements*

Measurements were made on artificial sea water to determine if the absorption coefficient of water is dependent on salinity. During the first set of measurements organic contaminants in the artificial sea water obscured any possible salinity dependence in the visible portion of the spectrum. The absorption by organics was evident as an exponentially increasing absorption towards shorter wavelengths which could be removed by filtering using an activated charcoal filter. The values of Ψ_S for wavelengths longer than 650 nm are provided in Table 5.4. At these longer wavelengths the absorption by dissolved organics is negligible in its effects on the determination of the salinity slope.

A second set of measurements were made with an activated charcoal filter added to remove organics. Measurements were made on NaCl solutions and artificial sea water. Results are provided in Table 5.4 where the NaCl concentration is provided as an equivalent salinity. Throughout most of the visible wavelengths the salinity slope is less than 0.00015 m^{-1}/PSU. For sea water samples of 35 PSU referenced to fresh water a slope of 0.00015 m^{-1}/PSU represents a 0.005 m^{-1} error. Unlike the temperature results, Table 5.4 does not pool the absorption and attenuation measurements. As can be seen in Figure 5.6, both the absorption and attenuation coefficients were found to be linearly dependent on salinity. The salinity slopes for the two measurements were found to have a statistically significant difference, however. The difference between the Ψ_S values was approximately 0.00015 m^{-1}/PSU at all

Table 5.4 The slopes of the absorption coefficient versus salinity based on linear regression analysis. For wavelengths longer than 715 nm only two samples were obtained. A constant of 0.00005 has been added to each measured Ψ_S to correct for changes in the primary reflectance at the instrument windows due to changes in salinity. Higher order reflections which are important in the absorption meter have not been accounted for in these results.

Wavelength	Ψ_S absorption	standard deviation absorption	Ψ_S attenuation	standard deviation attenuation
412	0.00023	0.00005	0.00012	0.00005
440	0.00013	0.00002	-0.00002	0.00002
488	0.00013	0.00002	-0.00002	0.00002
510	0.00014	0.00003	-0.00002	0.00003
532	0.00009	0.00006	-0.00003	0.00006
555	0.00013	0.00003	-0.00003	0.00003
650	0.00015	0.00003	0.00000	0.00003
676	0.00012	0.00002	-0.00002	0.00002
715	-0.00013	0.00006	-0.00027	0.00006
750	0.00075	0.00001	0.00064	0.00003
850	-0.00039	0.00001		
900	-0.00269	0.00003		
975	0.00226	0.00065		

wavelengths. In every case the Ψ_S for the attenuation coefficient was less than that for the absorption coefficient. Our results are presented together with the earlier results [10, 11] in Figure 5.7. From this figure it can be seen that our results lie well within the previous results.

The effect of reduced primary reflectance at the instrument windows with increasing salinity must be accounted for in the salinity measurements. The change in the index of refraction with salinity is approximately five times greater than that for temperature given the range of temperature and salinities used in this experiment[24].

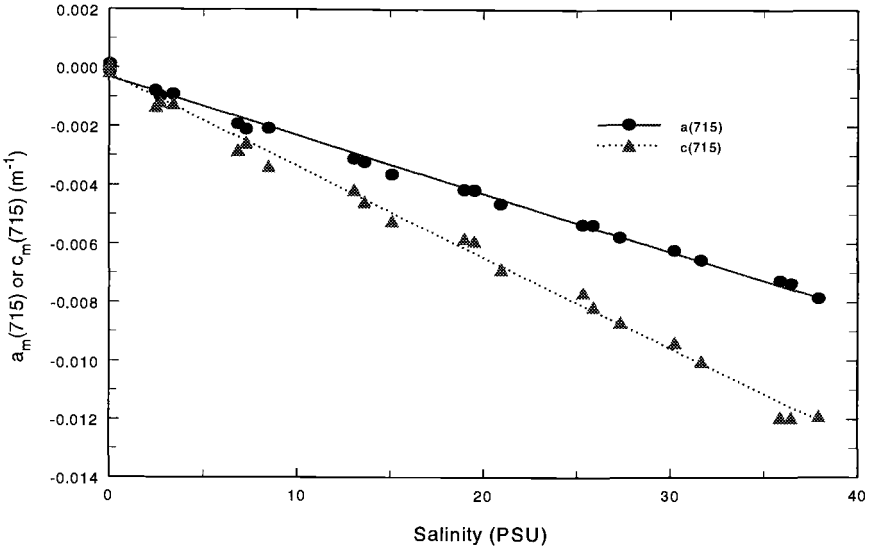

Figure 5.6. The absorption and attenuation coefficients at 715 nm as a function of salinity. Both parameters have a linear dependence on salinity but the slope of the dependence is significantly different for the two parameters.

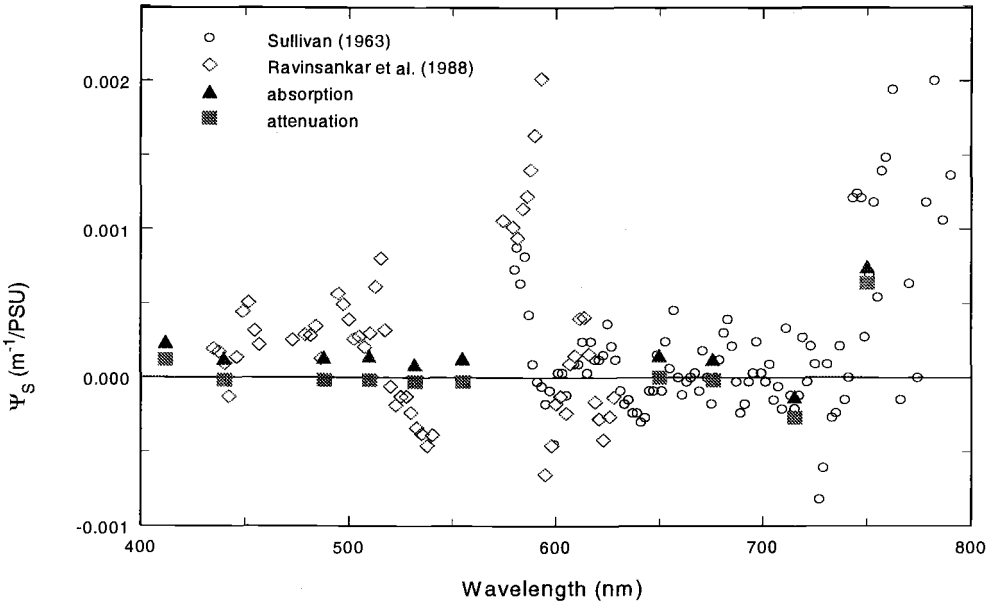

Figure 5.7. Our salinity results combined with the results of previous investigations. The two sets of results are in good agreement even allowing for the difference in slopes between our absorption and attenuation coefficients.

The index of refraction changes in a linear manner for the measured salinity range[24] which could add a linear dependence on salinity that is not related to changes in the absorption properties of water. Calculation of change in the reflectance at the fused quartz windows indicates that a change of salinities from 0 to 35 PSU causes the instruments to read 0.0017 m^{-1} lower. This may not seem important but it does represent a 0.00005 change in the measured value of Ψ_S for visible wavelengths. After accounting for the change in the reflectance at the windows the salinity slope in the visible region as measured using the attenuation meter is not significantly different from zero except at 412 nm.

A second effect must be accounted for in the absorption meter which contains a diffuser between the reciever window and the detector. Because of the potentially large portion of light reflected from the diffuser into the window we must account for multiple reflections within the window. As salinity increases, the index of refraction match between the water and window allows more light to be lost back into the sample water. The effect is to provide an apparent increase in the absorption coefficient with increasing salinity. If the diffuser reflected in a lambertian pattern, one half of the light received, the change in multiple reflections within the window could yield a $\Psi_S \approx$ 0.0005 m^{-1}/PSU. While the characteristics of the diffuser are not fully known, we suspect that the transmittance is higher and the diffusion pattern has less light at the larger angles than a lambertian. We thus expect that the multiple reflection effect is smaller than 0.0005 m^{-1}/PSU and is most likely the cause in the physically unrealistic

difference between the salinity slopes measured by the absorption and attenuation meters as shown in Figure 5.6.

5.5.2 Field Measurements

While the laboratory work is necessary for understanding how the absorption by water is affected by temperature and salinity, it is important to verify that the laboratory results make sense when applied to field measurements. During various cruises we have collected a large number of measurements of total absorption coefficients and dissolved-component absorption coefficients. We use the dissolved absorption results to discuss the dependence of field measurements on temperature and salinity for several reasons. First, the absorption by particulates is removed so that there is one less confounding factor. Second, the absorption by dissolved materials is low in the near-infrared portion of the spectrum where, based on the laboratory results, we expect the largest dependence on temperature and salinity.

A vertical profiles of the measured absorption by dissolved materials is shown in Figure 5.8. While the absorption by dissolved substances is not constant throughout the profile, the only wavelength in which the absorption coefficient seems to have an obvious correlation with temperature or salinity is 715 nm. Taking a closer look at the

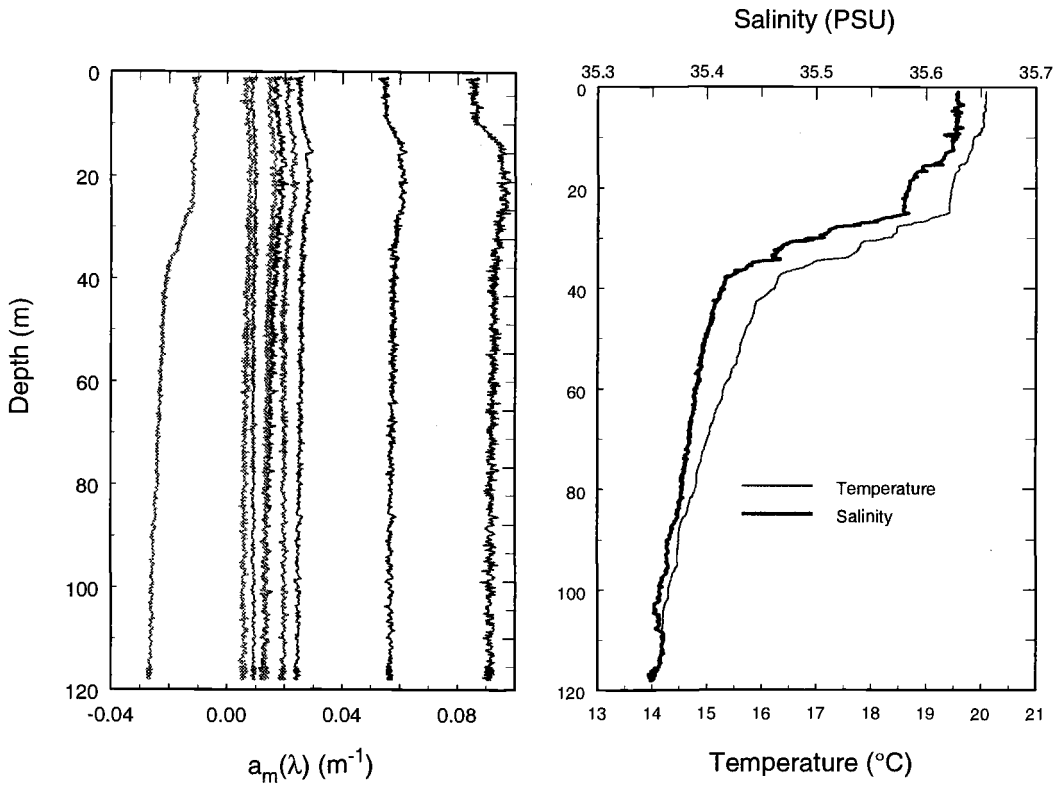

Figure 5.8. A profile of absorption of water passed through a 0.2 μm filter and the physical parameters temperature and salinity. Wavelength decreases from 715 nm at the left to 412 nm at the right. At 412 and 440 nm there is evidence of variability in the concentration of dissolved organics. Only at 715 nm is there evidence of changes in the measured absorption related to the physical parameters.

has a much different vertical profile than $a_{md}(650)$ (profiles A and D on figure 5.9). The vertical shape of the measured profile of $a_d(715)$ is changed to that of $a_d(650)$ when the measured absorption in the red and infrared shows the dependence of the absorption coefficient at 715 nm on temperature and salinity. Figure 5.9 illustrates the effect of applying the laboratory temperature and salinity corrections to $a_{md}(715)$. It can be seen that the measured $a_{md}(650)$ was nearly constant with depth. There is little

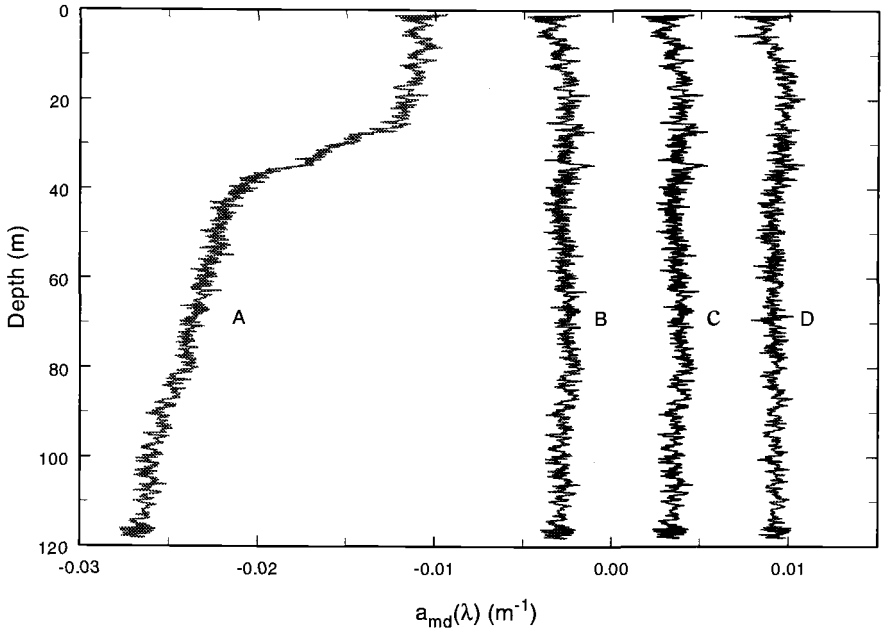

Figure 5.9. The laboratory values of Ψ_T and Ψ_S are applied to field measurements of $a_m(715)$ for water that has been passed through a 0.2 μm filter. Curve D is $a_m(650)$ and is expected to be similar in shape as well as slightly greater in magnitude than $a_m(715)$. Curve A is the measured value of $a_m(715)$. Curve B is $a_m(715)$ with the temperature correction applied. Note that curve B is similar to D but the magnitude is less than zero. Applying the salinity correction to the temperature corrected $a_m(715)$ gives curve C. Curve C is of the same shape and magnitude for the dissolved component given D as a reference.

expected difference between the vertical structures of $a_d(715)$ and $a_d(650)$ so that we expect the two wavelengths to have similar profiles. The measured $a_{md}(715)$, however, temperature correction is applied (profile B, figure 5.9). Even after the temperature correction is applied the measured value of $a_d(715)$ remains negative implying that the water is clearer than the calibration water. Because the range of salinity is small over this profile the salinity correction merely adds a constant related to the difference in

absorption between the pure and saline waters. Once the salinity correction given in Table 4 is applied, the $a_d(715)$ value becomes positive and slightly less than $a_d(650)$ in magnitude as would be expected for measurements of dissolved materials (profile C, figure 5.9). Measurements that include the particulate absorption also show the temperature and salinity dependence of the absorption coefficient at 715 and 750 nm (Fig. 5.10).

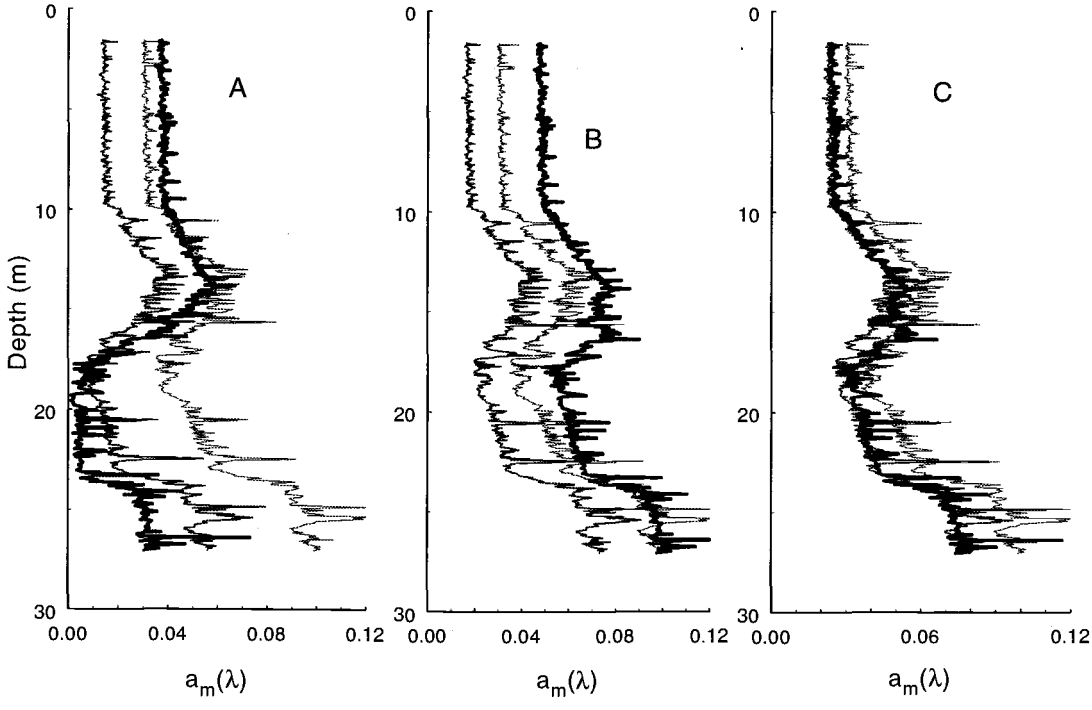

Figure 5.10. The application of temperature and salinity corrections to $a_m(715)$ (medium thickness line) and $a_m(750)$ (heavy line), compared to $a_m(650)$ (thin line) for samples of sea water absorption including both particulate and dissolved materials. Panel A gives the measured values. Panel B represents application of the temperature correction. Panel C is the data after both the temperature and salinity corrections have been applied.

If the temperature dependence in the visible region was on the order of 0.001 $m^{-1}/°C$ as has been suggested,[1, 4, 9] we should be able to see evidence of its effect on the measured profiles. We occasionally find vertical profiles of dissolved material absorption that are constant with depth even though a thermal structure may exist (Fig. 5.11). The application of a temperature correction of ± 0.001 ($m^{-1}/°C$)

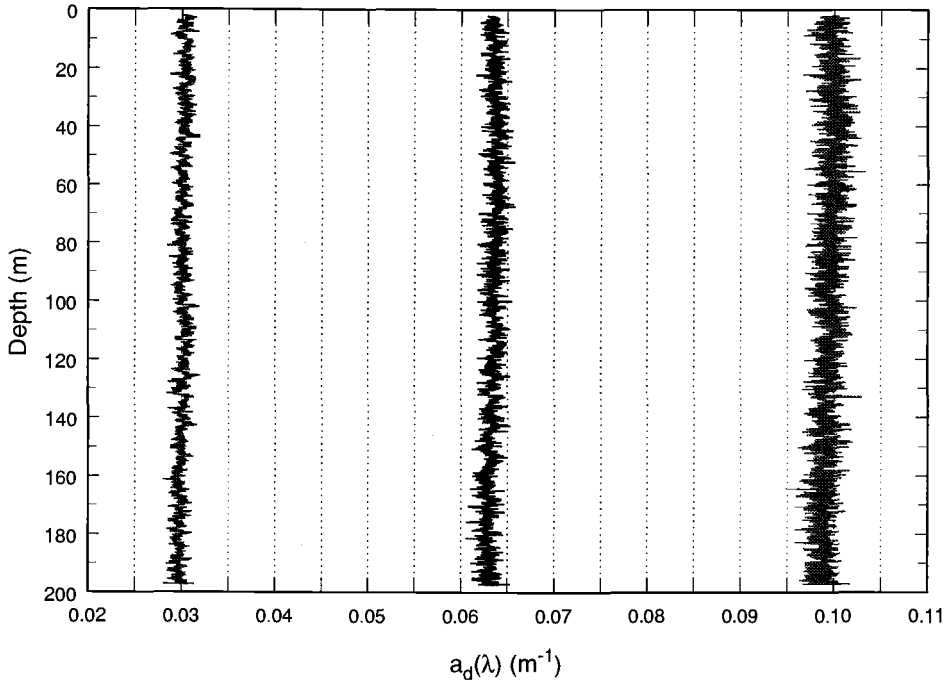

Figure 5.11 From left to right are the measured values of absorption by the dissolved component at 488, 440, and 412 nm. The water temperature changed by 5° over the depth of the profile. If the proposed constant temperature dependence of the order of 0.001 ($m^{-1}/°C$) existed, a change in the concentration of dissolved matter may compensate for the expected change in water absorption. However, a change in absorption by dissolved materials cannot match the expected change in water absorption at all three wavelengths. Since all three wavelengths exhibit the same vertical profile there cannot be a constant value of Ψ_T in the visible.

then causes the vertical profile of the dissolved absorption to mimic the temperature profile. There is a chance that at one wavelength the change in dissolved material absorption with depth compensates for the change in water absorption providing a vertically constant absorption profile. For the case in Figure 5.11 there was a 5° change in water temperature over the profile depth. If the measured $a_d(488)$ was constant because the dissolved absorption compensated for changes in the water absorption there would be a $\Delta a_d(488) = 0.005\ m^{-1}$ from the top of the profile to the bottom. Assuming that dissolved absorption can be modeled using an exponential function with 488 nm as a reference wavelength [25]:

$$a_d(\lambda) = a_d(488)*\exp(-0.015*(\lambda-488)) \tag{5.8}$$

then the expected $\Delta a_d(412)$ would be $0.016\ m^{-1}$. Subtracting the constant temperature dependence of $0.005\ m^{-1}$ leaves an expected change of $0.011\ m^{-1}$ which is not evident in Figure 5.11. Thus the field measurements do not support a constant temperature dependence on the order of $0.001\ m^{-1}/°C$ in the visible portion of the spectrum.

In cases where the absorption by dissolved materials does not vary with depth, the coefficient of the temperature dependence can be estimated by regressing the measured $a_d(\lambda)$ against temperature. The temperature variation in a typical profile is most often less than ten degrees. Combined with the small expected dependence of the absorption coefficient on temperature, the expected change in magnitude is in the third decimal place of the measurements. Errors in the temperature compensation of the

electronics can cause the measured absorption coefficients to vary at this level making it difficult to separate the two effects. A check on the quality of the electronic temperature compensation can be achieved by looking at both the up and down portions of a cast. Wavelengths with imperfect temperature calibrations will have a hysteresis in the profile related to the large thermal mass of the instrument. By performing a linear regression of the measured dissolved absorption against the temperature for the profile provided in Figure 5.11 we have estimated the magnitude of the temperature dependence for the wavelengths measured. The results of the regression analysis are provided in Table 5.5. With the exception of 555 nm the field results are in excellent agreement with the laboratory tests. The difference at 555 nm is attributed to instrumental temperature compensation errors.

Table 5.5 Slopes of linear regression of dissolved absorption coefficients measured in the ocean versus temperature. The data used is that presented in Figure 10 where the dissolved material absorption appears to be constant with depth. The up and down casts have been evaluated to ensure that the internal temperature compensation affected the measurement by less than 0.002 m^{-1}. While this is a small number it still represents a possible slope error of 0.0004 $m^{-1}/°C$. It is also possible that there is some vertical variability in dissolved material concentration which would affect the results most strongly at the shorter wavelengths.

Wavelength	Slope
412	0.0003
440	0.0002
488	0.0001
510	0.0004
555	0.0005
650	-0.0002
676	0.0001
715	0.0027

5.6 CONCLUSIONS

Our results verify that linear slopes can be used to correct the absorption coefficient for changes in both temperature and salinity encountered in natural waters. The temperature dependence was not statistically different for pure and saline water indicating that it is possible to ignore interaction terms of temperature and salinity in making corrections to the absorption coefficient.

The effects of temperature appear to be restricted to the central wavelengths of the overtones of the O-H vibrational frequencies. Neither laboratory nor field data provides any evidence of the previously reported [1, 4, 9] spectrally-constant temperature dependence in the visible region. The disagreement with the results of Trabjerg and Højerslev [9] in the blue-green portion of the spectrum is likely due to our inability to reproduce the long settling times that were required to obtain their results. With the exception of wavelengths near 610 nm it would appear that the magnitude of Ψ_T is less than 0.001 $m^{-1}/°C$ throughout the visible region of the spectrum. The measured temperature dependencies were modeled with a series of Gaussians fit to the absorption spectrum. The Gaussians peaked in the regions of the major absorption shoulders and the peaks had a temperature dependence of 0.5% of the magnitude of the Gaussian.

As was true with temperature the only significant salinity dependence measured was in the near infrared portion of the spectrum. Since temperature and salinity affect the absorption of liquid water by changing the molecular structure, we would not

expect salinity to cause variations in the absorption coefficient in regions where temperature is not important. The addition of ions affects water in a different manner than changing temperature [17] so that the direction of the temperature and salinity dependencies need not be the same. This is the case at 715 nm where increasing temperature increases the absorption coefficient but increasing salinity decreases the absorption coefficient. At wavelengths in the near infrared the magnitude of the salinity dependence was much less than the temperature dependence. Extrapolating this result into the visible region, we would expect the salinity dependence in the visible region to be negligible as was confirmed by the salinity effect on the measured attenuation coefficients. The only measured significant salinity dependence in the visible region was at 412 nm. The expected increase in the scattering coefficient[2] accounts for about half of the value of Ψ_S. The remainder may be the result of absorption by a salt or a shift in the ultraviolet absorption peak towards longer wavelengths. Without measurements at shorter wavelengths it is not possible to isolate the cause of the change in Ψ_S.

It is important to account for the changes in reflection at the water-glass interface with increasing salinity. The reflection properties of the attenuation meter are better understood than the absorption meter; therefore the values of Ψ_S from the attenuation meter are more accurate. Changes in the amount of light reflected back towards the diffuser, as a function of changes in the index of refraction, in the absorption meter cause the instrument to give an incorrectly high value of Ψ_S. Without knowing the spatial distribution of the reflected light and the exact transmittance of the

diffuser we cannot determine the magnitude of this error. The difference between the values of Ψ_S determined by the absorption and attenuation meters is well within a realistic range of possible error values, however. Because we cannot fully account for the difference in Ψ_S the values in Table 4 should be considered to have a possible error of ± 0.00015 m^{-1}/PSU with the true value most likely being near that measured by the attenuation meter. This error is smaller than the variability in earlier measurements[10,11].

The degree of precision in the slopes that is necessary to compensate observed values is generally different for temperature and salinity. The temperature of the calibration or reference water is commonly within 10 to 15 degrees of the water to be measured. A 0.0002 m^{-1}/°C error in the value of Ψ_T becomes a 0.003 m^{-1} error in the measured absorption value for a ΔT of 15 degrees. However, the reference water usually has a salinity of 0 PSU and sea water samples typically have a salinity of 35 PSU, which creates a 0.007 m^{-1} measurement error for a 0.0002 m^{-1}/PSU error in the value of Ψ_S. For the highest accuracy it is also important to account for the changes in reflectance at the windows when referencing a sea water sample to pure water. It is especially important for the interpretation of results from instruments such as the ac-9 to use the measured salinity dependences which include instrumental index of refraction effects as well as changes in the absorption coefficient of water.

The result that the absorption coefficient of water is dependent on the temperature and salinity is important to investigators that measure the optical properties of natural waters in the near infrared. For example, when the absorption coefficient at a wavelength in the near infrared is used for estimating the scattering

error in a measurement [26] it is important to account for the differences in temperature and salinity between the sample and the reference water. Variations in the optical properties of water may also account for baseline offsets that reportedly plague dissolve material absorption measurements. [7] These baselines commonly are obtained from measurements in the near infrared where the effects of temperature and salinity are largest.

5.7 REFERENCES

1. Buiteveld, H., J. M. H. Hakvoort, and M. Donze, "The optical properties of pure water," in *Ocean Optics XII,* J. S. Jaffe, ed., Proc. SPIE, **2258**, 174-183, (1994).

2. Morel, A., "Optical properties of pure water and pure sea water," in *Optical aspects of oceanography,* N. G. Jerlov & Nielsen, E. S., eds., (Academic Press, London, 1974), pp. 1-24.

3. Everett, D. H., "How much do we really know about water?," in *Water and aqueous solutions,* G. W. Neilson & Enderby, J. E., eds., Adam Hilger, **37**, 331-342, (1985).

4. Hojerslev, N. K., and I. Trabjerg, "A new perspective for remote sensing measurements of plankton pigments and water quality," Rep. 51 (Univ. Copenhagen Inst. Phys. Oceanogr., Copenhagen, 1990).

5. Pegau, W. S., *et al.*, "A comparison of methods for the measurement of the absorption coefficient in natural waters," J. Geophys. Res., **100,** 13,201-13,220, (1995).

6. Pegau, W. S., and J. R. V. Zaneveld, "Temperature-dependent absorption of water in the red and near-infrared portions of the spectrum," Limnol. Oceanogr., **38,** 188-192, (1993).

7. Green, S. A., and N. V. Blough, "Optical absorption and fluorescence properties of chromophoric dissolved organic matter in natural waters," Limnol. Oceanogr., **39,** 1903-1916, (1994).

8. Pegau, W. S., and J. R. V. Zaneveld, "Temperature dependence of the absorption coefficient of pure water in the visible portion of the spectrum," in *Ocean Optics XII,* J. S. Jaffe, ed., Proc. SPIE, **2258**, 597-604, (1994).

9. Trabjerg, I., and N. K. Hojerslev, "Temperature influence on light absorption by water and sea water in the visible and near-infrared spectrum," Applied Optics, (in press).

10. Ravisankar, M., A. T. Reghunath, K. Sathianandan, and V. P. N. Nampoori, "Effect of dissolved NaCl, $MgCl_2$, and Na_2SO_4 in seawater on the optical attenuation in the region from 430 to 630 nm," Appl. Opt., **27,** 3887-3894, (1988).

11. Sullivan, S. A., "Experimental study of the absorption in distilled water, artificial sea water, and heavy water in the visible region of the spectrum," J. Opt. Soc. Am., **53,** 962-968, (1963).

12. Collins, J. R., "Change in the infra-red absorption spectrum of water with temperature," Phys. Rev., **25,** 771-779, (1925).

13. Luck, W., "Beitrag zur Assoziation des flussigen Wassers. I. Die Temperaturabhangigkeit der Ultrarotbanden des Wassers," Ber. Bunsenges. Physik. Chem., **67,** 186-189, (1963).

14. Waggener, W. C., A. J. Weinberger, and R. W. Stoughton, "The absorption spectrum of H_2O an d D_2O in the near infrared region as a function of temperature from -20° to 250° C," Rep. ONRL-P-925 (Atomic Energy Commission, 1964).

15. Lin, J., and C. W. Brown, "Near-IR spectroscopic measurement of seawater salinity," Environ. Sci. Technol., **27,** 1611-1615, (1993).

16. Buckingham, A. D., "The structure and properties of a water molecule," in *Water and aqueous solutions,* G. W. Neilson & Enderby, J. E., eds., (Adam Hilger, Bristol, 1986), pp. 1-10.

17. Dera, J. ,*Marine Physics,* (Elsevier Science Publishing Company, Amsterdam, 1992).

18. Pope, R. M., "Optical absorption of pure water and seawater using the integrating cavity absorption meter," Ph.D. Thesis (Texas A&M, College Station, TX, 1993)

19. Quickenden, T. I., and J. A. Irvin, "The ultraviolet absorption spectrum of liquid water," J. Chem Phys., **72,** 4416-4428, (1980).

20. Halmann, M., and I. Platzner, "Temperature dependence of absortion of liquid water in the far-ultraviolet region," J Phys. Chem., **70,** 580-581, (1966).

21. Boivin, L. P., W. F. Davidson, R. S. Storey, D. Sinclair, and E. D. Earle, "Determination of the attenuation coefficients of visible and ultraviolet radiation in heavy water," Appl. Opt., **25,** 877-882, (1986).

22. Moore, C., "*In situ*, biochemical, oceanic, optical meters," Sea Technology, **35,** 10-16, (1994).

23. Pegau, W. S., C. A. Paulson, and R. J. V. Zanveld, "Optical measurements of frazil concentration," Cold Regions Science and Technology, (in progress).

24. Austin, R. W., and G. Halikas, "The index of refraction of seawater," Rep. SIO Ref 76-1 (Scripps Institution of Oceanography, San Diego, 1976).

25. Roesler, C. S., M. J. Perry, and K. L. Carder, "Modeling in situ phytoplankton absorption from total absorption spectra in productive inland marine waters," Limnol. Oceanogr., **34,** 1510-1523, (1989).

26. Zaneveld, J. R. V., J. C. Kitchen, and C. Moore, "The scattering error correction of reflecting-tube absorption meters," in *Ocean Optics XII,* J. S. Jaffe, ed., Proc. SPIE, **2258**, 44-55, (1994).

27. Shifrin, K. S. ,*Physical Optics of Ocean Water,* (American Institute of Physics, New York, 1988).

28. Smith, R. C., and K. S. Baker, "Optical properties of the clearest natural waters (200-800 nm)," Applied Optics, **20,** 177-184, (1981).

29. Tam, A. C., and C. K. N. Patel, "Optical absorptions of light and heavy water by laser optoacoustic spectroscopy," Applied Optics, **18,** 3348-3358, (1979).

30. Irvine, W. M., and J. B. Pollack, "Infrared optical properties of water and ice spheres," Icarus, **8,** 324-360, (1968).

31. Querry, M. R., D. M. Wieliczka, and D. J. Segelstein, "Water (H_2O)," in *Handbook of Optical Constants of Solids II,* (Academic Press, 1991), pp. 1059-1077.

32. Querry, M. R., P. G. Cary, and R. C. Waring, "Split-pulse laser method for measuring attenuation coefficients of transparent liquids: application to deionized filtered water in the visible region," Appl. Opt., **17,** 3587-3592, (1978).

33. Hale, G. M., and M. R. Querry, "Optical constants of water in the 200-nm to 200-υm wavelength region," Appl. Opt., **12,** 555-563, (1973).

34. Bayly, J. B., V. B. Kartha, and W. H. Stevens, "The absorption spectra of liquid phase H_2O, HDO and D_2O from 0.7 μm to 10 μm," Infrared Physics, 3, 211-222, (1963).

CHAPTER 6

OPTICAL MEASUREMENTS OF FRAZIL CONCENTRATION

W. Scott Pegau, Clayton A. Paulson, and J. Ronald V. Zaneveld

submitted to *Cold Regions Science and Technology*

6.1 ABSTRACT

Two commercially available oceanographic optical instruments were used to measure frazil concentration. The first of the two instruments was a single wavelength beam transmissometer with a pathlength of 25 cm. We calibrated the transmissometer in a laboratory flume and applied this calibration to field measurements made in an Arctic lead. An observed vertical profile of frazil ice concentration, which we believe is the first field observation to be reported, was dynamically consistent with the observed temperature and salinity profiles. This consistency supports the validity of the laboratory calibration. Because the transmissometer cannot differentiate between frazil and other kinds of particles, auxiliary measurements must be made to determine when frazil may be present. The transmissometer was capable of measuring frazil concentrations as low as 2×10^{-3} kg/m^3. The second instrument tested is a three-wavelength absorption meter with selected wavelength bands in the near infrared portion of the spectrum. In this region of the spectrum, water and ice have greatly different absorption characteristics. To remove the signal of non-ice particles the difference between the absorption coefficient measured at two wavelengths is used. The differential absorption technique can measure frazil ice concentrations as low as 5×10^{-2} kg/m^3. Both instruments provide the rapid and sensitive in situ measurements necessary for field and laboratory studies of frazil ice formation and evolution.

6.2 INTRODUCTION

Frazil is the collection of small ice crystals formed when heat is removed from a turbulent water body that is at or below the freezing point. The formation of frazil is an important component of the growth of ice in high latitude lakes, rivers, and oceans. For example, in most of the Weddell Sea 50% of the sea ice is composed of frazil ice crystals, and in some areas of the Weddell this proportion can increase to 80-90% (Gow et al., 1982; Lange et al., 1989). Sea ice in the central Arctic does not contain such high proportions of frazil with only 5% of the volume consisting of ice which was initially frazil (Weeks and Ackley, 1982). However, this proportion can be much higher for young ice within leads and polynyas where frazil production is high.

Frazil ice plays an important role in many processes in polar regions. The formation of frazil ice and its deposition at the downwind edges of leads and polynyas controls the area of open water which, in turn, affects the heat transferred to the atmosphere (Gow et al., 1990; Smith et al., 1990). Where frazil production is high, such as in wintertime polynyas, the brine rejected during formation may alter the regional circulation (Schumacher et al., 1983). Furthermore, deep formation, such as that observed by Penrose et al. (1994), and deep mixing of frazil provide mechanisms for sediment transport and entrainment of biological particles (Weeks and Ackley, 1982; Reimnitz et al., 1993). Knowledge of frazil concentration is also important for engineering reasons. Frazil ice can cause fouling of the intakes of power plants, ships,

and other water users (Martin, 1981; Daly 1984), with consequent damage to machinery.

Little is known about the dynamics of frazil ice despite the important role it plays in many processes. How frazil production depends on environmental conditions such as lead geometry, wind, current, and wave field is not well understood (Gow et al., 1990). To study the relationship between frazil production and environmental parameters requires the ability to make reliable and rapid measurements of frazil ice concentrations. The task of measuring frazil concentration is made difficult because the presence of frazil can be transitory in nature (Martin, 1981). The fluctuations in frazil concentration thereby require that the sampling system be able to make rapid measurements in order to provide information on the temporal variability.

Development of instruments capable of measuring frazil concentration has been limited. Tsang (1985) developed an instrument that used the resistivity of water to estimate frazil concentration. Daly and Rand (1990) developed a system that measures the water flow rate through a screen to indicate the presence of frazil ice. More recently, a calorimetric device has been used for laboratory measurements by Lever et al. (1992). These methods lack either the sensitivity or sampling speed necessary to be of practical use in many laboratory or field applications.

Notwithstanding the lack of observations, work has proceeded on numerical modeling of frazil growth and distribution (Omstedt, 1986; Liou and Ferrick, 1992; Daly 1994; Omstedt, 1994; Svensson and Omstedt, 1994). Verification and development of models requires measurements of frazil ice concentrations under a

variety of conditions and over a wide range of concentrations (10 to 10^{-4} kg/m^3, Lever et al., 1992). This range of concentration is important in the studies of frazil initiation and dynamics, but does not reach the concentrations expected during the formation of pancake ice or consolidation of frazil.

Instruments are needed for studies of frazil ice dynamics which are capable of rapidly measuring a wide range of concentrations under a variety of environmental conditions. We describe two optical instruments which are sufficiently sensitive and responsive to be used in the field and in the laboratory for frazil initiation and dynamics studies. These two instruments are a single-wavelength transmissometer and a three-wavelength absorption meter. The transmissometer is a commercially available instrument that has been used for a number of years by oceanographic institutions for measurement of particle concentrations in sea water (Gardner et al., 1985). The three-wavelength absorption meter is also commercially available and is normally used for measuring chlorophyll concentrations (Moore, 1994). While these instruments have not been used to measure frazil concentrations before now, they have been used on profiling and moored systems and are capable of making measurements under a wide range of environmental conditions.

Results are presented from two sets of measurements. The first set of measurements were made using both the transmissometer and the absorption meter in a laboratory flume. The second set of measurements were made in the Arctic using the transmissometer and represent what we believe to be the first measurements of frazil concentration within a lead.

6.3 LABORATORY MEASUREMENTS

During the spring of 1994 laboratory tests were conducted in the small frazil flume of the Ice Engineering Department of the U. S. Army Cold Regions Research and Engineering Laboratories (CRREL) (Fig. 6.1) (Lever et al, 1992). Five runs were made under a variety of seeding and supercooling conditions. Measurements were made using two single-wavelength transmissometers and the spectral absorption meter. A Sea Bird SBE-25 CTD was used to monitor water temperature in the flume. Unless otherwise noted the data has been averaged over 3-second intervals thus providing one datum every 3 seconds. The averaging was done to smooth high frequency fluctuations.

6.3.1 Transmissometers

One of the instruments used to measure the concentration of frazil ice is a Sea Tech. Inc., 25-cm-pathlength, single-wavelength (670 nm) transmissometer (Bartz et al., 1978). The transmissometer measures the transmitted portion of a collimated beam. A simplified schematic is presented in Figure 6.2. Scattering and absorption both reduce the intensity of the beam resulting in a lower transmitted beam strength. Frazil does not absorb strongly at 670 nm so that the signal measured by this device is dominated by light scattered out of the beam. The amount of scattered light depends on the concentration, index of refraction, size distribution and shape of the ice particles.

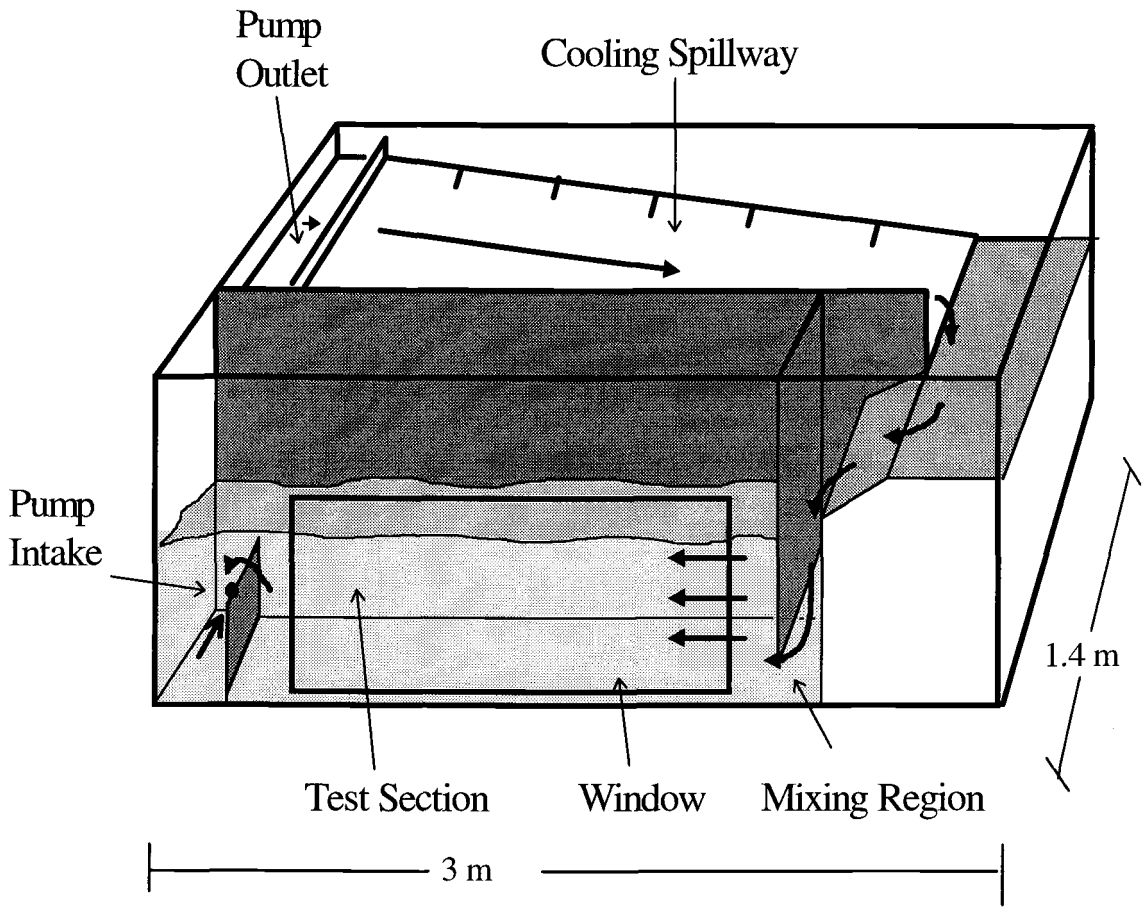

Figure 6.1. A diagram of the flume used for this experiment. The water flow is marked by the arrows. The starting point of the flow is the pump outlet section from which water overflows to the broad-shallow-cooling spillway. The water then turns and flows into the mixing region and underneath a baffle into the test section. A plexiglass window allows the flow in the flume to be observed. At the end of the test section there is a baffle and the pump inlet. The water is then pumped back up to the head of the spillway by a pump located under the spillway.

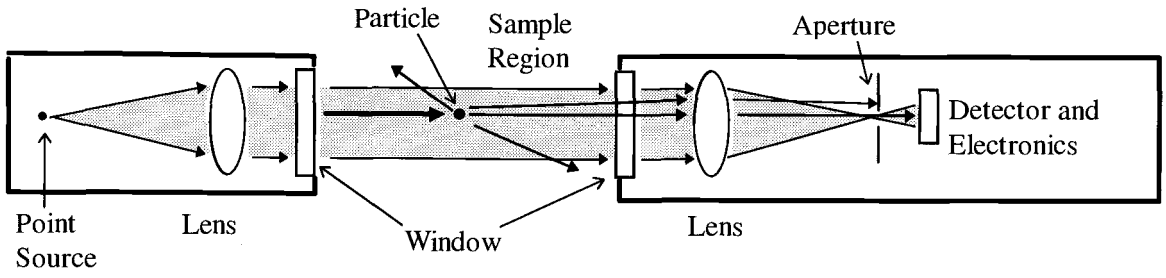

Figure 6.2. A schematic diagram of the optics of a beam transmissometer. Light is removed from the direct beam by scattering and absorption as illustrated by the particle in the beam. The aperture determines how much forward scattered light is accepted in the measurement. The beam transmissometers used in this work were Sea Tech., Inc. 660-nm 25-cm pathlength transmissometers with 1° acceptance angles. The instrument is 80 cm long and has a diameter of 10 cm.

To determine the frazil attenuation coefficient the measured signal is processed using:

$$c_f(\lambda) - c_{ref}(\lambda) = -\frac{1}{pathlength} \ln\left(\frac{V_{meas}}{V_{ref}}\right) \tag{6.1}$$

where c_f is the frazil attenuation coefficient, c_{ref} is the attenuation coefficient of a reference medium, V_{meas} is the measured voltage, and V_{ref} is the transmissometer voltage measured using the reference substance. In most cases pure water is used as the reference substance. However, since the transmissometer cannot distinguish the type of particles being measured, we use frazil-free water from the flume as the reference. In this manner the mean attenuation of background substances contained in the water is removed.

To calibrate the transmissometers, we used the run in which the least amount of seed crystals were added to the water. For negligible seeding, the ice concentration

within the flume can be determined from the temperature record (Fig. 6.3). The cooling rate was determined by regressing the temperature data against time for the period prior to seeding. The temperature versus time plot thus obtained was extrapolated to estimate the temperature that would have occurred if no ice had formed. The difference between the measured temperature and the extrapolated temperature (ΔT) was used to estimate the ice concentration according to the following equation:

$$I = \frac{\rho_w \tilde{c}_w \Delta T}{L_f} \tag{6.2}$$

where I is the ice concentration in kg/m^3, and ρ_w, $\tilde{c}_w$, and L_f represent the density, specific heat, and the latent heat of fusion for water, respectively.

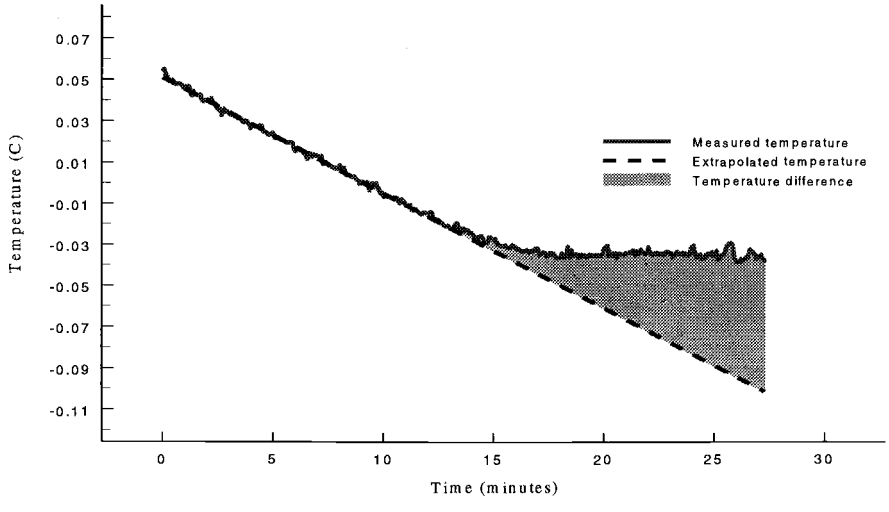

Figure 6.3. The measured temperature and the temperature extrapolated from a fit to the first 10 minutes of the run used for calibrating the transmissometers. The estimate of frazil concentration is based on the difference between the measured and extrapolated temperatures. All data has been averaged in 3-second intervals to filter out high-frequency fluctuations. The tank was seeded at approximately the 14 minute mark.

Calibration curves for the transmissometers were determined by linear regression of ice concentration versus attenuation coefficient (Fig. 6.4). The time period of the regression extended from one minute prior to seeding the flume to five minutes after the seeding. During this period the frazil was visibly observed to be well mixed in the test section and there was no observed surface accumulation. Because the frazil was well mixed we believe the temperature-based estimate of frazil concentration to be representative of the frazil concentration in the flume.

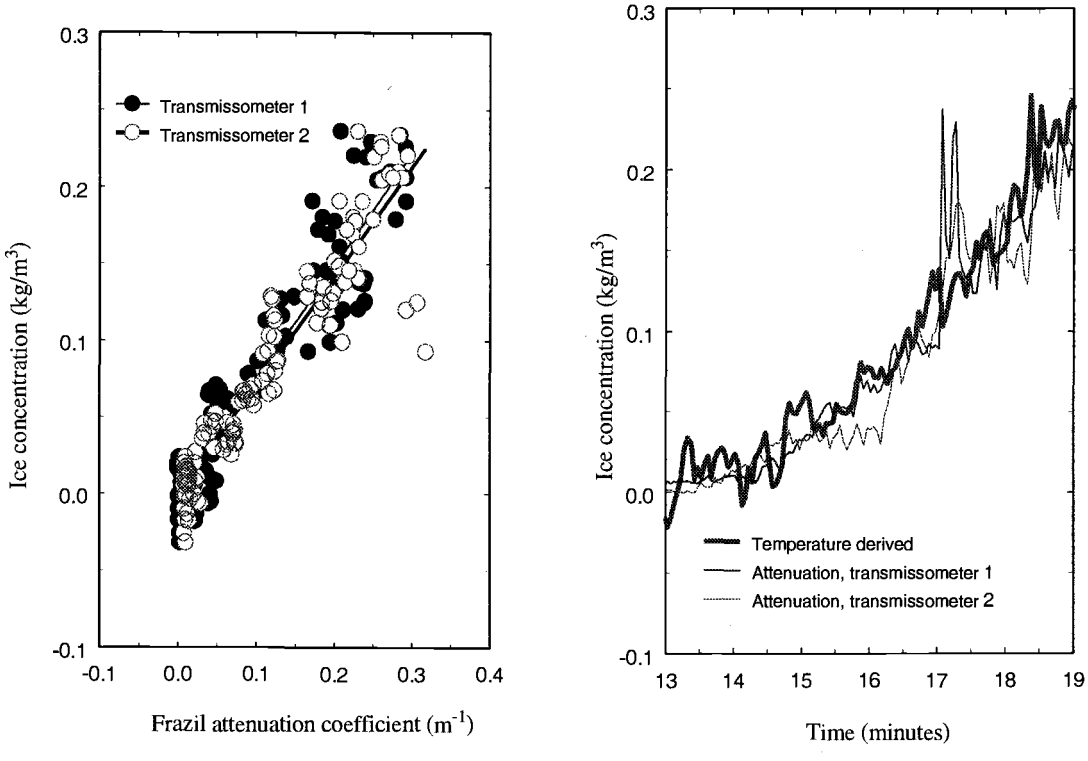

Figure 6.4. a) The regression of ice concentration versus beam attenuation by frazil used for calibrating the transmissometers. b) The resulting ice concentrations estimated from the temperature record and from the transmissometers based on the regression. The data used are from the run presented in Figure 3.

The regression was linear with a zero intercept which yielded a constant with which we can multiply the attenuation coefficient to obtain frazil concentration. For this test the coefficients were determined to be 7.5×10^{-1} and 7.6×10^{-1} ($kg/m^3/m^{-1}$) respectively, with the standard error of each being 2×10^{-2} for each of the two transmissometers. We used 7.5×10^{-1} ($kg/m^3/m^{-1}$) as the empirical calibration coefficient for the results presented here.

While the calibration of the transmissometers was performed at low frazil concentrations, it has been shown that the transmissometer signal is linearly dependent on particle concentrations as long as multiple scattering can be neglected (Gardner et al., 1985). For multiply scattered light to be detected by the transmissometer requires at least two and normally more scattering events at precise angles and positions within the path. Such a precise sequence of scattering events is highly unlikely. The maximum measurable concentration therefore depends on the length of the transmissometer used, with smaller pathlength instruments capable of measuring higher concentrations. The 25-cm pathlength transmissometer could be expected to reliably measure concentrations as high as 10 kg/m^3 provided no flocs have formed. The largest factor determining the transmissometer signal is particle concentration but the signal also depends on particle shape. At high frazil concentrations where the individual crystals have formed flocs a separate calibration for the transmissometer would be required.

6.3.2 Absorption Meter

In the near-infrared portion of the spectrum, the absorption coefficient of water is determined by the vibrational frequencies of the O-H bond. Because water is a polar molecule, it tends to form clusters by hydrogen bonding of individual molecules (Dera, 1990). The size of the clusters depends on temperature and the presence of ions in the solution. As the temperature increases, more of the hydrogen bonds are broken which results in more free molecules. When ions are present, their charge attracts a large number of water molecules which creates larger clusters than hydrogen bonding alone. Within the clusters of molecules, the O-H bonds are no longer able to move freely, which causes the vibrational frequencies to be altered and thus changes the absorption coefficient. Ice represents an extreme in the bonding process with vibrational overtones for the crystaline rather than liquid form of water. The absorption coefficient of ice is thus different than that of liquid water, as shown in Figure 6.5.

The difference in the spectral absorption coefficients for water and ice (Fig. 6.5) suggests that frazil ice concentration can be determined by measuring the absorption coefficient at two different wavelengths. We chose wavelengths of 900 and 975 nm. At 900 nm there is relatively little difference between the absorption coefficients of water and ice. At 975 nm there is a peak in the absorption spectrum of water, which is related to a vibrational frequency overtone, where there exists a maximal difference between the absorption coefficients of ice and water. As shown in earlier works, the absorption coefficient of water in the region of a vibrational overtone

is dependent on temperature (Collins, 1925; Luck, 1963; Pegau and Zaneveld 1993). This temperature dependence must be removed prior to calculating the ice concentration.

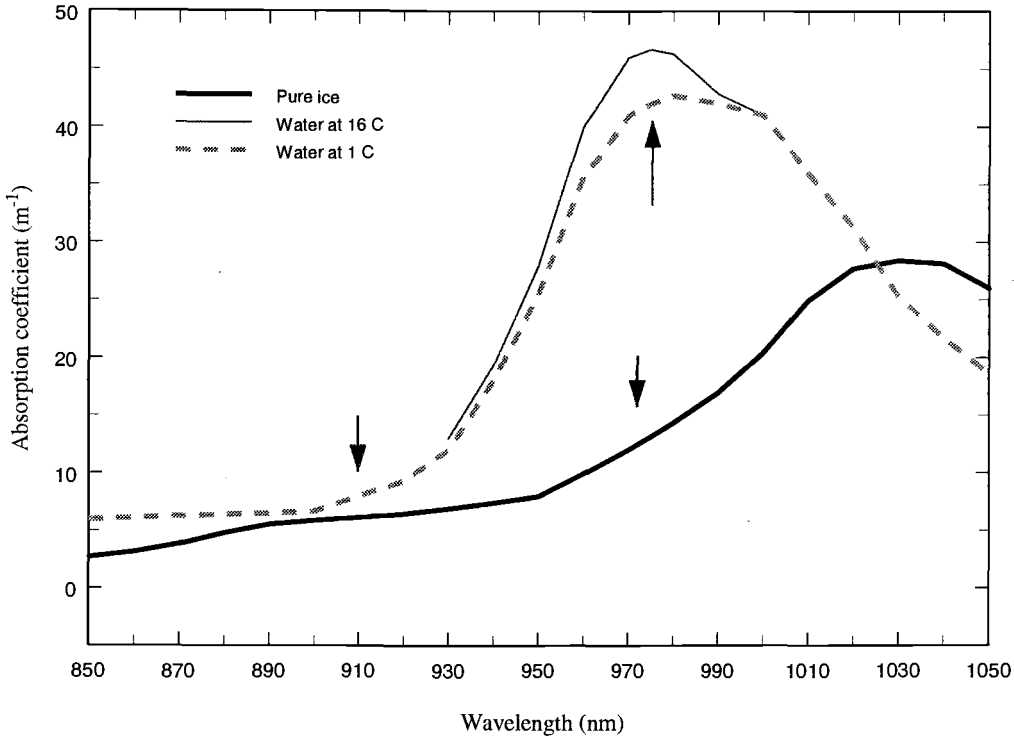

Figure 6.5. The absorption coefficients of water and ice in the spectral region of interest. The values for water are from Collins (1925) and the ice absorption coefficients are from Grenfell and Perovich (1981). The arrows indicate where the absorption coefficient is measured by the absorption meter.

We used a 10-cm-pathlength, WETLabs a-3, three-wavelength absorption meter (Moore, 1994) to measure the absorption coefficients. This instrument was originally designed to measure chlorophyll absorption in the ocean. We modified the

instrument to measure frazil by changing the interference filters which determine the wavelengths at which the absorption coefficient is measured. The interference filters are located in a rotating filter wheel on the source side of the instrument. The filter wheel rotates rapidly, allowing data at all three wavelengths to be collected at a frequency of 5.8 Hz. A simplified schematic of the instrument is given in Figure 6.6. From the source, the light beam enters a reflective flow tube. The water and frazil mixture is drawn through the flow tube by a submersible pump. At the other end of the flow tube is a diffuse collector and a detector which measures the direct and scattered light. The digital output from the instrument is stored on a computer.

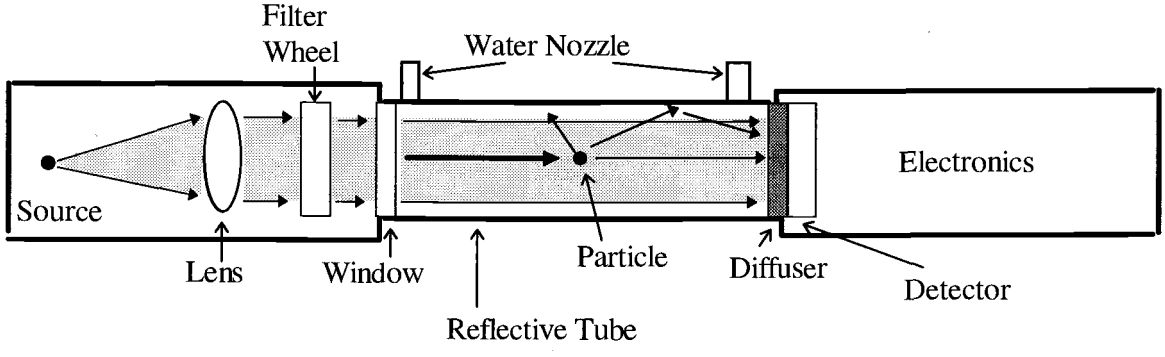

Figure 6.6. A simplified schematic diagram of the optics in the three-wavelength absorption meter. The flow tube pathlength is 10 cm and the beam width is 1 cm. The direct beam and forward scattered light reach the diffuser and are measured. The absorbed light and backscattered light are removed from the beam and determine the measured absorption coefficient. The WETLabs a-3 that was used is 50 cm long and has a diameter of 10 cm.

The reflective tube allows light scattered up to approximately 41° from the beam to be collected. The uncollected scattered light contributes to an error term in the

determination of the absorption coefficient (Zaneveld et al., 1994). The measured absorption coefficient is related to the true absorption coefficient by the following equation:

$$a_{meas}(\lambda)=a_{true}(\lambda)-a_{ref}(\lambda)+\varepsilon b(\lambda) \tag{6.3}$$

where a_{ref} is the absorption signal of a reference medium (normally pure water), b is the scattering coefficient, and ε is the proportion of the scattered light not collected by the instrument. The last term in (6.3) is the scattering error term. The measured absorption coefficient is a differential measurement, i.e., the difference between absorption of the medium and that of pure water at a specified temperature plus an error term. When no particles are present, a_{true} equals a_{ref} so a_{meas} is equal to zero. The measured absorption coefficient of the medium will be negative if the true absorption coefficient of the medium plus the error term is less than the absorption coefficient of the reference water. Because the absorption of ice at 975 nm is much less than that of water at the same wavelength (Fig. 6.5), the presence of ice in the flow tube will tend to make the measurement negative. Negative measurements can also occur if the sample temperature is less than that of the reference water.

To avoid mistaking the temperature signal as an ice concentration the absorption coefficients were corrected to a reference temperature of 0.0° C. The absorption coefficient is linearly dependent on temperature in the near infrared (Pegau and Zaneveld, 1993). The absorption coefficients were corrected for temperature effects using:

$$a(\lambda)_{meas_{TC}} = a(\lambda)_{meas} - S(\lambda)(T - T_{ref}) \tag{6.4}$$

where TC stands for temperature corrected values and S(λ) is the slope of the linear temperature dependence. To determine the values of S(λ) we regressed the measured absorption coefficients against temperature for temperatures near zero (Fig. 6.7). The values of S(975) and S(900) were determined to be 0.274 and 0.016 respectively.

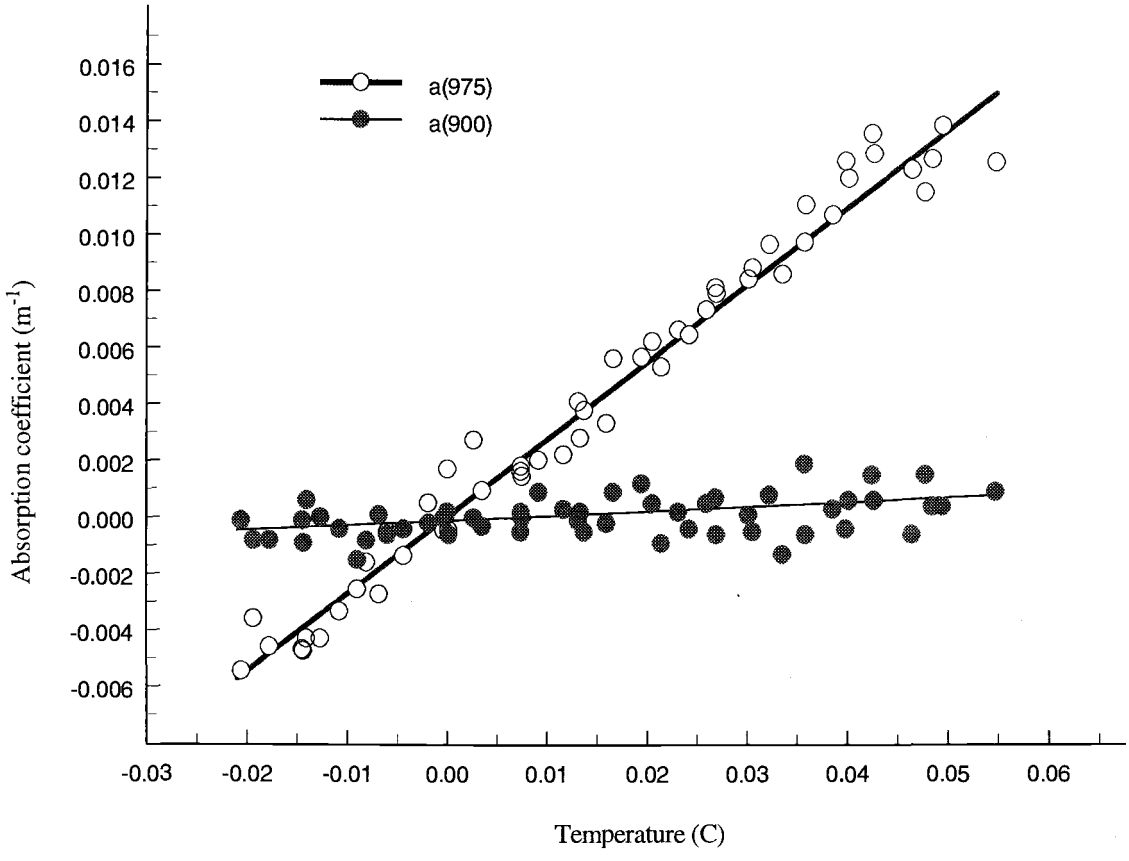

Figure 6.7. Linear fits of the absorption coefficients of water versus temperature at the two wavelengths used for temperatures near 0° C as measured during this experiment. These regressions are used to provide the slopes necessary for temperature compensation the measured absorption coefficients.

While the instrument makes measurements at three wavelengths we only used two wavelengths in this analysis. To determine the quantity of ice in a sample the following equation is used:

$$fractional\ volume\ of\ ice = \left(a(900)_{meas_{TC}} - a(975)_{meas_{TC}}\right) / \Theta \tag{6.5}$$

$$\Theta = [a_{pw}(975) - a_{ice}(975)] - [a_{pw}(900) - a_{ice}(900)]$$

where the pure water (pw) values are those measured at the reference temperature. The value of Θ at zero degrees is 27.6 m^{-1}. To obtain the ice concentration in kg/m^3 equation 6.5 is multiplied by the density of ice (900 kg/m^3).

We assume that the scattering error is wavelength independent in this portion of the spectrum, and thus the scattering errors are eliminated by subtracting the absorption coefficients in the numerator of equation 6.5. A wavelength dependent scattering correction could be applied if the third wavelength band in the instrument is chosen in a region where the absorption coefficients of ice and water are the same. A wavelength dependent function, such as a power function, could then be fitted to the a(900) and $a(\lambda_3)$ data which are measures of the scattering error. The scattering error at a(975) could then be extrapolated or interpolated from the fitted function depending on the value of λ_3. So long as the scattering error does not change its spectral characteristic, the scattering correction should work even at very high ice concentrations. In the flow-through configuration used during this experiment the maximum measured frazil concentration is limited by the ability to pump frazil through the system rather than by the optics.

It is also assumed that the absorption properties of the organic and inorganic particles are negligible compared to the difference between the absorption coefficients of water and ice and that any residual absorption that exists is spectrally flat in this portion of the spectrum. This assumption is consistant with the commonly made assumption in bio-optics that the absorption of phytoplankton is zero for wavelengths longer than 750 nm (Roesler et al, 1989; Kirk, 1994). Even if there is some residual absorption by particles at the longer wavelengths, so long as the absorption is spectrally flat these particles will have no effect on the difference in absorption coefficients at the two chosen wavelengths. In cases where the third wavelength is used to provide a spectral scattering correction function, the technique will remove residual absorption of the same spectral form. This instrument is thus able to identify ice in the presence of other particles in the water column.

Measurements of ice concentration in the frazil flume obtained with the absorption meter were compared with independent estimates of frazil concentration based on attenuation and temperature. To determine frazil concentration the temperature-corrected absorption coefficients were determined, as shown in Figure 6.8, and these absorption coefficients were used in equation 6.5. The positive measured absorption coefficients at a(900) and a(975) are attributed to the error caused by light scattering off the frazil crystals (eq. 6.4). If there had been no scattering signal, $a_{meas}(900)$ would be zero and $a_{meas}(975)$ would be negative because the absorption coefficient of ice is less than that of the reference medium (water). The assumption of

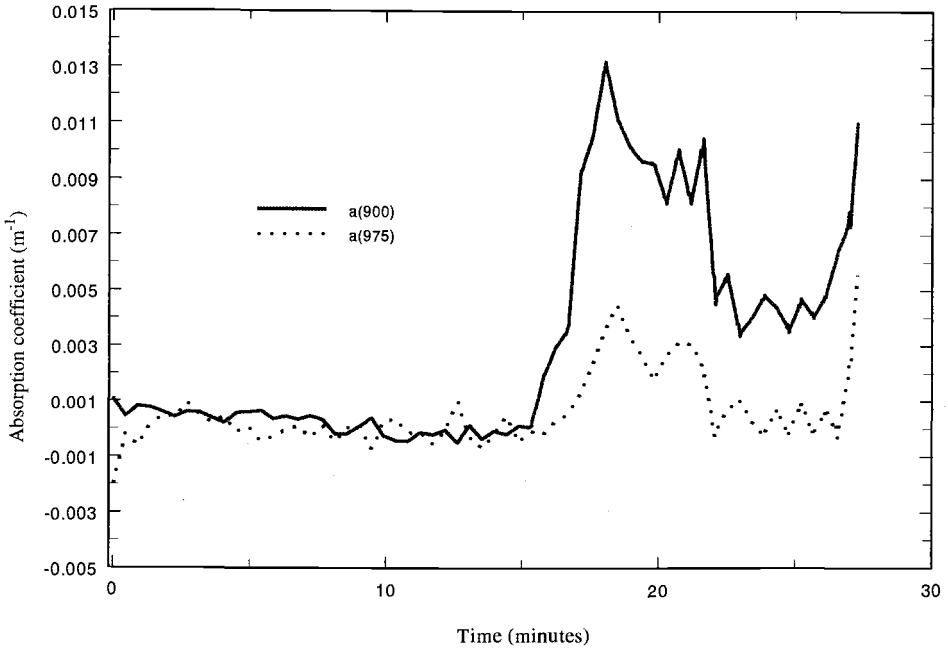

Figure 6.8. Measured values of a(900) and a(975) used to determine ice concentration. These data were collected during the run used to calibrate the transmissometers. The positive absorption values are due to the scattering error caused by the presence of frazil. The data have been smoothed using a locally weighted regression scheme over thirty second intervals.

the scattering being nearly the same at 900 and 975 nm is supported by the observation that the ice concentration derived from the differential absorption method agrees very well with both the temperature-derived concentration and the concentration estimates using the transmissometers between the 15 and 20 minute marks of the run used to calibrate the transmissometer (Fig. 6.9). After 20 minutes the agreement between the two optical instruments continues to be good while there is a departure from agreement between the optical and temperature estimates of ice concentration. The disagreement between estimates after 20 minutes can be attributed to the fact that the temperature

estimate does not account for removal of ice from the interior to the surface. One mechanism for the removal of frazil is the formation of flocs which rise to the surface (Omstedt, 1994). Another mechanism to remove heat without adding frazil to the volume is the growth of ice anchored to the flume surface. Both of these mechanisms would cause an overestimate of the frazil concentration in the sampling volume from the temperature record and both were observed to take place during each experimental run.

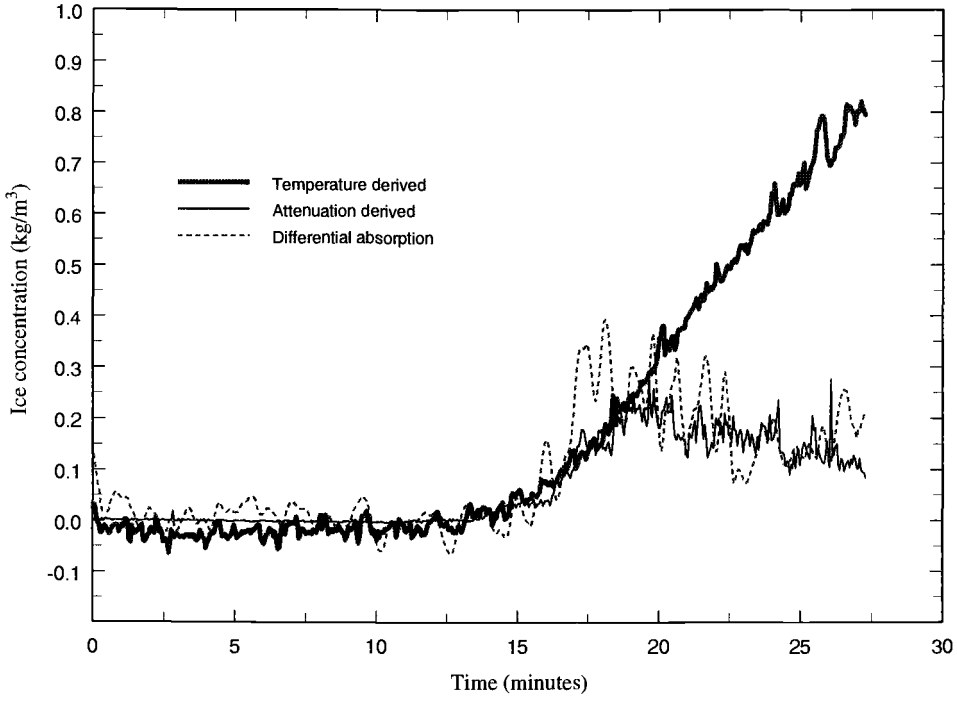

Figure 6.9. Comparison of the ice concentrations estimated from temperature, the transmissometer, and the differential absorption technique for the duration of the run used in the previous figures. The differential absorption data have been smoothed using a locally weighted regression scheme over a thirty second interval. The agreement between optical techniques remains good while deviating from the temperature based estimate of frazil concentration. This deviation is due to the temperature based estimation not accounting for removal of frazil crystals by flocculation or growth of anchor ice.

The ice concentration estimate from the differential absorption technique is inherently noisier than that from the transmissometer technique because the difference of two absorption measurements is required, whereas the transmissometer measures attenuation at a single wavelength. Measurements of pure water absorption show that the meter has a standard deviation of 0.002 m^{-1} for each wavelength, given a three second bin. This noise translates into a concentration error of approximately 0.1 kg/m^3 of ice. While much of the noise in the absorption measurements can be attributed to the instrument stability there are two other sources of noise. A portion of the noise in the absorption estimates of ice concentration can be attributed to the sequential absorption measurements, where each wavelength is measured at a different time (Δt = 0.057 s, ~ 1.5 mm at a flow rate of 1.5 l/min). Thus, the measurements are made on different crystal concentrations and orientations, introducing a non-constant scattering error. A thirty second boxcar average is applied to the measured absorption coefficients to smooth the scattering error. A second source of noise comes from the temperature correction. A one millidegree error in the temperature measurement translates into a $1x10^{-2}$ kg/m^3 error in the frazil measurement. During the laboratory experiment there was a small separation between the temperature sensor and the absorption meter (0.25 m). Hence there were differences in the temperature of the water being measured by each instrument at any given instance. The temperature records indicate that fluctuations of several millidegrees existed within the water of the flume (Figs. 6.3, 6.10). A portion of the noise in this set of measurements must therefore be attributed to differences in the water temperature being measured at the

temperature sensor and in the absorption meter. All three sources of noise are reduced by averaging over longer time periods.

6.3.3 Other Laboratory Results

An interesting feature of Figure 6.3 is that the measured temperature does not exhibit the recovery that is expected when ice forms in supercooled water (Daly, 1984; Omstedt, 1994). The very light seeding of the flume caused enough frazil formation to stop the cooling of the water but not enough to allow the temperature to rise. Another run exhibited the stalled cooling but after a few minutes of frazil formation the cooling continued at a much lower rate (Fig. 6.10a). This time probably corresponds to the initiation of flocculation and removal to the water surface. Once the frazil is removed from the water volume there are not enough secondary nucleation sites available to support frazil formation (Daly, 1994) and cooling continues at a slower rate. In cases where the seeding was heavier, the temperature displays the expected evolution, with recovery to a residual supercooling level after seeding has occurred (Fig. 6.10b). The unusual results observed at low seeding levels may be a result of the low turbulence levels in the flume during this series of experiments. Why the low seeding levels appear to be able to produce enough frazil to stop the cooling trend but not enough to cause temperature recovery is an interesting question.

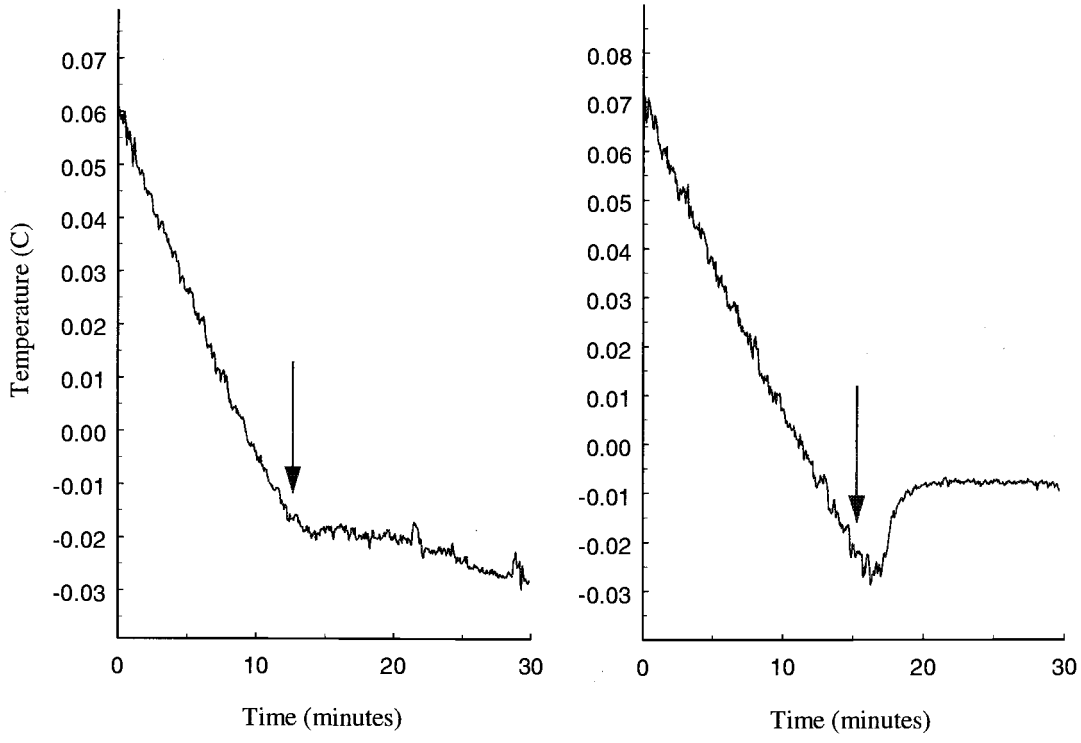

Figure 6.10. a) Water temperature versus time of a run where the temperature does not exhibit a recovery upon seeding. The temperature remains supercooled and continues to cool even though frazil was present. b) Water temperature versus time of a run that exhibited a temperature recovery upon seeding. In this case the seeding level was much higher than in the previous case. The arrows indicate the approximate seeding times in each case.

None of the instruments for detecting frazil, including the two discussed here, are capable of distinguishing between ice formed in the water and ice introduced from an outside source. This is important when the amount of added seed crystals is large. Figure 6.11 presents the optically and temperature derived ice concentrations for a run where the external seed crystals are the dominant source of ice. While the optical and temperature derived estimates are substantially different, the quantity of seed crystals

required to account for the difference is only 1/20th the mass of water blown into the air by the seeding device. The agreement between the differential absorption technique and the transmissometer is good (until icing occurs) even when both optical measurements differ significantly from the temperature based estimate. The agreement between the independent optical systems supports the premise that the ice concentration is dominated by the seed crystals that were added to the flume. The increase in the attenuation derived concentration seen in Figure 6.11 after the 20 minute mark is the result of crystals accumulating on the transmissometer window. When the transmissometer was cleaned at the 30 minute mark the two optical signals come back into agreement. The difference between the optically and temperature derived concentrations evident in Figure 6.11 shows the importance of knowing the quantity of ice from external sources when comparing measurements to model predictions.

Figure 6.11 illustrates the importance of ensuring that the flow past the transmissometers is high enough to prevent frazil from collecting around or forming on the windows. With a flow-through system, such as used by the absorption meter, it is important to have a high flow rate (>1.5 l/min) to prevent the intake from being clogged by ice. The high flow rate also helps to keep the optical surfaces free of ice. We suspect that the heat generated by the electronics and incandescent source also helped to maintain the windows free of ice. Throughout the duration of these experiments the internal temperature of the absorption meter remained at about 4° C which would allow the temperature of the windows to remain above freezing.

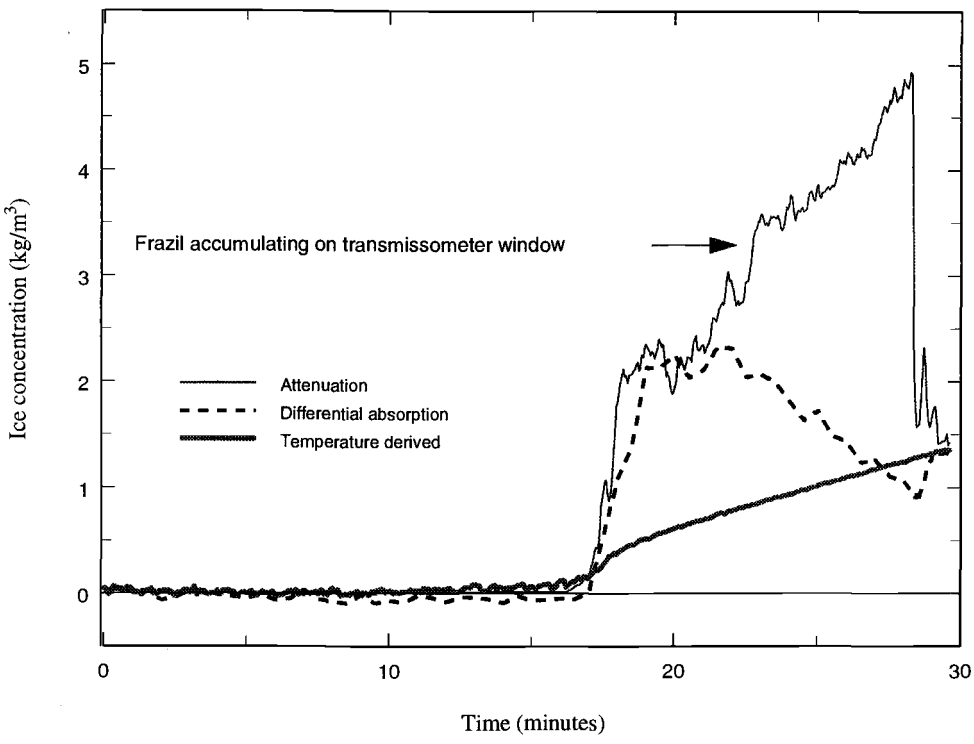

Figure 6.11. Ice concentration estimates for a run where a large quantity of seed crystals were introduced into the system. The difference between optical and temperature based estimates of frazil concentration is attributed to the large quantity of seed crystals. In such a case the temperature estimate of frazil concentration is not valid because it represents a small fraction of the ice in the system. The good agreement between the optical systems (until the time that the transmissometer began to have icing problems) is a good indicator that the transmissometer calibrations are valid even at ice concentrations greater than covered during the calibration run.

6.4 FIELD MEASUREMENTS

In the spring of 1992 an experiment was conducted north of Alaska to study lead processes (Morrison et al., 1993). As part of this experiment a Sea Tech. Inc., single wavelength transmissometer was attached to a Sea Bird SBE-25 CTD and used

to measure the optical and physical properties within leads. To ensure that the transmissometer windows were free of ice the unit was lowered below the mixed layer. By holding the instruments there the relatively warm waters could melt any ice that might have formed when immersing the instrument package.

There are two difficulties in using the transmissometer for field measurements of frazil concentration. The first is that the single-wavelength transmissometer cannot distinguish ice particles from biological particles. To ensure that we are not measuring non-ice particles we must determine the background particle loading and use auxiliary indicators of the presence of frazil. During the early portion of the field experiment the transmissometer signal in the ice-free mixed layer varied only within the noise level of the instrument, which indicates that the surface waters of the high Arctic during early spring are as free of particles as any in the world. We use the transmissometer voltage in the ice-free portion of the mixed layer as the reference value for the field measurements. If there were particles present, this technique would remove the background attenuation associated with those particles. Although the waters are extremely clean, we use the auxiliary measurements of temperature and salinity as indicators of the presence of frazil. Brine rejection during frazil formation will cause the salinity to be elevated from background levels. The temperature is expected to be at or below the freezing point for the formation of frazil. When the temperature and salinity signal are combined with an increase in the particulate attenuation coefficient, such as seen in Figure 6.12, the attenuation may be ascribed to frazil.

The second potential difficulty involves using the frazil ice calibration determined in the laboratory. The transmissometer signal depends on the size distribution, shape, and index of refraction as well as concentration of particles. We assumed that the natural frazil ice has the same characteristics as the laboratory frazil. To obtain a second estimate of frazil concentration, we calculated the frazil concentration necessary to stabilize the water column. The rejection of brine during frazil formation creates water that is denser than the water it overlies. The presence of frazil can lower the mixture's density to create

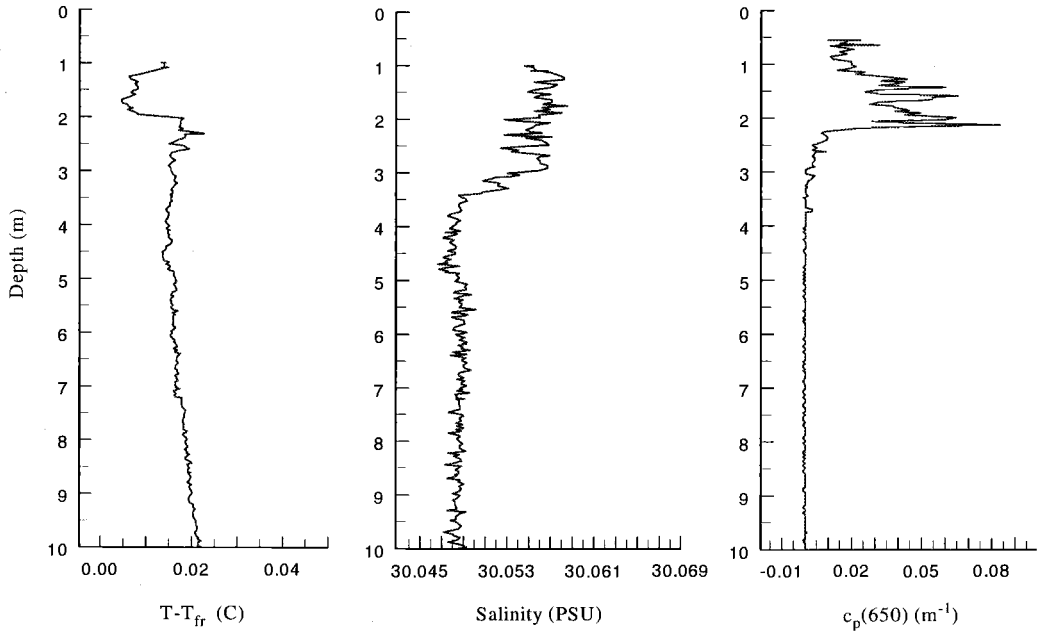

Figure 6.12. Measurements made in a lead during the Arctic Lead experiment. a) Profile in the upper 10 m of the measured temperature minus the freezing temperature. Negative values would indicate supercooling. b) Salinity profile in the upper 10 m. c) The profile of the beam attenuation coefficient for particles. Note that the temperature and salinity profiles have different shapes near the surface. Such differences would not be expected if the mixing was being driven by the wind. The increased salinity at the surface is an expected result of local ice formation and would not be expected if ice crystals in the water were the result of snow being mixed into the water by the wind.

a neutrally stable water column. Therefore there are two competing buoyancy forces, the higher salinity waters have a negative buoyancy while the frazil exerts a positive force. When the water starts to descend it can entrain frazil which will remain in the water until such a time when the positive buoyancy of the crystals separate them from the water. As the crystals flocculate they will ascend at higher speeds and sweep other frazil crystals from the mixture. These rising crystals can thus create small regions where the frazil concentration is higher than would be expected from stability. In such regions there will be an upward flux of ice and downward flux of water. For the mixture to descend it must have a negative buoyancy and thus the frazil concentration has to be lower than that required to create a stable water column. Therefore, on the large scale, the frazil concentration calculated to create a neutrally stable column represents an upper limit to the possible concentration in buoyancy driven mixing. Frazil and blowing snow can also be mixed into the water by the wind. Ice crystals from blowing snow do not have an associated increase in salinity as they are not formed locally. The temperature and salinity profiles given in Figure 6.12 suggest that the frazil is being mixed by the descent of the denser water formed with frazil and that the stability estimate is a good indicator of the upper limit to the frazil concentration. The frazil concentration determined using the laboratory calibrations of the transmissometer and from stability are in good agreement (Fig. 6.13). Based on this result it appears reasonable that the laboratory calibrations may be applied to the field measurements.

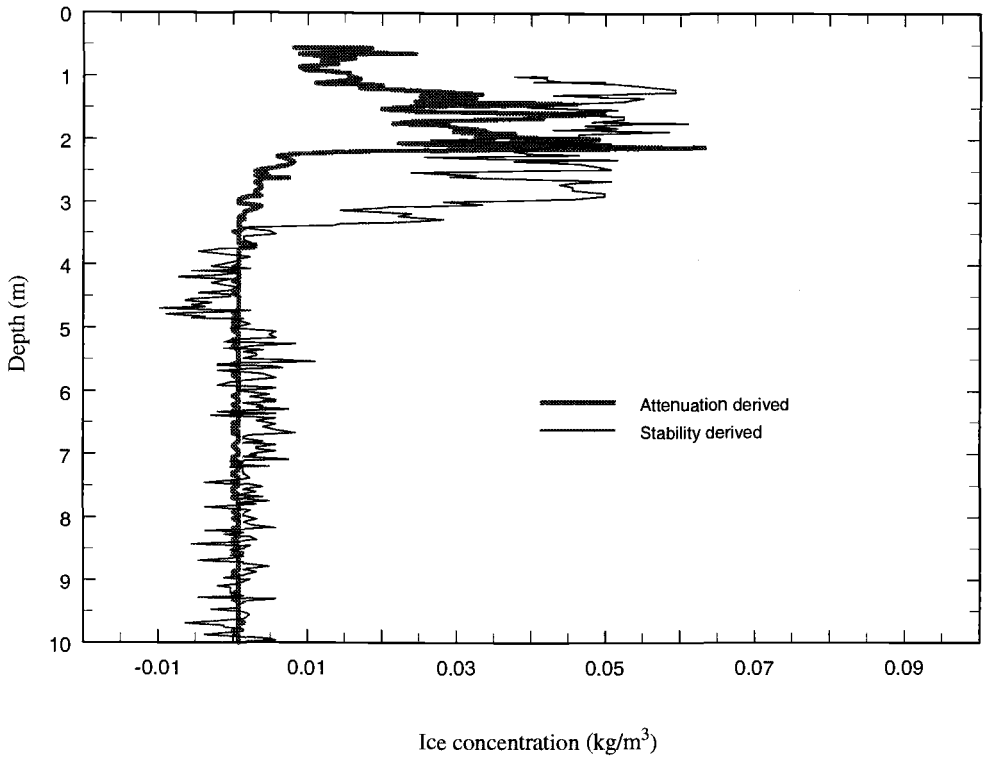

Figure 6.13. The estimates of frazil concentration obtained from the attenuation coefficient and those obtained using the assumption of a stable water column. These measurements correspond to those presented in Figure 6.12. The stability estimate of frazil concentration represents the upper limit on frazil. Where the frazil is measured to be less than is required by stability the water mass is descending.

6.5 CONCLUSIONS

Methods for the rapid and accurate determination of frazil ice concentration are needed for the investigation of frazil ice dynamics. Two optical instruments, a transmissometer and an absorption meter, have been shown to be useful for measuring frazil ice concentration.

The transmissometer can be used to measure frazil concentrations as low as 2×10^{-3} kg/m^3. The laboratory derived calibrations appear to apply to the field measurements, providing evidence that the properties of the laboratory and natural frazil crystals are similar. The single wavelength transmissometer is unable to discriminate between kinds of particles. It is necessary, therefore, to make auxiliary measurements to show that the particles may be frazil and to use a reference measurement that incorporates any non-frazil background particle load. It may be possible to use spectral transmissometers to distinguish between the types of particles being measured removing the need for auxiliary measurements. With the Sea Tech. Inc. transmissometers used in these experiments, care needs to be taken to ensure that the flow past the windows of the instrument is high enough to prevent frazil from collecting around or forming on the windows.

Differential absorption measurements of frazil ice concentration are calibrated theoretically rather than empirically. The instrument in its present configuration is capable of measuring concentrations as low as 5×10^{-2} kg/m^3. The instrumental noise should be reduced by specifically designing an instrument for the measurement of frazil instead of modifying a chlorophyll measuring device to detect frazil. The precision of this instrument could be improved further by using a simultaneous detection scheme rather than the present sequential system and by monitoring temperature within the sampling cell. The significant advantage of this system is that it can potentially discriminate frazil particles from biological or geological particles.

6.6 REFERENCES

Bartz, R., J. R. V. Zaneveld, and H. Pak, 1978, A transmissometer for profiling and moored observations in water, *In* Ocean Optics V, Proc. SPIE, 160, 102-108.

Collins, J. R., 1925, Change in the infra-red absorption spectrum of water with temperature, Phys. Rev., 25, 771-779.

Daly, S. F., 1984, Frazil ice dynamics, USA Cold Regions Research and Engineering Laboratory, Monograph 84-1.

Daly, S. F., 1994, Frazil ice dynamics, , In, "Report on frazil ice", Steven F. Daly ed., USA Cold Regions Research and Engineering Laboratory, Special report 94-23.

Daly, S. F., and J. H. Rand, 1990, Development of an underwater frazil-ice detector, Cold Reg. Sci. Technol., 18, 77-82.

Dera, J, 1990, "Marine Physics", Elsevier Oceanography Series, Vol. 53, Elsevier, Amsterdam, 515 pp.

Gardner, W. D., P. E. Biscaye, J. R. V. Zaneveld, and M. J. Richardson, 1985, Calibration and comparison of the LDGO nephelometer and the OSU transmissometer on the Nova Scotian Rise, Mar. Geol., 66, 323-344.

Gow, A. J., S. F. Ackley, W. F. Weeks, and J. W. Govoni, 1982, Physical and structural characteristics of Antarctic sea ice, Ann. Glaciol., 3, 113-117.

Gow, A. J., D. A. Meese, D. K. Perovich, and W. B. Tucker III, 1990, The anatomy of a freezing lead, J. Geophys. Res., 95, 18221-18232.

Grenfell, T. C., and D. K. Perovich, 1981, Radiation absorption coefficients of polycrystalline ice from 400-1400 nm, J. Geophys. Res., 86: 7447-7450.

Kirk, J. T. O., 1994, "Light & Photosynthesis in Aquatic Ecosystems", 2nd edition, Cambridge University Press, Cambridge, 509 pp.

Lange, M. A., S. F. Ackley, P. Wadhams, G. S. Dieckmann, and H. Eicken, 1989, Development of sea ice in the Weddell Sea, Ann. Glaciol., 12, 92-96.

Lever, J. H., S. F. Daly, J. H. Rand and D. Furey, 1992, A frazil concentration meter, In: Proceedings, International Association of Hydraulic Research 11th International Symposium on Ice, Banff, Alberta, pp. 1362-1376.

Liou, C. P., and M. G. Ferrick, 1992, A model for vertical frazil distribution, Water Resource Res., 28, 1329-1337.

Luck, V. W., 1963, Beitrag zur assoziation des flüssigen Wassers. I Die Temperaturabhängigkeit der Ultrarotbanden des Wassers, Ber. Bun. Ges., 67: 186-189.

Martin, S., 1981, Frazil ice in rivers and oceans, Ann. Rev. Fluid Mech., 13: 379-397.

Moore, C., 1994, *In-Situ*, biochemical, oceanic, optical meters, Sea Tech., 35, 10-16.

Morrison, J. et al., The LeadEx experiment, EOS, 74, 393-396.

Omstedt, A., 1986, Modeling initial ice formation in rivers and oceans, In. Proceedings, International Association for Hydraulic Research Symposium on Ice, Iowa City, pp. 559-568.

Omstedt, A., 1994, Numerical simulations of frazil ice, In, "Report on frazil ice", Steven F. Daly ed., USA Cold Regions Research and Engineering Laboratory, Special report 94-23.

Pegau, W. S., and J. R. V. Zaneveld, 1993, Temperature-dependent absorption of water in the red and near-infrared portion of the spectrum, Limn. Oceanogr., 38, 188-192.

Penrose, J. D., M. Conde, and T. J. Pauly, 1994, Acoustic detection of ice crystals in Antarctic waters, J. Geophys. Res. 99: 12,573-12,580.

Roesler, C. S., M. J. Perry, and K. L. Carder, 1989, Modeling in situ phytoplankton absorption from total absorption spectra in productive inland marine waters, Limnol. Oceanogr., 34, 1510-1523.

Schumacher, J. D., K. Aagaard, C. H. Pease, and R. B. Tripp, 1983, Effects of a shelf polynya on flow and water properties in the Northern Bering Sea, J. Geophys .Res., 88: 2723-2732.

Smith, S. D., R. D. Muench, and C. H. Pease, 1990, Polynyas and leads: an overview of physical processes and environment, J. Geophys. Res., 95, 9461-9479.

Svensson, U., and A. Omstedt, 1994, Simulation of supercooling and size distribution of frazil ice dynamics, Cold Reg. Sci. Technol., 22: 221-233.

Tsang, G., 1985, An instrument for measuring frazil concentration, Cold Reg. Sci. Technol., 10: 235-249.

Weeks, W. F., and S. F. Ackley, 1982, The growth, structure, and properties of sea ice, USA Cold Regions Research and Engineering Laboratory, monograph 82-1.

Zaneveld, J. R. V., J. C. Kitchen, and C. C. Moore, 1994, Scattering error correction of reflecting-tube absorption meters. *In* Ocean Optics XII, Jules S. Jaffe, Editor, Proc. SPIE 2258, 44-55.

CHAPTER 7

GENERAL CONCLUSIONS

This thesis describes the different manners in which the absorption coefficient is measured in natural waters. A practical IOP closure equation is developed for testing the consistency of absorption coefficient measurements. The roles of the environmental parameters of temperature and salinity are investigated using laboratory and field measurements of the absorption coefficient. Finally, the temperature dependence of the absorption coefficient is used to develop a method for measuring frazil concentration within the water column.

The difficulty of measuring the absorption coefficient is shown in Chapter 2 where several of the techniques presently used for measuring the absorption coefficient of natural waters were compared. It was found that the temporal and spacial variability in the optical properties of the water played a significant role in comparing the results of the instruments. The natural variability not only creates problems in comparing separate measurements, but also illustrates the difficulty in reporting the optical properties of a given water mass. A single or even several profiles may not be sufficient to fully define the optical properties of a water mass. When possible, it is important to separate the total absorption coefficient into its component contributions to facilitate isolating which components create differences in the measurements using the various techniques. Allowing for the natural variability, it was found that the

measurements were in better agreement at longer wavelengths where the absorption by water is a larger component of the total absorption coefficient. In the blue region of the spectrum there were more instrumental effects included in the performance of the instruments. For this reason it was recommended that further comparisons focus initially in the green region where instrumental effects are smaller. No significant differences between techniques were found that could be attributed to the volume of water included in the measurement (scale effect), the use of a pure water reference, or possible wavelength errors in the instrumentation.

In Chapter 3 an IOP closure equation was developed that is practical within the reality of measurements. It is stressed that perfect measurements of each component in the IOP closure equation is not necessary, but it is very important that all light be accounted for once and only once. The IOP closure equation cannot be used to prove that a measurement is correct. Single point evaluations of the IOP closure equation do not provide any information as there are an infinite number of possible combinations of errors that can provide apparent closure in the measurements. When closure can be maintained over a wide range of optical conditions, the possible measurement errors are reduced to a single multiplier applied to all three measurements. When the measurements are made independently then it is unlikely that the same error would affect all three measurements and it is probable that the measurements of the IOPs are accurate. Because of natural variability in the optical properties it is important to minimize the time and space scales between individual measurements.

In Chapter 4 we began to investigate the role of temperature and salinity in determining the magnitude of the absorption coefficient of water. It was found that the absorption coefficient in the near-infrared portion of the spectrum was linearly dependent on temperature between 5 and 40 °C. It was also shown that in the regions of the overtones of the O-H vibrational frequency, the shape of the spectral absorption curve was dependent on temperature. For wavelengths in the visible region this includes wavelengths near 660, 600, 550, and 515 nm. To correct for variations between samples, we assumed that there was no temperature dependence at 685 nm and required all measured a(685) values to have the same value. In doing this, we were unable to confirm the claim of a constant temperature dependence throughout the visible region [Højerslev and Trabjerg, 1990]. The salinity dependence for wavelengths longer than 735 nm were found to be smaller than those reported by Sullivan [1963]. It was found that influence of temperature on the absorption coefficient of water can dramatically alter spectrophotometeric measurements of the absorption by dissolved materials. Measurement of dissolved material absorption using a clean water reference at a different temperature will provide inaccurate measurements in the near infrared region. It is at these longer wavelengths that the baseline correction of the dissolved component measurements is commonly determined so that temperature based errors are propagated throughout the measurement.

In Chapter 5 we further investigate temperature and salinity effects on the absorption coefficient of water. The experiments discussed in this chapter have less

spectral resolution, but are much better suited for determination of absolute changes in the absorption coefficient. For the wavelengths measured in the visible region there were no areas with temperature dependencies of practical importance i.e. >0.001 $m^{-1}/°C$. The measurements did not include all of the overtone regions in the visible portion of the spectrum. A series of Gaussian curves used to model the spectral absorption of pure water were used to develop a continuous spectral temperature dependence curve. In the regions of the O-H vibrational overtone peaks a constant 0.5% of the absorption coefficient at 20 °C was used. From this model it was apparent that the only wavelength region below 700 nm with a temperature dependence of the order of 0.001 $m^{-1}/°C$ is around 610 nm. A constant temperature dependence throughout the visible band was not found in the laboratory measurements. Using field measurements of the absorption by dissolved materials we were able to demonstrate that a constant temperature dependence, of the magnitude previously reported [Højerslev and Trabjerg, 1990; Buiteveld et al., 1994; Trabjerg and Højerslev, 1996], could not exist.

The effect of the addition of salts on the index of refraction must be accounted for when determining the salinity dependence. Changes in reflectivity at the glass-water interfaces of the windows accounted for the changes in the measured attenuation coefficient in the visible region except at 412 nm. Full compensation of the index of refraction effects on the absorption meter is not possible without detailed knowledge of the transmittance and reflection pattern of the diffuser. Differences found in the salinity dependence using the absorption and attenuation meters can be accounted for

by including multiple reflections in the window at the receiver end of the absorption meter. In the infrared portion of the spectrum salinity has a stronger role in determining the magnitude of the absorption coefficient. Like the temperature dependence the salinity dependence is caused by the changing molecular structure of liquid water. The two mechanisms alter the structure of water in different manners so that the salinity dependence does not necessarily follow that of temperature. The salinity and temperature effects must be accounted for when making measurements in the near infrared using instruments that require a pure water reference.

In Chapter 6 an application of the temperature dependence is developed and tested. The application discussed is the measurement of frazil concentration. The use of a multiple-wavelength absorption scheme may enable the measurement of frazil concentration in the presence of other particles in the water. Temperature, attenuation, and absorption based estimates of frazil concentration are in good agreement for measurements made in a laboratory flume. Field measurements using a transmissometer and applying the laboratory calibrations are consistent with the frazil concentration required to create a stable water column. The optical methods appear to be well suited for making measurements of frazil concentration both in the laboratory and in the field. These methods are thus the first to be capable of making continous vertical profiles of frazil concentration in the field.

BIBLIOGRAPHY

Austin, R., and G. Halikas, The index of refraction of seawater, *Ref. 76-1*, 105 pp, Univ. Calif. SIO, La Jolla, California, 1976

Bartz, R., J. R. V. Zaneveld, and H. Pak, A transmissometer for profiling and moored observations in water, in *Ocean Optics V*, Proc. SPIE, 160, 102-108, 1978.

Bayly, J. B., V. B. Kartha, and W. H. Stevens, The absorption spectra of liquid phase H_2O, HDO and D_2O from 0.7 μm to 10 μm, Infrared Physics, 3, 211-222, 1963.

Bennett, G. T., E. S. Fry, and F. M. Sogandares, Photothermal measurements of the absorption coefficient of water at 590 nm. in *Ocean Optics VIII*, M. A. Blizard, ed., Proc. SPIE, 637, 172-180, 1986.

Boivin, L. P., W. F. Davidson, R. S. Storey, D. Sinclair, and E. D. Earle, Determination of the attenuation coefficients of visible and ultraviolet radiation in heavy water, *Appl. Opt.*, 25, 877-882, 1986.

Bricaud, A., A. Morel and L. Prieur, Absorption by dissolved organic matter of the sea (yellow substance) in the UV and visible domains. *Limnol. Oceanogr.*, 26, 43-53, 1981.

Buckingham, A. D., The structure and properties of a water molecule, in *Water and aqueous solutions,* Neilson, G.W. & Enderby, J.E., eds., Adam Hilger, Bristol, pp. 1-10, 1986

Buiteveld, H., J. M. H. Hakvoort, and M. Donze, The optical properties of pure water, in *Ocean Optics XII,* J. S. Jaffe, ed., Proc. SPIE, 2258, 174-183, 1994.

Cleveland, J. S., R. M. Pope, and E. S. Fry, Spectral absorption coefficients measured with an integrating cavity absorption meter, in *Ocean Optics X*, R. W. Spinrad, ed., Proc. SPIE, 1302, 176-186, 1990.

Cleveland, J. S., and A. D. Weidemann, Quantifying absorption by aquatic particles: A multiple scattering correction for glass-fiber filters, *Limnol. Oceanogr.*, 38, 1321-1327, 1993.

Collins, J. R., Change in the infra-red absorption spectrum of water with temperature, *Phys. Rev.*, 25, 771-779, 1925.

Daly, S. F., Frazil ice dynamics, *Monograph 84-1*,47 pp, USA Cold Regions Research and Engineering Laboratory, Hanover, New Hampshire, 1984.

Daly, S. F., Frazil ice dynamics, , in, *Report on frazil ice, Special report 94-23*, S. F. Daly ed., USA Cold Regions Research and Engineering Laboratory,. Hanover, New Hampshire, 1994.

Daly, S. F., and J. H. Rand, Development of an underwater frazil-ice detector, *Cold Reg. Sci. Technol.*, 18, 77-82, 1990.

Dera, J, *Marine Physics*, Elsevier Oceanography Series, Vol. 53, Elsevier, Amsterdam, 515 pp., 1990.

Doss, W., and W. Wells, Undersea compound radiometer, *Appl. Opt.*, 31, 4268-4274, 1992.

Elterman, P., Integrating cavity spectroscopy, *Appl. Opt.*, 9, 2141-2142, 1970.

Everett, D. H., How much do we really know about water?, in *Water and aqueous solutions,* Neilson, G.W. & Enderby, J.E., eds., Adam Hilger, Bristol, pp. 331-342, 1985.

Franks, F., Water, the unique chemical, in *Water: a comprehensive treatise,* vol. 1, F. Franks ed., Plenum Press, New York, pp.1-20, 1972

Fry, E. S., G. W. Kattawar, and R. M. Pope, Integrating cavity absorption meter, *Appl. Opt.*, 31, 2055-2065, 1992.

Gardner, W. D., P. E. Biscaye, J. R. V. Zaneveld, and M. J. Richardson, Calibration and comparison of the LDGO nephelometer and the OSU transmissometer on the Nova Scotian Rise, *Mar. Geol.*, 66, 323-344, 1985.

Georgiev, G. M., T. K. Kalkanjiev, V. P. Petrov, and Zh. Nickolov, Determination of salts in water solutions by a skewing parameter of the water Raman band, *Appl. Spectrosc.,* 38, 593-595, 1984.

Gershun, A., The Light Field, *J. Math. Phys.*, 18, 51-151, 1939.

Gordon, H. R., Simple calculation of the diffuse reflectance of the ocean, *Appl. Opt.*, 12, 2803-2804, 1973.

Gordon, H. R., Sensitivity of radiative transfer to small-angle scattering in the ocean: Quantitative assessment, *Appl. Opt.*, 32, 7505-7511, 1993.

Gow, A. J., S. F. Ackley, W. F. Weeks, and J. W. Govoni, Physical and structural characteristics of Antarctic sea ice, *Ann. Glaciol.*, 3, 113-117, 1982.

Gow, A. J., D. A. Meese, D. K. Perovich, and W. B. Tucker III, The anatomy of a freezing lead, *J. Geophys. Res.,* 95, 18221-18232 1990.

Green, S. A., and N. V. Blough, Optical absorption and fluorescence properties of chromophoric dissolved organic matter in natural waters, *Limnol. Oceanogr.,* 39, 1903-1916, 1994.

Grenfell, T. C., and D. K. Perovich, Radiation absorption coefficients of polycrystalline ice from 400-1400 nm, *J. Geophys. Res.,* 86: 7447-7450, 1981.

Hale, G. M., and M. R. Querry, Optical constants of water in the 200-nm to 200-μm wavelength region, *Appl. Opt.,* 12, 555-563, 1973.

Halmann, M., and I. Platzner, Temperature dependence of absortion of liquid water in the far-ultraviolet region, *J Phys. Chem.,* 70, 580-581, 1966.

Hirschfeld, T., Salinity determination using NIRA. *Appl. Spectrosc*, 39, 740-741, 1985.

Højerslev, N. K., Inherent and apparent optical properties of the Western Mediterranean and the Hardagerfjord, *Report 21,* 23 pp, Institut for Fysisk Oceanografi, Københavns Universitet, Copenhagen, Denmark, 1973.

Højerslev, N. K., Inherent and apparent optical properties of the Baltic, *Report 23,* 41 pp, Institut for Fysisk Oceanografi, Københavns Universitet, Copenhagen, Denmark, 1974.

Højerslev, N. K., A spectral light absorption meter for measurements in the sea, *Limnol. Oceanogr.*, 20, 1024-1034, 1975.

Højerslev, N. K., and I. Trabjerg, A new perspective for remote sensing measurements of plankton pigments and water quality, *Report 51*, 10 pp, Institut for Fysisk Oceanografi, Københavns Universitet, Copenhagen, Denmark, 1990.

Irvine, W. M., and J. B. Pollack, Infrared optical properties of water and ice spheres, *Icarus,* 8, 324-360, 1968.

Jerlov, N. G., *Marine Optics,* Elsevier Oceanography Series, 14, Amsterdam, 231 pp., 1976.

Kennedy, C. D., Integrating cavity spectral absorption meter, Masters Thesis, December 1992, Long Memorial Library, University of New Orleans, New Orleans, La.

Kiefer, D. A. and J. B. Soohoo, Spectral absorption by marine particles of coastal waters of Baja California. *Limnol. Oceanogr.*, 27, 492-499, 1982.

Kirk, J. T. O., Monte Carlo modeling of the performance of a reflective tube absorption meter, *Appl. Opt.*, **31**, 6463-6468, 1992.

Kirk, J. T. O., *Light & Photosynthesis in Aquatic Ecosystems*, 2nd edition, Cambridge University Press, Cambridge, 509 pp, 1994.

Lange, M. A., S. F. Ackley, P. Wadhams, G. S. Dieckmann, and H. Eicken, Development of sea ice in the Weddell Sea, *Ann. Glaciol.,* 12, 92-96, 1989.

Lever, J. H., S. F. Daly, J. H. Rand and D. Furey, A frazil concentration meter, in: *Proceedings, International Association of Hydraulic Research 11th International Symposium on Ice*, Banff, Alberta, pp. 1362-1376, 1992.

Lin, J., and C. W. Brown, Near-IR spectroscopic measurement of seawater salinity, *Environ. Sci. Technol.,* 27, 1611-1615, 1993.

Liou, C. P., and M. G. Ferrick, A model for vertical frazil distribution, *Water Resource Res.*, 28, 1329-1337, 1992.

Luck, W, Beitrag zur assoziation des flüssigen wassers. I Die temperaturabhängigkeit der ultrarotbanden des wassers, *Ber. Bun. Ges.,* 67, 186-189, 1963.

Maffione, R. A., and J. S. Jaffe, The average cosine due to an isotropic light source in the ocean, *J. Geophys. Res.*, 100, 13,179-13,192, 1995.

Maffione, R. A., R. C. Honey, and R. A. Brown, Experiment for testing the closure property in ocean optics, Proc. SPIE, 1537, 115-126, 1991.

Maffione, R. A., K. J. Voss, and R. C. Honey, Measurement of the spectral absorption coefficient in the ocean with an isotropic source, *Appl. Opt.*, 32, 1993.

Martin, S., Frazil ice in rivers and oceans, *Ann. Rev. Fluid Mech.,* 13: 379-397, 1981.

Miles, E., and W. H. Wells, Revised results from the underwater compound radiometer, Report to ONR under contract N 00014-88-C-0715, Dec. 1993. (available from Tetra Tech. Data Systems Inc. 2451a Impala Dr. Carlsbad, CA 92008)

Mobley, C. D., *Light and water: radiative transfer in natural waters,* Academic Press, New York, 592 pp., 1994.

Mobley, C. D., B. Gentili, H. R. Gordon, Z. Jin, G. W. Kattawar, A. Morel, P. Reinersman, K. Stamnes, and R. H. Stavn, Comparison of numerical models for computing underwater light fields, *Appl. Opt.*, **36**, 7484-7504, 1993.

Moore, C., *In-Situ*, biochemical, oceanic, optical meters, *Sea Tech.,* 35, 10-16, 1994.

Moore, C., J. R. V. Zaneveld, and J. C. Kitchen, Preliminary results from an *in situ* spectral absorption meter, in *Ocean Optics XI*, G. D. Gilbert, ed., Proc. SPIE, 1750, 330-337, 1992.

Morel, A., Optical properties of pure water and pure sea water, in *Optical aspects of oceanography,* Jerlov, N.G. & Nielsen, E.S., eds., Academic Press, London, pp. 1-24, 1974.

Morel, A., Light and marine photosynthesis: a spectral model with geochemical and climatological implications, *Prog. Oceanog.*, 26: 263-306, 1991.

Morrison, J. et al., The LeadEx experiment, EOS, 74, 393-396.

Mueller, J. L., Integral method for irradiance profile analysis, *CHORS Tech. Memo. 007- 91*, San Diego, CA., 1991.

Mueller, J. L. and R. W. Austin, Ocean optics protocols for SeaWiFS validation, SeaWiFS Technical Report Series, Vol. 5. Hooker, S.B. and E.R. Firestone, eds., *NASA TM-104566*, Vol. 5, NASA Goddard Space Flight Center, Greenbelt, MD. 43pp, 1992.

Omstedt, A., Modeling initial ice formation in rivers and oceans, in. *Proceedings, International Association for Hydraulic Research Symposium on Ice*, Iowa City, pp. 559-568, 1986

Omstedt, A., Numerical simulations of frazil ice, in, *Report on frazil ice, Special report 94-23,* Steven F. Daly ed., USA Cold Regions Research and Engineering Laboratory, Hanover, New Hampshire, 1994.

Pegau, W. S., J. S. Cleveland, W. Doss, C. D. Kennedy, R. A. Maffione, J. L. Mueller, R. Stone, C. C. Trees, A. D. Weidemann, W. H. Wells, and J. R. V. Zaneveld, A comparison of methods for the measurement of the absorption coefficient in natural waters, *J. Geophys. Res.,* 100, 13,201-13,220, 1995.

Pegau, W. S., C. A. Paulson, and R. J. V. Zanveld, Optical measurements of frazil concentration, *Cold Reg. Sci.Tech.,* in progress.

Pegau, W. S., and J. R. V. Zaneveld, Temperature-dependent absorption of water in the red and near-infrared portion of the spectrum, *Limn. Oceanogr.,* 38, 188-192, 1993.

Pegau, W. S., and J. R. V. Zaneveld, Temperature dependence of the absorption coefficient of pure water in the visible portion of the spectrum, in *Ocean Optics XII,* J. S. Jaffe, ed., Proc. SPIE, 2258, 597-604, 1994.

Penrose, J. D., M. Conde, and T. J. Pauly, Acoustic detection of ice crystals in Antarctic waters, *J. Geophys. Res.,* 99: 12,573-12,580, 1994.

Petzold, T. J., Volume scattering functions for selected ocean waters, *SIO Ref. 72-78,* 79 pp, Scripps Inst. of Oceanogr., La Jolla, Calif., 1972.

Pope, R. M., Optical absorption of pure water and sea water using the integrating cavity absorption meter, Ph. D. Thesis, Texas A&M University, December 1993.

Preisendorfer, R. W., *Hydrologic Optics,* 6 volumes, Pacific Mar. Environ. Lab/NOAA, Seattle, WA, 1976.

Querry, M. R., P. G. Cary, and R. C. Waring, Split-pulse laser method for measuring attenuation coefficients of transparent liquids: application to deionized filtered water in the visible region, *Appl. Opt.,* 17, 3587-3592, 1978.

Querry, M. R., D. M. Wieliczka, and D. J. Segelstein, Water (H_2O), in *Handbook of Optical Constants of Solids II,* Academic Press, pp. 1059-1077, 1991.

Quickenden, T. I., and J. A. Irvin, The ultraviolet absorption spectrum of liquid water, *J. Chem Phys.,* 72, 4416-4428, 1980.

Rao, C. N. R., Theory of hydrogen bonding in water, in *Water: a comprehensive treatise,* vol. 1, F. Franks ed., Plenum Press, New York, pp.93-113, 1972.

Ravisankar, M., A. T. Reghunath, K. Sathianandan, and V. P. N. Nampoori, Effect of dissolved NaCl, $MgCl_2$, and Na_2SO_4 in seawater on the optical attenuation in the region from 430 to 630 nm, *Appl. Opt.,* 27, 3887-3894, 1988.

Richards, W. G., *Ab initio* methods and the study of molecular hydration, in *Water: a comprehensive treatise,* vol. 6, F. Franks ed., Plenum Press, New York, pp.47-120, 1979.

Roesler, C. S., M. J. Perry, and K. L. Carder, Modeling in situ phytoplankton absorption from total absorption spectra in productive inland marine waters, *Limnol. Oceanogr.,* 34, 1510-1523, 1989.

Sathyendranath, S., L. Lazzara, and L. Prieur, Variations in the spectral values of specific absorption of phytoplankton, *Limnol. Oceanogr.*, 32, 403-415, 1987.

Schumacher, J. D., K. Aagaard, C. H. Pease, and R. B. Tripp, Effects of a shelf polynya on flow and water properties in the Northern Bering Sea, *J. Geophys .Res.*, 88: 2723-2732, 1983.

Shifrin, K. S. ,*Physical Optics of Ocean Water,* American Institute of Physics, New York, 285 pp., 1988.

Smith, R. C., and K. S. Baker, Optical properties of the clearest natural waters (200-800 nm), *Appl. Opt.*, 20, 177-184, 1981.

Smith, S. D., R. D. Muench, and C. H. Pease, Polynyas and leads: an overview of physical processes and environment, *J. Geophys. Res.,* 95, 9461-9479, 1990.

Sorenson, G., and R. C. Honey, Instrumentation for measuring visibility-limiting characteristics of sea water, Proc. SPIE, 12, 115-122, 1968.

Spitzer, D., and M. R. Wernand, *In situ* measurements of absorption spectra in the sea, *Deep-Sea Res.*, 28A, 165-174, 1981.

Stamnes, K, S.-C. Tsay, W. Wiscombe, and K. Jayaweera, Numerically stable algorithm for discrete-ordinate-method radiative transfer in multiple scattering and emitting layered media, *Appl. Opt.*, 27, 2502-2509, 1988.

Sullivan, S. A., Experimental study of the absorption in distilled water, artificial sea water, and heavy water in the visible region of the spectrum, *Opt. Soc. Am. J.*, 53: 962-968, 1963.

Svensson, U., and A. Omstedt, Simulation of supercooling and size distribution of frazil ice dynamics, *Cold Reg. Sci. Technol.,* 22: 221-233, 1994.

Tam, A. C., and C. K. N. Patel, Optical absorptions of light and heavy water by laser optoacoustic spectroscopy, *Appl. Opt.*, 18, 3348-3358, 1979.

Trabjerg, I., and N. K. Hojerslev, Temperature influence on light absorption by water and sea water in the visible and near-infrared spectrum, *Appl. Opt.*, in press.

Trees, C. C., and K. J. Voss, Optoacoustic spectroscopy and its application to molecular and particle absorption, in *Ocean Optics X*, R. W. Spinrad, ed., Proc. SPIE, 1302, 149-156, 1990.

Tsang, G., An instrument for measuring frazil concentration, *Cold Reg. Sci. Technol.*, 10: 235-249, 1985.

Tyler, J. E., Radiance distribution as a function of depth in an underwater environment, *Bull. Scripps Inst. Oceanogr. Univ. Calif.*, **7**, 363-412, 1960.

Voss, K. J., Use of the radiance distribution to measure the optical absorption coefficient in the ocean, *Limnol. Oceanogr.*, 34, 1614-1622, 1989.

Voss, K. J., Electro-optic camera system for measurement of the underwater radiance distribution, *Optical Engineer.*, 28, 241-247, 1989.

Voss, K. J., and R. W. Austin, Beam-attenuation measurement error due to small-angle scattering acceptance, *J. Atmosph. and Oceanic Technol.*, 10, 113-121, 1993.

Voss, K. J., and A. L. Chapin, Next generation in-water radiance distribution camera system, in *Ocean Optics XI*, G. D. Gilbert, ed., Proc. SPIE, 1750, 384-387, 1992.

Waggener, W. C., A. J. Weinberger, and R. W. Stoughton, The absorption spectrum of H_2O an d D_2O in the near infrared region as a function of temperature from -20° to 250° C, *Rep. ONRL-P-925* Atomic Energy Commission, 1964.

Walrafen, G. E., Raman spectral studies of the effects of temperature on water structure, *J. Chem. Phys.*, 47, 114-126, 1967.

Weeks, W. F., and S. F. Ackley, The growth, structure, and properties of sea ice, *monograph 82-1*, USA Cold Regions Research and Engineering Laboratory, Hanover, New Hampshire, 1982.

Wells, W. H., Techniques for measuring radiance in sea and air, *Appl. Opt.*, 22, 2313-2321, 1983.

Whetsel, K. B., Near-infrared spectrophotometry, *Appl. Spectrosc. Rev.*, 2, 1-67, 1968.

Wiscombe, W. J., The Delta-M method: rapid yet accurate radiative flux calculations for strongly asymmetric phase functions, *J. Atmos. Sci.* **34**, 1408-1422, 1977.

Wood, D. W., Computer simulation of water and aqueos solutions, in *Water: a comprehensive treatise,* vol. 6, F. Franks ed., Plenum Press, New York, pp.279-392, 1979.

Yentsch, C. S., Measurement of visible light absorption by particulate matter in the ocean, *Limnol. Oceanogr.*, 7, 207-217, 1962.

Zaneveld, J. R. V., Optical closure: from theory to measurement, in *Ocean Optics,* R. W. Spinrad, K. L. Carder, and M. J. Perry editors, Oxford University Press, New York, 283 pp, 1994.

Zaneveld, J. R. V., and R. Bartz, Beam attenuation and absorption meters, in *Ocean Optics VII,* M. A. Blizzard, ed., Proc SPIE, 489, 318-324, 1984.

Zaneveld, J. R. V., R. Bartz, J. C. Kitchen, Reflective-tube absorption meter, in *Ocean Optics X*, R. W. Spinrad, ed., Proc. SPIE, 1302, 124-136, 1990.

Zaneveld, J. R. V., J. C. Kitchen, A. Bricaud, and C. Moore, Analysis of *in situ* spectral absorption meter data, in *Ocean Optics XI*, G. D. Gilbert, ed., Proc. SPIE, 1750, 187-200, 1992.

Zaneveld, J. R. V., J. C. Kitchen, and C. C. Moore, Scattering error correction of reflecting-tube absorption meters. in *Ocean Optics XII*, Jules S. Jaffe, Editor, Proc. SPIE 2258, 44-55, 1994

Zaneveld, J. R. V., and H. Pak, Some aspects of the axially symmetric submarine daylight field, *J. Geophy. Res.*, 77, 2677-2680, 1972.